Photo-oxidation Kinetics of Poly-3-hexylthiophene Thin Films

Dissertation

der Mathematisch-Naturwissenschaftlichen Fakultät

der Eberhard Karls Universität Tübingen

zur Erlangung des Grades eines

Doktors der Naturwissenschaften

(Dr. rer. nat.)

vorgelegt von

Holger Hintz

aus Remagen

Tübingen

2011

Tag der mündlichen Qualifikation:	23.2.2012
Dekan:	Prof. Dr. Wolfgang Rosenstiel
1. Berichterstatter:	Prof. Dr. Thomas Chassé
2. Berichterstatter:	PD. Dr. Hans-Joachim Egelhaaf

Ich erkläre hiermit, dass ich die zur Promotion eingereichte Arbeit selbständig verfasst, nur die angegebenen Quellen und Hilfsmittel benutzt und wörtlich oder inhaltlich übernommene Stellen als solche gekennzeichnet habe.

Holger Hintz, Tübingen den 19.12.2011

Parts of this work have been published in:

Publications (peer reviewed):

***H.Hintz**, H.-J.Egelhaaf, H.Peisert, T.Chassé,* Wavelength dependent pathways of P3HT photo degradation as studied by UV/VIS and FTIR spectroscopy, in preparation

***H.Hintz**, C.Sessler, H.-J.Egelhaaf, T.Chassé,* The role of humidity in the photo oxidation of P3HT, in preparation

***H. Hintz**, H.-J. Egelhaaf, H. Peisert, T. Chassé* Oxygen induced p-doping during photo oxidation of P3HT as studied by photoelectron spectroscopy (XPS/UPS), *J. Phys. Chem. C,* **2011**,115, 13373-13376

***H. Hintz**, H.-J. Egelhaaf, H. Peisert, T. Chassé, L. Lüer, J. Hauch,* Photo degradation of P3HT - a systematic study of environmental factors, *Chem. Mater.*, **2011**, 23, 145–154

H.Hintz, *H.-J.Egelhaaf, H.Peisert, T.Chassé,* Photo oxidation and ozonization of Poly(3-hexylthiophene) thin films as studied by UV/Vis and Photoelectron Spectroscopy, *Polymer Degrad. Stab.*, **2010**, 95, 818-825

H. Hintz, H. Peisert, U. Aygül, F. Latteyer, I. Biswas, P. Nagel, M. Merz, S. Schuppler, D. Breusov, S. Allard, U. Scherf, T. Chassé, Electronic structure and interface properties of a model molecule for organic solar cells, *ChemPhysChem*, **2010**, 11, *269–275.*

D. Zhang, X. Wang, K. Braun, H.-J. Egelhaaf, M. Fleischer, L. Hennemann, **H. Hintz**, C. Stanciu, C. J. Brabec, D.P.Kern, A.J.Meixner , *J. Raman Spectrosc.* , **2009**, 40, 1371–1376.

Content:

Abbreviations:

OFET	Organic Field Effect Transistor
OLED	Organic Light Emitting Diode
OPV	Organic Photovoltaic
P3HT	Poly-3-Hexylthiophene
PPV	Poly(paraphenylenvinylene)
FTIR	Fourier Transform Infrared
UV/Vis	Ultraviolet/Visible
PES	Photoelectron Spectroscopy
XPS	X-ray Photoelectron Spectroscopy
UPS	Ultraviolet Photoelectron Spectrosocopy
AFM	Atomic Force Microscopy
AM1.5	Air Mass 1.5
PL	Photoluminescence
FQ	Fluorescence Quenching
TFAA	Trifluoroaceticanhydride
TFA	Trifluoracetic acid
PE	Polyethylene
PET	Polyethylenterephthalate
PP	Polypropylene
PMMA	Poly(methyl methacrylate)
NIST	National Institute of Standards and Technology

I. Introduction:

The interest in organic semiconductors has strongly increased over the last decade due to their application in optoelectronic devices like organic field effect transistors[1] (OFET), organic light emitting diodes (OLED) and organic photovoltaics (OPV). The first commercial launch of OPV devices by Konarka in 2009 additionally boosted the effort spent on this topic. Although organic materials cannot compete with their inorganic counterparts in terms of device efficiency so far [2] they are interesting as their properties can be easily tuned via chemical synthesis both in small molecule (e.g. phthalocyanines[3]) and polymeric materials (e.g. thiophene based materials). "Bulk heterojunction" devices, whose photoactive layer consists of a blend of electron donor (usually a π-conjugated polymer) and an electron acceptor (usually a fullerene), can be processed cost effectively via solution based techniques like spin coating, doctor blading or roll to roll (e.g. Konarka Company) printing. Another approach for multilayer devices is the vacuum evaporation of small molecules at a commercial scale without high temperature processing steps (e.g. Heliatek). Generally OPV devices exhibit some major advantages compared to silicon based devices. These advantages are cheaper and less energy consuming manufacturing, semi-transparency and a variable band gap leading to different colours making them attractive for building integrated applications. Disadvantages of OPV so far are given by the relatively low power conversion efficiency (<10%) compared to their inorganic counterparts (~20% for crystalline silicon and 8-9 % for amorphous silicon based devices[4]). Therefore most of the effort spent in organic electronics was focused on the improvement of device performance (i.e. power conversion efficiency in the case of OPV) for both small molecule and polymer based materials. Although this is still a field of intensive research, it turned out that besides device performance, the life time of organic materials under operational conditions is a key challenge, which has to be faced in order to allow broad commercialization[5,6,7,8]. Although there are effective encapsulation methods[9,10] which reduce oxygen and water induced degradation effects by orders of magnitude, their use in OPV technology is prevented by their tremendous costs. To make organic solar cells competitive to established technologies, the intrinsic stability of the materials constituting the devices has to be improved to achieve the desired lifetimes of more than 10 years[8]. In order to meet these requirements a more detailed knowledge of the basic degradation mechanisms of the organic solar devices is required. Major degradation pathways comprise ageing of the active layer morphology[6,11], delamination of the different organic layers[5], corrosion of low work function metal electrodes[5,12], and several oxygen induced degradation pathways of the active layer [5,6]. The latter are the topic of this thesis. In principle, both components of the active layer, i.e., polymer and fullerene are prone to oxidation. As the p-type component is reported to be significantly less stable than the n-type constituent, the present work will concentrate on the oxidation of the polymer.

Although there are many other thiophene based polymers which show better performance in organic photovoltaic devices[5], poly-3-hexylthiophene (P3HT) has still, by far, the highest commercial relevance in OPV. So far only P3HT based organic solar cells are commercially available. It is among the polymers with the largest data base on degradation and thus serves as a model system for degradation studies[13]. Moreover, it serves as a prototypical example, as many of the most promising polymers for organic photovoltaic applications contain thiophene based moieties[5,14]. P3HT contains neither vinylene bonds nor fluorene moieties and thus does not have obvious weak points as poly(paraphenylenvinylene)s and polyfluorenes have. Understanding of the degradation mechanisms of P3HT will make it possible to synthesize a broad variety of new polymers with enhanced stability.

Polymers in general are prone to different degradation pathways under ambient conditions. The oxygen-induced mechanisms have the biggest practical relevance. These mechanisms comprise photo-oxidation, thermal oxidation and decomposition by ozone. These pathways are certainly also operative in the degradation of P3HT. However, the importance of these mechanisms under realistic conditions has not been determined quantitatively so far. Some π-conjugated polymers, represented by P3HT, reveal some additional features of interaction with oxygen. The simultaneous exposure of P3HT to light and oxygen leads to the degradation of device properties[11,15,16]. This degradation has both reversible and irreversible components[15]. A reversible component has been characterized as light induced oxygen doping[17] via the formation of polymer-oxygen charge transfer complex[18,19] whereas the irreversible part is assigned to the destruction of the π-conjugated system in both, solution[20] and the solid state[24]. In solution, the degradation is known to originate from the production of singlet oxygen sensitized by the polymer[20, 21]. However, the mechanistic situation in the solid state seems to be completely different from that in solution. Even at high concentrations of singlet oxygen, P3HT films are reported to remain undegraded[22]. Thus, the mechanism has been proposed to proceed via a radical pathway[23,24,25], at least under white light conditions. It has been suggested that the radical mechanism proceeds via hydrogen abstraction at the alpha carbon of the alkyl side chain[23,26] with subsequent formation of hydrogen peroxide and oxidation of the aromatic and alkylic system, accompanied by crosslinking[23,26] and the formation of volatile species[25]. However, the origin of the first reactive centers which triggers the reaction remains unclear. Despite the effort spent on understanding the degradation of P3HT in the solid state there is still a lack of understanding of the details of the degradation mechanism especially about ambient factors entering the complex reaction mechanism. Literature reporting on the quantitative influence of illumination conditions, temperature and atmospheric conditions is not available, although these are key factors in polymer aging. Only detailed knowledge about the nature and relevance of single reaction steps will allow the synthesis of materials with enhanced stability absolutely necessary for the commercial success of organic electronics. In order to overcome this obstacle and to get deeper insights into the complex mechanism, the influence of the mentioned environmental conditions on the photo degradation rate of P3HT is

screened in this work identifying the dominating reaction pathways under ambient conditions. As the studies require the rigorous control of environmental conditions, a setup for polymer degradation under defined, online monitored conditions was constructed first. This will be presented in section II. Subsequently single ambient parameters (e.g. humidity from 0% to100% relative humidity, oxygen partial pressure from 1mbar to 8000 mbar) and their relevance for the material aging are screened first by UV/VIS spectroscopy. Doing so, the dominating pathways in the overall degradation process are identified. Herein UV/VIS absorption spectroscopy is employed as the polymer strongly absorbs in the visible range, and this type of spectroscopy can be easily adapted to the online tracing of the degradation process under different conditions. At last UV/VIS spectroscopy is directly probing the properties of π-conjugated system which are of major importance.

After the screening, defined limiting cases are investigated using different spectroscopic techniques (FTIR, PL, PES) revealing a deeper insight into the decomposition process and the contribution of single degradation steps (section III). Here FTIR is used to probe bulk chemical properties during the degradation process especially by using isotopic labeling techniques. Photoelectron spectroscopy with its high surface sensitivity is employed to study the chemical processes near the surface compared to those in the bulk. Furthermore, photoelectron spectroscopy gives insights into the electronic structure of the organic semiconductor.

The consequences of degradation for the material properties like the electronic structure (e.g. doping by oxygen), photo physical behaviour (quenching of excited polymer states) or chemical reactions (disruption of the π-conjugated system and the polymer backbone) will be addressed together with their respective relation in section III. Furthermore, the presence of reversible and irreversible oxygen effects together with their occurrence on the timescale of the complete degradation process is illustrated in section III. The observed reaction kinetics of the π-conjugated system during the decomposition process are approached by a numerical simulation dealing with basic photochemical considerations (Lambert Beer Absorption, polymer chain fragmentation, mobility of reactive centres).

In order to be able to draw a most complete picture of the degradation process from initial reversible effects to latest irreversible effects the results are discussed altogether in section IV. Finally a degradation process is proposed there.

II Theory and fundamentals

II.1 Interaction of electromagnetic radiation with matter

If electromagnetic radiation hits matter there are three possibilities of interaction: Transmission (T), reflection (R) and absorption (A). Absorption accounts for a loss of intensity due to the excitation of matter to a higher energy level. The loss of intensity is described by the Lambert Beer law:

$$I(\lambda) = I_0(\lambda) \cdot 10^{-\varepsilon(\lambda)cx} \qquad \textbf{Eq.1}$$

The intensity decreases exponentially, with the exponent containing the wavelength dependent molar absorption coefficient ε(λ), the concentration c and the path length x through the matter. The spectroscopic measurement is done by wavelength resolved comparison of the intensity before and after passing the matter. This is written as absorbance

$$E(\lambda) = \log\frac{I_0(\lambda)}{I(\lambda)} = \varepsilon(\lambda)cx \qquad \textbf{Eq.2}$$

Depending on the used wavelength, excitation to higher rotational, vibrational or electronic states is possible. Using radiation of higher energy e.g. deep UV or X-ray radiation, electrons can be even shifted above the vacuum level.

The sum of transmitted, reflected and adsorbed intensity equals the incident intensity I_0,

$$T + R + A = 1 \qquad \textbf{Eq.3}$$

where $T = \frac{I_T}{I_0}$ $R = \frac{I_R}{I_0}$ $A = \frac{I_A}{I_0}$ **Eq. 4**

II.2 UV/VIS Spectroscopy

Using light of the ultraviolet or visible region for excitation, spectroscopic transitions from a vibronic ground state S_0^0 to a higher energy final state S_1^n can be obtained and evaluated according to the Lambert-Beer law. In this notation S means a singlet state, while the superscript describes the vibrational state and the subscript the number of the electronic state, starting with zero from the ground state. After excitation to this level several primary steps of relaxation are possible. These are shown in Tab. 1

Tab. 1: possible primary steps after absorption of a photon.

Primary step	Explanation
Thermal equilibration (TE)	Relaxation to the vibrational ground state of the respective electronic state by energy transfer to the environment
Fluorescence (F)	Emission of radiation, in organic molecules usually the transition $S_1^0 \rightarrow S_0^n$
Intersystem crossing (ISC)	Transition between two systems of different spin multiplicity, in organic molecules usually from S_1^0 to a triplet state T_1^n
Internal conversion (IC)	(Radiationless) transition from S_1^0 to S_0^n
Photochemical steps (PS)	The absorbed energy can be used for activation of chemical reactions
Phosphorescence (P)	Radiative transition between two states of different spin multiplicity, e.g., the transition $T_1^0 \rightarrow S_0^n$
Energy transfer (ET)	Transfer of energy between two chromophores, by, e.g., Förster transfer.

For each process a quantum efficiency q_i can be defined:

$$q_i = \frac{N_i}{N_0} \leq 1 \qquad \textbf{Eq. 5}$$

where N_0 is the number of absorbed photons and N_i is the number of molecules undergoing process i triggered by the absorbed photon.

II.3 Photoluminescence spectroscopy and quenching phenomena

Contrary to UV/VIS absorption, photoluminescence (PL) spectroscopy deals with the emission of photons after the absorption process. Upon excitation into a higher vibronic state (e.g. S_1^n) the molecule relaxes reaching the vibrational ground state (S_1^0) via thermal equilibration. The further deactivation of the molecule is represented by several pathways, which may be both, radiative (e.g. fluorescence and phosphorescence) and non radiative processes (e.g. Internal conversion, quenching by other molecules, photochemical steps). The emission spectrum is generally shifted towards lower energies compared to the absorption spectrum due to the fact that the thermal deactivation process directly after excitation reduces the energy of the following radiative transitions (Stokes shift).

The intensity of the PL is given by the product of the emission quantum efficiency Q_{PL} and the number of absorbed photons $I_{Absorbed}$

$$PL = Q_{PL} \cdot I_{Absorbed} \xrightarrow{LambertBeer} PL = Q_{PL} \cdot I_0 (1 - 10^{-\varepsilon c d}) \qquad \textbf{Eq.6}$$

using Lambert Beer`s law with ε the absorption coefficient, c the concentration of the respective species and d the thickness of the illuminated pathway. The quantum efficiency Q_{PL} is given by

$$Q_{PL} = \frac{N_{PL}}{N_{Absorbed}} \qquad \textbf{Eq.7}$$

with the number of emitted photons N_{PL} and the number of absorbed photons $N_{Absorbed}$. Whereas the latter one is easily accessible via the incident intensity and the absorption spectrum of the corresponding sample the number of emitted photons critically depends on the rate constants of primary steps after excitation. The deactivation of excited states can be expressed as

$$dN_{Excited} = -k \cdot N_{Excited} \cdot dt \xrightarrow{Integration} N_{Excited} = N_{Excited}(0) \cdot e^{-kt} \qquad \textbf{Eq.8}$$

With k being the decay constant representing the sum of all rate constants of all decay channels

$$k = \sum_i k(i) \xrightarrow{e.g} k_{Fluorescence} + k_{InterSystemCrossing} + k_{Internalconversion} \ldots\ldots\ldots\ldots \qquad \textbf{Eq.9}$$

Therefore the quantum efficiency of photoluminescence becomes:

$$Q_{PL} = \frac{k_{PL} \cdot N_{excited}}{\sum_i k(i) \cdot N_{excited}} = \frac{k_{PL}}{\sum_i k(i)} = k_{PL} \cdot \tau \qquad \textbf{Eq.10}$$

with the natural lifetime given by:

$$\tau = \frac{1}{\sum_i k(i)}$$

Upon the presence of quenching sites the photoluminescence is reduced due to the presence of additional decay pathways of the excited state yielding the reduced quantum efficiency, in the case of homogeneously distributed quenching sites of the density N_{Quench}:

$$Q_{Quench} = \frac{k_{PL}}{\sum_i k(i) + k_{Quench} \cdot N_{Quench}} \qquad \textbf{Eq.11}$$

Comparing the photoluminescence quantum efficiency in absence (Q_{Pl}) and presence (Q_{Quench}) of quenching phenomena yields the Stern Volmer equation

$$\frac{Q_{Pl}}{Q_{Quench}} = \frac{\sum_i k(i) + k_{Quench} \cdot N_{Quench}}{\sum_i k(i)} = 1 + k_{Quench} \cdot N_{Quench} \cdot \tau \xrightarrow{k_{Quench} \cdot \tau = K_{SV}} 1 + K_{SV} \cdot N_{Quench} \qquad \textbf{Eq.12}$$

with K_{SV} representing the Stern Volmer constant. Under experimental conditions the photoluminescence intensities are used to describe the photoluminescence quenching in presence of a quenching site PQ according to:

$$PQ = \frac{Pl_0}{Pl_{Quench}} - 1 = K_{SV} \cdot N_{Quench} \qquad \textbf{Eq. 13}$$

Therefore the density of quenching sites can be calculated, if both the natural lifetime τ and the rate constant of the quenching process k_{Quench} are known.

II.4 Fourier Transform Infrared Spectroscopy (FTIR)

Absorption of light in the infrared region can lead to the excitation of the molecule into a higher rotational-vibrational state which is typically expressed in terms of the Lambert-Beer law. The vibration modes strongly depend on the chemical nature of the molecule which makes IR spectroscopy a suitable tool to identify chemical functions in a specific molecule. The number of molecular vibrations is given for non-/linear molecules according to:

F = 3N-5 and F = 3N-6, respectively. **Eq.14**

However, of these vibrational modes only those are observed in FTIR spectroscopy, which are associated with a changing dipole moment. In a first approximation the frequency of a molecular vibration can be described assuming a harmonic oscillator and a 2-atomic molecule. Then the frequency is given by the respective Eigen-frequency:

$$\upsilon = \frac{1}{2\pi}\sqrt{\frac{k}{\mu}} \qquad \textbf{Eq.15}$$

with k being the force constant of the corresponding vibration. The reduced mass μ of the two atoms with mass m1 and m2 participating in the vibration is calculated according to:

$$\mu = \frac{m_1 m_2}{m_1 + m_2} \qquad \textbf{Eq.16}$$

Eq.16 reveals that FTIR spectroscopy is sensitive to isotopic labelling. Therefore FTIR can be used to investigate whether a specific atom of a certain molecule participates in a chemical process or not. Changing the reduced mass by using isotopic labeling therefore leads to shifts of the molecular vibrations $\upsilon_{(1)}$ to the new frequency $\upsilon_{(2)}$ according to:

$$\upsilon_{(2)} = \upsilon_{(1)} \cdot \sqrt{\frac{\mu_{(1)}}{\mu_{(2)}}} \qquad \textbf{Eq.17}$$

The expected factors for the spectral shifts according to Eq. 17 are summarized in Tab. 2 for different chemical groups upon ^{18}O and deuterium labeling.

Tab. 2: Scaling factors for spectral FTIR features upon isotopic labeling according to Eq.17.

Chemical group	Exchanged Isotope	$\sqrt{\frac{\mu_{(1)}}{\mu_{(2)}}}$
C-O or C=O	^{16}Oxygen by ^{18}Oxygen	0.976
OH	Hydrogen by Deuterium	0.728
OH	^{16}Oxygen by ^{18}Oxygen	0.993
CH	Hydrogen by Deuterium	0.738

In order to unambiguously state about chemical species which show overlapping bands in the FTIR (e.g. different carbonyl functions with similar force constants) chemical derivatization of sample can be employed to identify the detailed chemical nature of these groups.

Although it is possible to assign the observed FTIR bands to certain functional groups e.g. carbonyls or hydroxyls due to their spectral position, the assignment to specific chemical structures (e.g. ketones or esters) is not easily accessible as the frequencies might depend on the surrounding matrix and corresponding interactions. Therefore chemical derivatization experiments can be employed to probe single chemical species in polymer degradation. The derivatization agents used in this thesis and the expected products are presented in Tab.3.

Exposure to water vapor is a sensitive test to the presence of anhydrides, which decompose to form acids. In the presence of anhydrides, the exposure to water vapor should therefore lead to a substantial increase in the hydroxyl range and spectral shifts in the carbonyl range.

Derivatization with ammonia can be used to identify any kind of acidic hydroxyl function, which becomes evident from a substantial loss in the hydroxyl range and simultaneous occurrence of a new carbonyl signal both originating from the deprotonation of the acid leading to $RCOO^{-}NH_4^{+}$. Furthermore ammonia may react with anhydrides and esters to form amide functions. In this case, the carbonyl band shifts to lower wave numbers due to the formation of an amide C=O function. Simultaneously, the hydroxyl region experiences enhanced absorption due to the formation of alcohols or acids.

Trifluoroaceticanhydride (TFAA) is a strong esterification agent and can be used to identify alcoholic functions [27,28]. Upon exposure to TFAA, the alcohol functions react according to Tab.3 forming a TFA-ester, whose carbonyl signal is located at the high wave number side of the carbonyl region. Furthermore, due to the decomposition of the alcohol function, the hydroxyl range experiences a significant loss of absorbance. The remaining TFA acid has a clearly different absorbance spectrum

than the created ester [27] and shows a high vapor pressure of 150 hPa. Therefore it is rather unlikely that the TFA acid remains at the surface.

Heating of photo-degraded samples under vacuum condition should lead to the desorption of adsorbed water and to the decomposition of hydroperoxides. However it has to be kept in mind that any reaction product with an equal or higher vapor pressure than water will also desorb from the surface.

Tab.3 Overview about chemical derivatization agents, probed groups and the corresponding chemical reactions

Derivatization Agent	Probed groups	Reaction scheme
Water	Anhydrides	$R(CO)O(CO)R + H_2O \rightarrow RCOOH + RCOOH$
NH_3	Acids, Esters Anhydrides	$RCOOH + NH_3 \rightarrow RCOO^- + NH_4^+$ $RCOOR + NH_3 \rightarrow RCONH_2 + R-OH$ $R(CO)O(CO)R + NH_3 \rightarrow RCONH_2 + RCOOH$
TFAA	Alcohols	$CF_3(CO)O(CO)CF_3 + ROH \rightarrow CF_3COOR + CF_3COOH$

II.5 Photoelectron Spectroscopy (XPS/UPS)

The basic concept of photoelectron spectroscopy is the photo electric effect discovered by Hertz. Electrons are removed from matter by energetically shifting them above the vacuum level using an external excitation source with defined energy. These electrons have, due to their chemical and physical state in matter, a specific kinetic energy after leaving the matter. This kinetic energy is analyzed and the number of electrons is counted. The kinetic energy is converted to the binding energy E_B scale, with the origin referred to the Fermi level E_F for condensed matter. As sample and spectrometer are in electrical contact the Fermi levels E_F of both align. Therefore the surface work function of the spectrometer $\Phi_{spectrometer}$ has to be considered in the calculation of the binding energy according to:

$$E_B = E_{excitation} - E_{kin} - \Phi_{spectrometer} \qquad \textbf{Eq.18}$$

Using ultra violet for excitation radiation (typically He I radiation with 21.21 eV) valence states are probed. The sample work function is calculated using the binding energy of the secondary cutoff of the spectrum according to:

$$\phi_{Sample} = h\nu_{Exciation} - E_{B,Cutoff} \qquad \textbf{Eq.19}$$

Higher excitation energies (typically Al Kα 1486.6 eV and Mg Kα 1253.6 eV in laboratory environment) are used to gain information about core level states (e.g carbon C1s). The binding energy position of the core level signals is given by the respective element and modified by the effective charge distribution around the emitting atom (chemical shift). If electron density is removed by neighbour atoms due to higher electron negativity, the result is a shift to higher binding energies. The fine structure of the signal is given by spin-orbit interaction of electrons; therefore a signal can consist of a singlet or a doublet feature with defined intensity ratio. Furthermore a fine structure may originate from spin-spin interaction between the emitted photoelectron and unpaired electrons. This makes XPS a powerful method to quantitatively identify the sample composition in terms of element distributions, and their respective oxidation states.

In order to calculate the relative elemental ratio of the sample, the integrated intensities of the photoemission signals have to be calculated by:

$$I = I_{X-ray} \cdot A \cdot N \cdot \lambda \cdot \sigma \qquad \textbf{Eq.20}$$

with the primary photon flux I_{X-ray} , the excited sample area A, the emitter density N, the mean free path length λ and the ionization cross section σ for the respective element and orbital under consideration. Assuming a constant mean free path length λ, the elemental ratio of the two elements is then given by:

$$\frac{N(1)}{N(2)} = \frac{I(1) \cdot \sigma(2)}{I(2) \cdot \sigma(1)} \qquad \textbf{Eq.21}$$

Although the penetration depth of the incident radiation is certainly in the micron range, PES is a strongly surface sensitive method due to the fact that the emitted photoelectrons experience energy losses on their way to the surface originating from interactions with the surrounding matter. The mean free path length λ of photoelectrons in organic matter can be approximated by [29]:

$$\lambda_d = 49E^{-2} + 0.11E^{1/2}[mg/m^2] \qquad \textbf{Eq.22}$$

with E being the kinetic energy of photoelectrons depending on the primary energy. In order to estimate λ for a certain material, the corresponding density has to be considered resulting in λ = 2-3 nm in organic materials (e.g. carbon C1s and sulfur S2p signal) using typical laboratory X-ray sources like Al Kα or Mg Kα radiation and assuming a closed layer. Therefore, the information depth $D = 3 \cdot \lambda$, representing 95% of all electrons leaving the sample is limited roughly to the first 10 nm below the surface. In order to perform PES spectroscopy with varying information depth the energy of the primary excitation can be tuned, which requires access to synchrotron facilities. Another possibility to enhance the surface sensitivity in the laboratory is to vary the polar angle P between the sample surface normal and the analyzer axis as indicated in Fig.1:

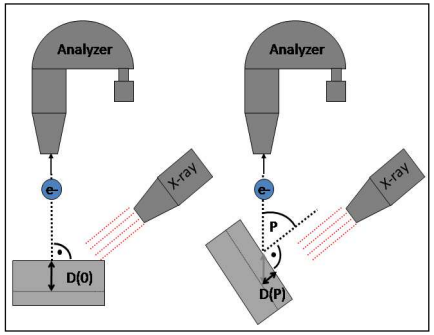

Fig.1 Left: Information depth D(0) of PES for an polar angle of 0° (normal emission); right: Reduced information depth D(P) for an polar angle P.

For larger polar angles, the effective distance which photoelectrons have to overcome to reach the sample surface increases. Therefore, the information depth D is reduced according to:

$$D(P) = D(0) \cdot \cos(P) \qquad \textbf{Eq.23}$$

Besides the primary photoelectron signals, several satellite structures may appear in the PES spectrum. Excitation with non monochromatic X-ray radiation (eg. Al Kα with Al Kβ) leads to the occurrence of satellite structures in defined energetic distance to the main PES signal, characteristic for the separation between the primary X-ray lines. Energy loss satellites located at higher binding energies originate from the possible excitation of distinct transitions (e.g. plasmons, HOMO-LUMO) by the photoelectron on its way to the surface.

II.6 Poly-3-hexylthiophene (P3HT) properties

Poly-3-hexylthiophene is a widely employed semiconducting polymeric material consisting of hexyl-substituted thiophene monomers. According to the unsymmetrical substitution of the monomers, several different possibilities for polymeric isomers arise upon coupling (2,2 head-to-head or 5,5 tail-to-tail or 2,5 head-to-tail coupling)[30]. A quantitative number for the occurrence of different coupling regimes within the polymer is the regio-regularity which can be obtained by nuclear magnetic resonance spectroscopy (NMR)[30]. Regio-regularity denotes the percentage of signal intensity of the isomer under consideration within the complete polymer signal. For example, a value of 97% regio-regularity represents a polymer with 97% of all thiophene units coupled with the same geometry (e.g. head tail). A high degree of regio-regularity is beneficial for the coplanar alignment of the polymer strand, enabling efficient overlap of the π-orbitals. The substitution with alkyl side chains strongly increases the solubility of the polymer in common solvents and influences both morphological and electronic properties of the material. The regio-regularity strongly affects the materials properties such as the spectral position of the absorption in the visible range, the conductivity, the photophysical properties and the morphology in the solid state. Fig. 2 shows the monomeric unit of the 2,5- poly3-hexyl-thiophene used in this work.

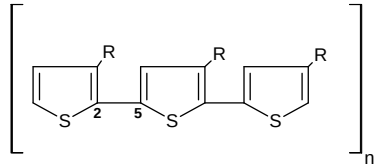

Fig. 2 Structure of the region-regular 2,5-poly-3-hexyl-thiophene. The connecting ring positions are labeled with 2 and 5.

Whereas regio-regular P3HT absorbs in the visible region of the electromagnetic spectrum with the absorption maximum located between 520 and 550 nm, the regio-random polymer absorbs at roughly 440 nm due to the fact that the effective conjugation length is smaller. Furthermore, the regio-regular isomer shows a strongly structured absorption spectrum in the solid state with the vibronic bands located at roughly 520 nm, 554 nm and 610 nm. The vibronic sub-bands at 554 nm and 610 nm are strongly affected by interchain interactions, which in turn depend on the crystallinity of the polymer film[31] .

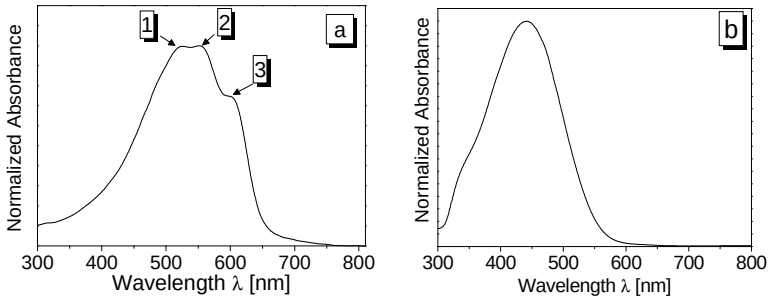

Fig. 3 Absorption spectra of P3HT thin films. Panel a: Absorption spectrum of regio-regular P3HT with transitions at 520 nm (1), 554nm (2) and 610 nm (3). Panel b: Absorption spectrum of regio-random P3HT

The film morphology and therefore the spectral shape of the regio-regular spectrum is strongly dependent on both the preparation conditions and thermal annealing steps after the thin film application. As a consequence the absolute absorption maximum is located at 520 nm in rather amorphous films whereas it is located at 554 nm in more crystalline films. It will be shown in section II.2.2.6 that the photochemical stability does not significantly depend on the degree of crystallinity and that the both the kinetic evaluation of the 520nm band and of the 554 nm show the same results.

II.7 Reaction pathways in polymer oxidation

Organic polymeric materials are prone to deterioration upon exposure to ambient conditions. Different degradation pathways have been described in literature with the dominating decomposition process depending on the type of polymer and the ambient conditions, such as the oxygen partial pressure, the light level, ambient temperature and humidity. In the following, the limiting cases of oxidative degradation pathways discussed in literature will be shortly reviewed.

Radical induced photo oxidation

The photo-induced oxidation of polymeric materials such as PE, PET, PP and PMMA, which are highly transparent in the visible range and only absorb in the near UV range below 320 nm, has been widely investigated over the last decades. This interest was mainly motivated by the tremendous commercial relevance of these materials. The dominating photo-degradation pathway of these materials has been shown to be a radical chain mechanism **(**Scheme 1**),** initiated by a polymer radical with subsequent formation of hydroperoxides and the formation of carbonyl products via oxygen uptake [33]. Both of these species are known to be photo-chemically active upon UV irradiation, leading to chain scission of the polymer backbone. Besides photo-induced reactions also thermally induced reactions can occur, however they seem to play a minor role at ambient temperatures. The nature of the initiating radical is commonly discussed in terms of intrinsic defects or impurities due to the synthesis and application procedure [32]. Neverthless, the primary photochemical step leading to the very first reactive centers remains unclear in many cases.

Scheme 1: Kinetic scheme of polymer degradation by a radical chain mechanism (adopted from Audouin et al.[33]). (1) Initiation process via radical generation, (2) and (3) chain propagation via peroxides/hydroperoxides, (4) and (5) termination steps via radical recombination.

(1) $P \xrightarrow{G} P\bullet$

(2) $P\bullet + {}^3O_2 \xrightarrow{k_2} PO_2\bullet$

(3) $PO_2\bullet + PH \xrightarrow{k_3} PO_2H + P\bullet$

(4) $P\bullet + P\bullet \xrightarrow{k_4} inactive\ species$

(5) $PO_2\bullet + PO_2\bullet \xrightarrow{k_6} inactive\ species$

In the steady state the polymer is consumed at the rate [33]

$$-\frac{d[P]}{dt}=\frac{k_2\cdot(G/k_4)^{0.5}\cdot[^3O_2]}{(k_2/k_3\cdot P)\cdot(k_6/k_4)^{0.5}\cdot[^3O_2]+1} \qquad \textbf{Eq.24}$$

Singlet oxygen induced photo oxidation

Differently from classical polymers like PE or PMMA, organic semiconducting materials strongly absorb in the visible range according to their application e.g. in OLEDs and OPV. Over roughly the last two decades their stability has been mainly investigated in solution, revealing that the dominating degradation mechanism is given by the presence of highly reactive singlet oxygen sensitized by the excited triplet state of the polymer [23] according to Scheme 2:

Scheme 2: Kinetic scheme of polymer degradation by singlet oxygen. Groundstate of the polymer P, excited singlet polymer state $^1P^*$, excited triplet polymer state $^3P^*$, groundstate oxygen $^3O_2$, singlet oxygen $^1O_2$, generation constant G, fluoresence constant k_F, deactivation constant k_d, quenching constant k_q, reaction constant k_r, deactivation constant k_5

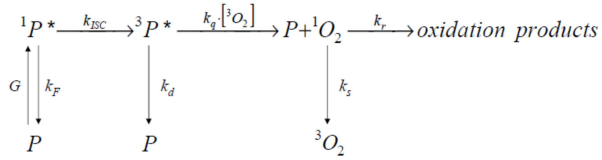

The rate of polymer degradation by singlet oxygen (Scheme 2) is determined by the production of singlet oxygen in the collisional quenching of triplet states of the polymer by ground state oxygen

$$\frac{d[^1O_2]}{dt}=k_q[^3O_2]\cdot[^3P^*]-(k_r\cdot[P]+k_s)[^1O_2]\cdot \qquad \textbf{Eq.25}$$

The triplet state is formed from the singlet excited state by ISC and decays both spontaneously and due to the quenching by ground state oxygen

$$\frac{d[^3P^*]}{dt}=k_{ISC}[^1P^*]-(k_q\cdot[^3O_2]+k_d)\cdot[^3P^*] \qquad \textbf{Eq.26}$$

In the steady state, the concentrations of the transient species are constant, so that the overall degradation rate is obtained as

$$-\frac{dP}{dt}=k_r\cdot P\cdot{}^1O_2=\frac{G\cdot\phi_{ISC}\cdot\phi_r}{\left(1+\frac{k_d}{k_q\cdot{}^3O_2}\right)}=\frac{G\cdot\phi_{ISC}\cdot\phi_r}{\left(1+\frac{k_d}{k_q\cdot S\cdot p_{O_2}}\right)} \qquad \textbf{Eq.27}$$

Considering that the oxygen concentration in the film is given by the atmospheric pressure p_{O_2} and the solubility S. G is the generation rate of singlet excitons, ϕ_{ISC} is the quantum yield of triplet population from the excited singlet state of the polymer, and ϕ_r is the quantum efficiency of singlet oxygen deactivation by chemical reaction (as opposed to deactivation by physical deactivation). The role of singlet oxygen in the degradation of π-conjugated polymers in the solid state is still under debate[22].

II.8 Determination of reaction rates and effectiveness of photo degradation

The reaction rate of P3HT decomposition is represented by the destruction of single thiophene rings which can be obtained from the loss of UV/Vis absorbance, ΔE_{max}, of a P3HT film of thickness d according to:

$$\frac{d[P]}{dt} = \frac{\Delta E_{max}}{d \cdot \varepsilon_{max}(T)} \qquad \textbf{Eq.28}$$

Inserting a molar extinction coefficient per thiophene ring [34] of $\varepsilon_{max}(T) \approx 10^4\ M^{-1}cm^{-1}$. This proportionality of absorbance loss and the concentration of destroyed thiophene rings is valid irrespective of the degradation mechanism as long as both spectral shape and position of the absorbance do not change significantly during the reaction. This is at least the case in the early stages of degradation, as for chains of more than ten thiophene units (n > 10) the spectral position of the absorption maximum depends only weakly on the conjugation length [35]. A true differential quantum efficiency of the degradation process cannot be given, as the nature of the absorbing species during photo oxidation is not clear and several other factors besides light enter the reaction. However a quantitative value for the reaction is the wavelength dependent effectiveness $\Im(\lambda)$ [36], yielding the activation spectrum:

$$\Im_\lambda = \frac{dN_{tr}/dt}{I_{incident}(\lambda)} \qquad \textbf{Eq.29}$$

with dN_{tr}/dt being the number of destroyed thiophene rings per unit area and time. dN_{tr}/dt is calculated from the decay of the absorbance dE/dt at 554 nm and the molar absorption coefficient per thiophene ring $\varepsilon_{tr} = 10^4\ M^{-1}cm^{-1}$ according to:

$$\frac{dN_{tr}}{dt} = \frac{dE}{dt} \cdot \frac{N_A}{\varepsilon_{tr}} \qquad \textbf{Eq.30}$$

II.9 Oxygen diffusion coefficients determined from fluorescence quenching of P3HT

The sorption of oxygen into a P3HT thin film can be monitored using the decay trace of the polymer fluorescence F(t) upon contact to oxygen leading to the partial quenching of emissive states according to the Stern Volmer equation[55]:

$$FQ = \frac{F(t=0)}{F(t)} = K_{SV} \cdot [O_2](t) + 1 \qquad \textbf{Eq.31}$$

The time dependent oxygen concentration $[O_2](t)$ here contains the desired diffusion coefficient D according to Fick´s second law:

$$\frac{\partial [O_2]}{\partial t} = D \frac{\partial^2 [O_2]}{\partial x^2} \qquad \textbf{Eq.32}$$

This equation is solved under the following boundary conditions: oxygen access is possible only from the surface, whereas both side walls and the substrate reflect oxygen. Furthermore it is assumed that the surface concentration of oxygen, C_0, may react delayed upon changing the partial pressure of oxygen to the new value C_0 according to:

$$\frac{C}{C_0} = 1 - e^{-\beta t} \qquad \textbf{Eq.33}$$

with β being the time constant for reaching the equilibrium of oxygen concentration between C and C_0 at the surface of the sample polymer. The amount of sorbed oxygen in a polymer film with thickness l is then given by:

$$M = 2lC_0 \left[1 - \left(\frac{D}{\beta l^2} \right)^{\frac{1}{2}} e^{-\beta t} \tan\left(\frac{\beta l^2}{D} \right)^{\frac{1}{2}} - \frac{8}{\pi^2} \sum_{n=0}^{\infty} \frac{e^{\frac{-(2n+1)^2 \pi^2 D t}{4l^2}}}{(2n+1)^2 \left[1 - (2n+1)^2 \frac{D\pi^2}{4\beta l^2} \right]} \right] \qquad \textbf{Eq.34}$$

Fitting this function[37] to the experimental decay trace of a polymer with known thickness l yields the diffusion coefficient D, which is the only free parameter. The influence of β is negligible as the

experimental switching time between vacuum and several bars of oxygen leads to rapid equilibration at the surface much faster than the complete diffusion process into the polymer film. Fig. 4 shows how the fluorescence signal is connected to the oxygen sorption into the film.

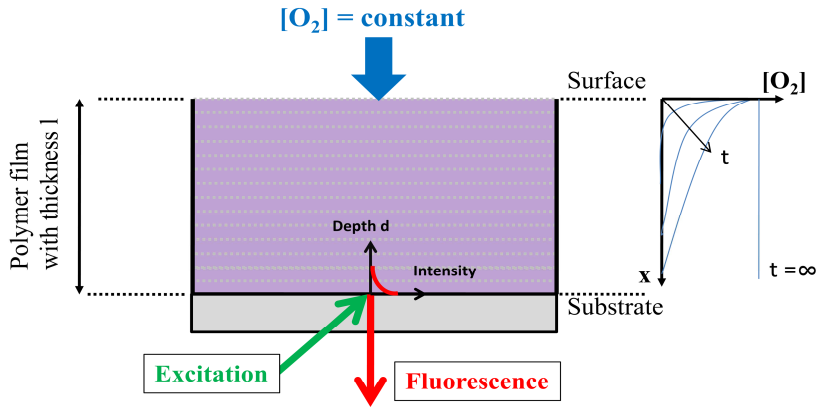

Fig. 4 Oxygen sorption experiment for a polymer film with thickness l. The fluorescence probe is limited by the penetration depth d. Oxygen access is only possible from the surface. The temporally and spatially resolved oxygen profile is given at the right hand side.

The information depth d of the fluorescence signal is limited by the penetration depth d of the excitation beam I_0 (520nm) to roughly 100 nm in the case of P3HT due to absorption according to Lambert Beer`s law. In order to avoid artifacts by the illumination geometry the film thickness must be l>>d. At time t = 0 the oxygen partial pressure is applied with the full fluorescence intensity obtained. Since l >>d, the emission remains constant until the diffusion front reaches the probing area, causing the fluorescence quenching FQ.

II. Experimental section

II.1 Sample preparation

P3HT thin films (~100 nm in thickness as determined by atomic force microscopy and optical absorption measurements) were prepared under ambient conditions by doctor blading (Erichsen Coatmaster 509) or spin coating on microscope slides using a 1% (w/w) solution of regio-regular (Merck, number-average molecular weight 83 000 g mol^{-1}, weight-average molecular weight 113 000 g mol^{-1}; RR = 95 %, 2,5 connected) and regio-random P3HT (Merck), in chloroform (Uvasol, Merck). Thicker films of several microns were prepared via drop coating from a 1% solution (o-Xylene, Merck) on microscope slides respectively Indium-Tin-Oxid (ITO) covered glass substrates. Regio regular P3HT with deuterated alpha methylene unit was purchased from the group of Prof. Dr. Ulrich Scherf, Bergische Unversität Wuppertal. Solvents were bubbled with nitrogen in order to get rid of dissolved oxygen and water. Prior to polymer deposition the substrates were cleaned in chloroform using an ultrasonic bath for 5 min. Thermal annealing of the samples was performed under nitrogen (170 °C, 30 min, N_2 purity 5.0) in the dark. Afterwards the samples were transferred to the reaction chamber in the absence of light. For combined UV/VIS and FTIR investigations CaF_2 windows with a thickness of 5mm (Korth GmbH) were used. These windows were cleaned in chloroform with subsequent annealing at 600°C for 15 min under ambient air.

II.2 Spectroscopic equipment

II.2.1 UV/VIS spectroscopy and absolute Photon flux measurements

UV/VIS spectra were recorded in transmission mode using a homemade set up containing fibre optic spectrometers from ocean optics (Maya2000 pro and PC2000) both with a spectral resolution of approximately 3 nm. The time resolution was set between milliseconds (Maya2000pro, minimum 13 ms, PC2000, minimum 3 ms) and days, depending on the reaction rate.

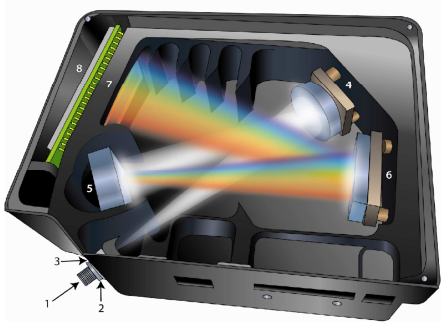

Fig 5: Optical path of the Maya 2000 pro fibre optic UV/VIS spectrometer. Fibre connector (1), entrance slit (2), filter (3), collimating mirror (4), grating (5), focusing mirror (6), second order filter (7), CCD array (8) [38]

Calibration for wavelength resolved recording of the absolute light intensity was performed using a calibrated (National Institute of Technology, NIST) white light source (Ocean Optics DH Cal2000) in the range from 200 nm to 1050 nm. Therefore an optical fibre equipped with a cosine corrector (both Ocean Optics) was positioned directly at the sample position in the reaction chamber. The optical fibre was connected to the calibrated Maya 2000 pro spectrometer. In this manner it is possible to measure absolute, wavelength resolved photon fluxes directly on the sample surface which are not depending on the spectral sensitivity of the detector. Several white light sources were used for recording UV/VIS spectra during this work (Mueller, 450W Xenonarc, Ocean optics DH BAL 2000). The influence of the spectrometer light beam on the stability of the corresponding sample was checked for each light source.

II.2.2 Fourier transformation Infrared (FTIR) spectroscopy

FT-IR spectra were recorded using a standard Bruker Vertex 70v spectrometer in transmission mode with a resolution of better than 1 cm^{-1}. The base pressure of this vacuum spectrometer was better than 1 mbar. Furthermore a Bruker Vertex 70 flooded with dry nitrogen (rel.hum.< 2% at 25°C) was used. Samples were prepared on CaF_2 substrates in order to allow simultaneous investigation of FTIR UV/VIS transmission spectroscopy. Samples were transferred from the reaction chamber to the FTIR spectrometer with only short exposure time to ambient air in darkness (roughly 5 min) which is negligible compared to the observed reaction rates under photo oxidative conditions.

II.2.3 Photoelectron spectroscopy (XPS/UPS)

Photoemission measurements (X-ray photoemission spectroscopy (XPS) as well as valence band ultraviolet photoemission spectroscopy (UPS)) were performed using a multi-chamber UHV-system (base pressure $2 \cdot 10^{-10}$ mbar), equipped with a Phoibos 150 cylindrical hemispherical analyzer (SPECS), a monochromatic Al Kα source and a high flux He discharge lamp (UVS 300, SPECS). The energetic resolution determined from the width of the Fermi edge for XPS and UPS was about 400 meV and 100 meV, respectively. The spectra were energetically calibrated to reproduce the binding energy (BE) of Au $4f_{7/2}$ (84.0 eV) eV $Ag3d_{5/2}$ (368.3 eV) and $Cu2p_{3/2}$ (923.7 eV). A gold sample was mounted next to the investigated polymer film to further confirm the energy reproducibility by recording the Au $4f_{7/2}$ energy before every measurement. The reproducibility of the energy measurement determined from the recorded Au4f spectra is about 0.05eV. The raw data were fitted using a numerical routine[39]. UPS measurements were performed using a He discharge lamp, He I β and He I γ satellites were subtracted from the data. The high binding energy cutoff of the UPS spectrum (which reflects the work function of a sample) was determined applying a bias voltage in the range from -5 V and -10V to the sample. Then the onset of the cutoff was determined graphically placing two tangents. The intercept point of these tangents is used as onset value (Fig.6). The same procedure was used for estimating the HOMO onset.

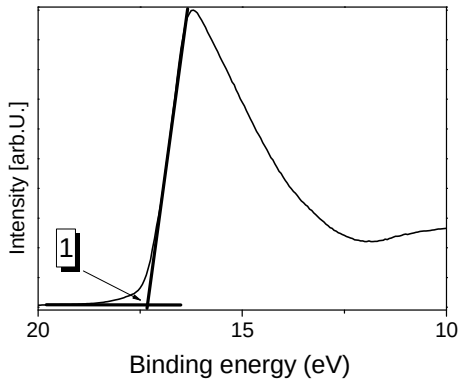

Fig.6 Typical high binding energy cutoff with applied 7V Bias voltage. The intercept point of the applied tangents yields the cutoff position 1.

II.2.4 Photoluminescence spectroscopy and quenching experiments

The diffusion coefficients of oxygen in thick films of P3HT (7 µm) were determined by monitoring the time trace of the oxygen induced fluorescence quenching with a Spex Fluorolog 222. For this aim, the sample was placed in the reaction chamber with shortest time to ambient air in darkness. Subsequently, the chamber was evacuated (total pressure <1 mbar) and finally flooded with oxygen (in less than 0.3 seconds, final pressure $p_{O_2} = 8\ bar$). During the measurement, the sample was continuously excited with monochromatic light at 550 nm and the fluorescence intensity was monitored at the maximum of the emission spectrum at 700 nm. Fluctuations of the light source (< 2% of the total intensity) were corrected by using the signal of the reference photomultiplier of the Fluorolog 222. The temperature of the sample was adjusted using cartridge heaters attached to the sample cell and controlled by a Ni-NiCr thermocouple directly attached to the sample surface. Later experiments were performed with the home made spectrometer which will be described in section II.3.5.

II.3 Construction of equipment for polymer aging:

The mechanistic investigation of chemical reactions requires the detailed control of environmental conditions during the chemical reaction. In the case of solid state polymer aging these are mainly temperature, light intensity, spectral light distribution and atmospheric conditions. In order to disentangle their effects on the reaction rate, all relevant parameters have to be monitored and kept constant during the complete timescale of the reaction. Since it is not clear how the single environmental factors affect the chemical pathway of polymer aging it is a useful approach to investigate their influence step by step. Therefore several specialized setups were designed during this work serving both, the simultaneous degradation of polymer samples and the spectroscopic tracing via optical methods (UV/VIS absorption and fluorescence). In order to easily access a broad range of optical experiments, a CCD-based UV/VIS fibre optic spectrometer (Ocean Optics Maya 2000 pro) was chosen as described in section II.2.1.

II.3.1 Reaction chamber and environmental control

In order to control the atmospheric conditions during the degradation experiments a closed reaction chamber (Fig. 7) with the polymer sample situated between two quartz windows embedded in an aluminum body was designed. The usage of quartz windows enables illumination experiments in the wavelength range down to 200 nm without significant losses of the primary irradiation intensity. The free volume of the chamber is roughly 1 ml which provides fast exchange of the atmosphere through the attached gas supply connectors on the side. Constant gas flow using a gas mixing facility and constant pressure in the range from 10^{-1} mbar to 8 bar can be both realized. The oxygen partial pressure was monitored by a pressure sensor (Newport Omega PAA21R-V-10, error 1%), directly attached to the reaction chamber. The temperature was recorded with a home-made Ni/NiCr thermo pair (DIN 43710, error 1 K) which was directly at the sample surface using silver glue. Different humidity levels were realised mixing dry (directly from the oxygen bottle) and wet (100% rel.hum. at 295 K) oxygen with different flow rates via a gas mixing facility (Westphal WMR4000 Controller electronic, Brooks mass flow controller). The humidity was monitored by positioning a calibrated sensor (Driesen & Kern company, DKRF400, 2% error) in the chamber and applying a constant flow of humidified oxygen and/or synthetic air.

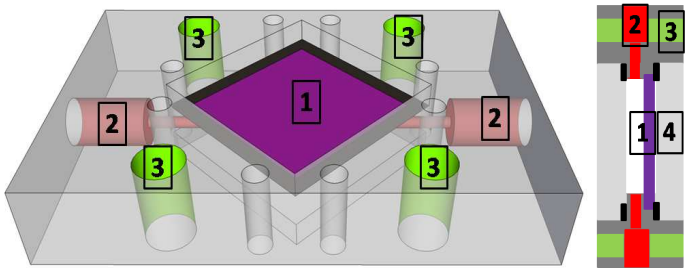

Fig. 7 Left: 3D sketch of the reaction chamber with sample (1), gas supply connectors (2) and connectors for the optical bench (3), windows are not shown. Right: 2D sketch of sample cell including quartz windows (4) top covers for the windows are not shown.

The sensor data about humidity, temperature and atmosphere in the reaction chamber were monitored online during the reaction using automated (National instruments, LabView) read out electronics specially designed for this purpose (Institute for explorative data analysis Hamburg,SAB-S16-N12-P)

II.3.2 Setup for white light experiments

The reaction chamber and the optical path of the light used for degradation experiments under white light conditions are described in Fig.8. The white light of a 450W Xenon high pressure lamp (Müller lamps/electronics) is focussed on the entrance port of an integrating sphere (Ulbricht sphere). Prior to the integrating sphere the light passes a homebuilt infrared filter consisting of a quartz pipe filled with water (10 cm optical path) in order to reduce thermal stress on the following optical parts and the sample. Due to the multiple diffuse reflectance of the beam inside the sphere, the intensity profile of the xenon arc vanishes. This produces a highly homogeneous intensity profile, which is the prerequisite for obtaining accurate degradation kinetics. The light which leaves the integrating sphere is collimated using several quartz lenses before being focussed on the sample with a focus diameter of 10 mm. After passing the sample, the transmitted light is then collected by an optical fibre connected to the UV/VIS spectrometer which enables continuous monitoring of the degradation process. The complete optics is based on a commercially available microbench system (QIOPTIQ company). The temperature recorded on the sample surface using a Ni/NiCr thermo pair revealed that the samples are not significantly heated due to illumination (<1K).

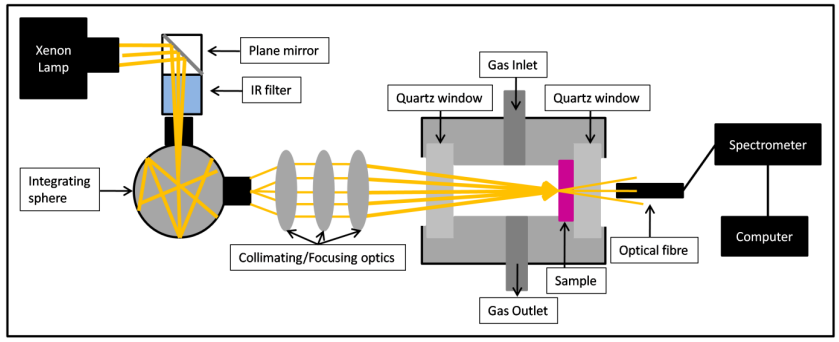

Fig.8 Reaction chamber, optical pathway of degradation and probe beam used during white light degradation experiments.

The spectral power distribution of the used Xenon lamp on the sample surface is presented in Fig. 9.

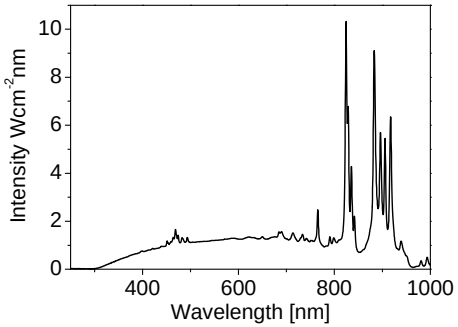

Fig. 9 Spectral power distribution of the incoming Xenon white light. The spectrum was recorded on the sample surface position depicted in Fig.8.

II.3.3 Setup for single wavelength experiments: Mercury arc lamp based

Degradation experiments carried out under monochromatic illumination conditions were realized using a 350 W mercury lamp (Müller lamps/electronics, with OSRAM HBO bulb) with attached infrared filter (water), monochromator (Horiba Jobin Yvon H10UV) and collimating optics consisting of several quartz lenses. Single wavelengths were chosen according to the emission lines of the mercury arc source (313 nm, 333 nm, 369 nm, 405 nm, 436 nm, 547 nm). The sample was kept under controlled atmospheric conditions using the sample cell described in section II.3.1. UV/VIS spectra were recorded by removing the sample cell and placing it into an UV/VIS setup containing the Maya2000 pro directly besides the irradiation setup. High accuracy in the sample positioning was achieved by fixing the sample cell with several metal tracks.

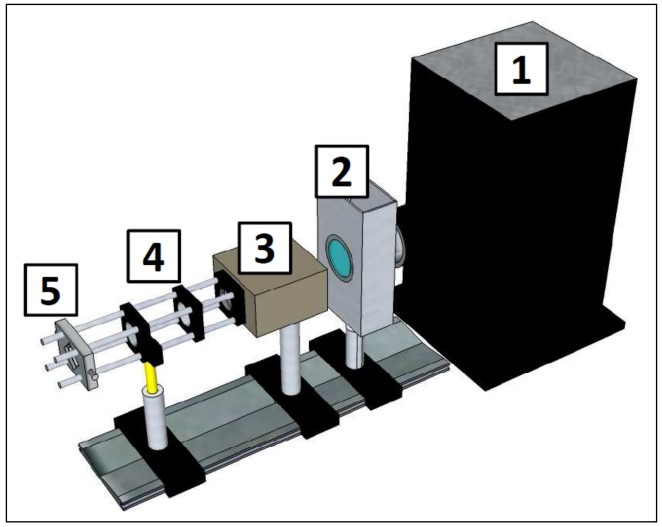

Fig. 10 Setup for single degradation experiments with monochromatic illumination: Mercury 150W lamp (1), infrared filter (2), monochromator (3), collimating optics (4), reaction chamber with sample (5) mounted on the micro bench system

II.3.4 Setup for single wavelength experiments: Light emitting diode based

Over the last decades monochromatic illumination sources in photochemistry were based on high power Xenon or mercury lamps with attached monochromator or interference filter. Several optics elements are needed to achieve highly homogeneous power distribution over the light spot. Very often high lateral homogeneity, high power and large illumination area are not accessible at the same time. In order to overcome these limitations, a light emitting diode (LED) based light source for monochromatic, high power, large area and low cost illumination was created, which can be easily parallelized. Inorganic LEDs have experienced a strong enhancement over the last years which led to the development of the so called high power LEDs with emission out puts of more than 0.3 W on an area of 2x2 mm [40] in a narrow emission band of 20-40 nm half width and lifetimes (80% remaining emission after more than 10000 hours). The light source consists of an array of single high power LEDs (Phillips, Luxeon Rebel, emitter size ~1.5x1.5mm[40]) distributed on a commercially available SMD chip (20x30 mm)

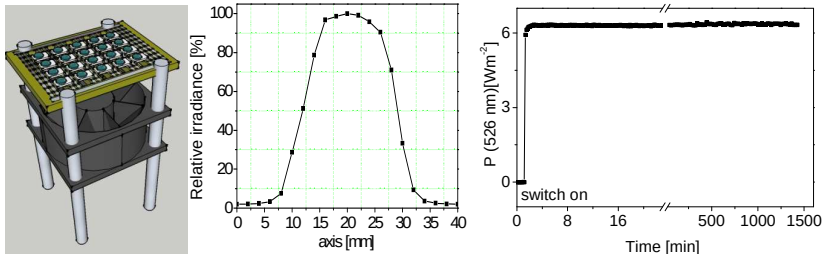

Fig. 11 Left: LED base light source for monochromatic illumination. LEDs are attached on an SMD chip. The chip material placed below the emitter of each single LED spot was removed to allow easy cooling from the backside using a cooling fan. Middle: Line scan of a LED array operating at 10 V, 0.5 A in a distance of 4.5cm from the LED surface using the Maya 2000 pro spectrometer. Right: Time scan of the emission at 526 nm of a green LED array, with a mean power output of 6.31 Wm^{-2} and a noise of 0.2%.

Cooling of the LED array is typically done using a passive cooling element for each LED. However in the present case cooling is realized using a 12 V fan in order to avoid temperatures above 50 °C. Increased temperature would result in weaker emission, accelerated LED aging or in the worst case immediate destruction of the array. The geometric power distribution of the emitted light spot in a distance of 4.5 cm from the LED array covers an area of roughly 20 mm diameter where the intensity variation is below 3%. The size of this area can be simply enlarged by increasing the array size or the distance to the emitting surface. In order to ensure a stable power output, the light source is operated under both constant voltage and constant current conditions resulting in a stable output rapidly reached

within the first two minutes, with no detectable intensity loss within 24 hours, and with an intensity fluctuation below 1%. In order to parallelize monochromatic illumination experiments several LED light sources were attached on a bread board directly in front of the sample cells. Above these sample cells, a fiber optic UV/VIS transmission spectrometer (containing a spectrometer and a light source) is attached on a carriage which can be moved side wards and both up and downwards. This allows the parallel UV/VIS spectroscopic investigation of up to 6 polymeric samples, irradiated with different wavelengths (365 nm, 400 nm, 460 nm, 526 nm, 610 nm, 630 nm, 695 nm) under controlled atmospheric conditions.

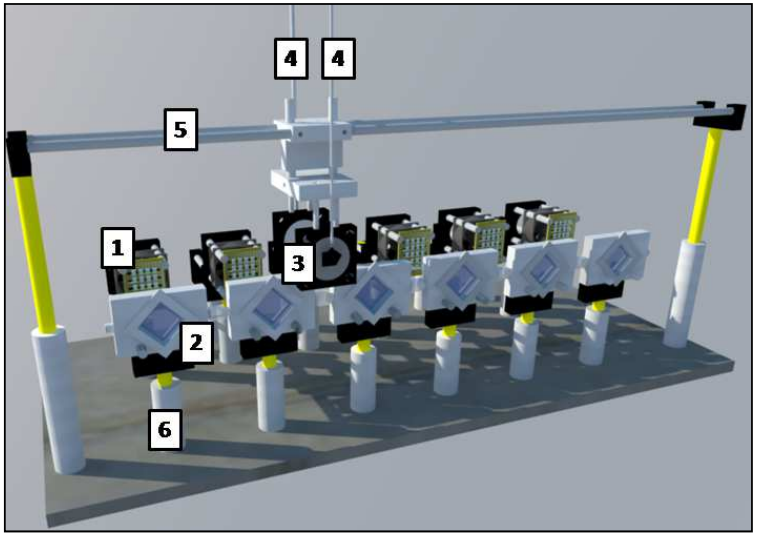

Fig.12 Parallelized setup for monochromatic photo degradation experiments with LED based light sources (1), sample cells (2), transmission UV/VIS optics on a moving carriage (3), fibre optic connector to both spectrometer and light source (4), guide way for the optics (5)

II.3.4 Setup for oxygen doping experiments using PES

Ambient atmosphere may induce electronic changes in organic semiconductors which can be probed using XPS and UPS spectroscopy in the ultra high vacuum. However ambient pressure during a XPS measurement cannot be realized due to fact that ultra high vacuum is needed. Therefore the sample has to be treated in an external chamber which can be switched between ambient pressure with controlled atmosphere and vacuum conditions, in order to allow transfer to the ultra high vacuum. These requirements are realized in a vacuum chamber (base pressure $1 \cdot 10^{-4}$mbar to 1000 mbar) equipped with a gas supply (e.g. for oxygen or nitrogen), a quartz window on top for illumination experiments and a homemade heating system (Fig. 13). The chamber is directly connected to the UHV system, therefore samples can be treated in different ways with subsequent transfer to the ultra high vacuum avoiding contact to ambient air which may influence the polymer film.

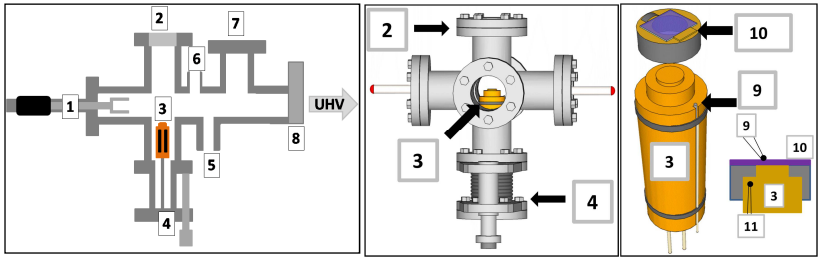

Fig. 13 Left: Vacuum chamber for oxygen doping experiments, transfer arm (1), quartz window for illumination experiments (2), sample heater (3) mounted on an lift (4), vacuum pump connector (5), gas supply (6), load lock (7), valve against UHV (8) Middle: Front view of the constructed chamber. Right: Detail drawing of the heating unit with sample thermo couple (9), sample on holder (10) and heater thermo couple (11).

The heating system consists of two cartridge heaters in a copper block with attached Ni/NiCr thermopair all together mounted on a lift. The copper block directly contacts both the sample holder and the sample backside in order to ensure good mechanical contact crucial for heat transfer under vacuum conditions. A second Ni/NiCr thermopair can be placed on the sample surface which enables calibration of the heating system (temperature on sample surface as function of copper block surface). In later experiments the sample surface cannot be equipped with a thermopair due to the necessity of several transfers in the UHV system. Prior heating of the copper block with subsequent contact to the sample enables heating of the sample to 150 °C within 2-3 minutes.

II.3.5 Setup for correlated UV/VIS / Fluorescence experiments

In order to probe the effect of polymer aging on both ground and excited state properties a setup for the simultaneous recording of UV/VIS transmission and fluorescence spectra under controlled atmospheric conditions was constructed. The UV/VIS transmission path consists of a commercially available white light source (DH Bal 2000, Ocean optics with manual shutter) and the Maya 2000 Pro spectrometer both with attached optical fibre and collimator (Ocean Optics 74UV Collimating lens). The polymer thin film is placed in a closed sample cell which can be operated in discharge of gases or high pressure as mentioned in section II.3.1.

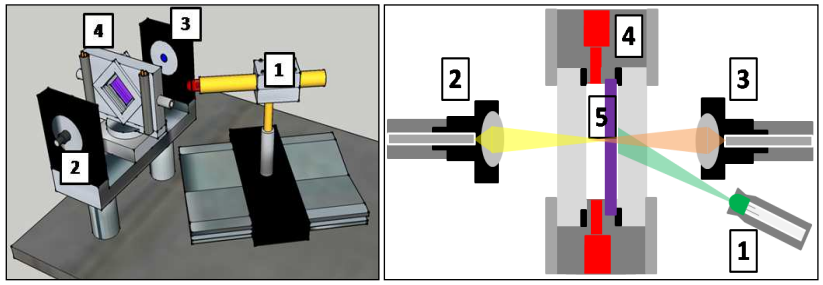

Fig. 14 Setup for simultaneous UV/VIS transmission and steady state fluorescence spectroscopy; LED excitation light source (1), optical fiber connector for UV/VIS light source (2), optical fibre connector for spectrometer (3), sample cell with attached heating cartridge and gas connectors (4), polymer sample (5)

The excitation source for fluorescence spectroscopy consists of a single LED mounted in an angle of 45° compared to the surface plane. The emitted photons are recorded via the same optical path used for UV/VIS transmission Fig. 14. Since the emission intensity depends on the primary intensity I_0 this value needs to be monitored for later reference at least in a relative way. Therefore the realized geometry allows a small fraction of I_0 to become reflected at the sample cell. The reflected light is monitored so that possible fluctuations in I_0 can be referenced although this is not an absolute reference. Due to the usage of LEDs the wavelength of the excitation source can be changed easily representing an extremely cost and time effective method. The typical correlated experiment between UV/VIS transmission and emission spectroscopy simply requires switching between the two light sources 2 and 1 in Fig. 14.

II.3.7 Setup for degradation under constant ozone concentrations

Ozone degradation experiments were performed using a self made ozone generator directly attached to a reaction chamber (Volume ~ 500 ml) containing the corresponding sample. The ozone generator consisted of a Hg arc lamp (UV Consulting Peschl, GPH287T5VH/4 , 14W) with main emission lines 187 nm and 254 nm) irradiating a quartz pipe with a constant oxygen flow (purity 99.998%) of 100 ml/min at ambient pressure (Fig.15). Special care was taken to avoid irradiation of the sample by the light produced by the ozone generator.

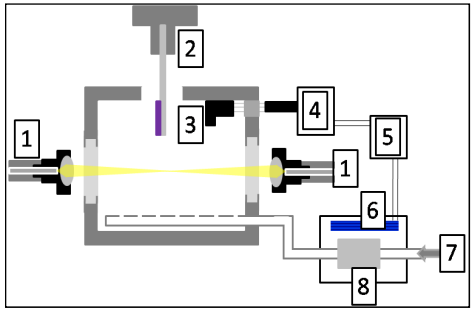

Fig.15 Setup for ozone degradation experiments, UV/VIS transmission spectroscopy (1), holder with sample (2), ozone sensor (3), sensor electronics (4), power supply UV lamp (5), ozone generator with UV lamp (6) and oxygen flow (7) through a quartz pipe (8)

The ozone produced in this way was then pumped through the sample chamber at a flow rate of 100 ml/min. The ozone concentration is continuously monitored using a sensor (Ecosensor Os-4 range from 0.05 ppm to 20 ppm) placed directly in sample chamber. Different ozone concentrations were simply realized by varying the length of the illuminated part of the quartz pipe. Upon reaching a stable concentration of ozone the sample was placed in the chamber and immediate (Δt <5 sec.) start of the spectroscopic tracing. Degradation of P3HT was monitored by recording the UV/Vis transmission spectra of the film using an Ocean Optics fibre optic spectrometer (Maya2000 pro). Photo-oxidation by the spectrometer beam was ruled out by control experiments in ozone free oxygen atmosphere. In later experiments the ozone generator was further improved by establishing a control loop between the ozone sensor (with set upper and lower limit values) and the power supply of the Hg arc lamp. Upon reaching the set ozone limits the light source was switched on and off. Both methods were capable of producing constant ozone concentration within the error bars. However with the control loop method, the life time of the Hg arc lamp was dramatically decreased.

II.3.8 Validation of equipment

The fiber optic spectrometer Maya 2000 Pro was calibrated in order to perform absolute irradiance measurements using an NIST calibrated light source. Further validation was neverthless performed in order to ensure the elimination of systematic errors in the estimation of absolute photon flux.

As a first step the spectrometer was calibrated and the spectrum of a Steuernagel Solar simulator with defined Air Mass 1.5 (AM1.5) spectrum was recorded (Fig. 16 panel a). The relative deviation RD (Fig. 16 panel b) was calculated according to:

$$RD[\%] = \frac{P(\lambda)_{May\,2000\,pro} - P(\lambda)_{Steuernagel}}{P(\lambda)_{May\,2000\,pro}} \cdot 100 \qquad \textbf{Eq.35}$$

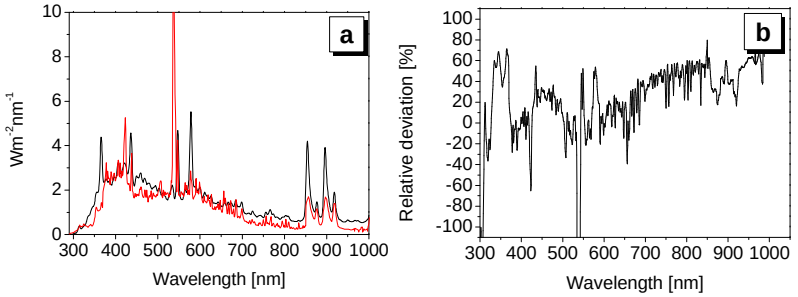

Fig. 16 Panel a: Absolute irradiance spectrum of a Steuernagel AM1.5 Simulator recorded with the Maya 2000 pro spectrometer (black) and data obtained from Steuernagel (red). Panel b: Relative deviation of the spectra according to equation 35

It is obvious that the order of magnitude of the spectral power distribution is certainly correct, however there are differences of roughly 50% in average. The occurrence of this difference however cannot be explained in detail since no reference was found, how the literature values were recorded. Anyhow these findings proof that the calibration with the NIST light source is certainly trustworthy with only minor error bars.

Besides the calibration of the spectrometer itself, the optical pathway might be the origin of systematic errors due illumination geometry (e.g. focusing of the irradiation beam, substrate etc.). In order to further proof the setup of the optics, the fluorescence excitation spectrum of P3HT was recorded Fig. 17 using the Hg arc lamp based optics already shown in section II.3.3. From literature it is known that

the excitation spectrum directly follows the absorption spectrum of P3HT [41]. This enables another crosscheck whether the relative intensity distribution is correctly recorded.

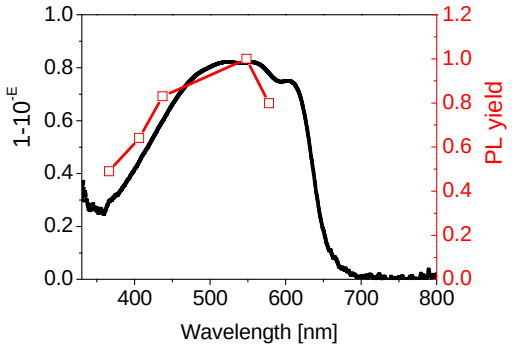

Fig. 17 Photoluminescence excitation spectrum (red connected dots) and absorption of a P3HT thin film (black solid line). The photoluminescence yield was calculated according to equation 36.

The incoming photon flux of the light source was directly recorded at the sample position for each of the wavelengths. Subsequently, the sample, which was kept under nitrogen flux in order to reduce photo oxidation, was introduced and the emission spectrum of it was recorded. The photoluminescence yield was then calculated according to:

$$\Phi PL = \frac{\int_{\frac{600nm}{\lambda 2}}^{850nm} N_{Emission}(\lambda)d\lambda}{\int_{\lambda 1} N_{Incoming}(\lambda)d\lambda} \qquad \textbf{Eq.36}$$

with λ1 and λ2 being the onset respectively offset of the narrow excitation band. As can be seen from figure Fig. 17, the fluorescence yield and the absorption spectrum of P3HT are in good accordance as reported in literature[41]. In summary the spectrometer was calibrated with an NIST calibrated white light source. The absolute irradiance mode was confirmed recording the spectrum of a defined light source (Steuernagel AM1.5 solar simulator). Possible errors originating from the optics which were used for wavelength resolved degradation experiments were checked recording the fluorescence excitation spectrum of P3HT within the same illumination geometry. Therefore the validation of the optical system was performed using three independent methods assuring that absolute photon flux can be estimated using the optics developed for this work.

III. Results:

III.1 Reversible oxygen effects on P3HT

III.1.1 Oxygen induced fluorescence quenching of P3HT

Upon admission of oxygen to a P3HT film, the fluorescence of P3HT is reduced by three different mechanisms, which take place on significantly different time scales: collisional quenching (in milliseconds to seconds, due to the encounter of polymer excited states with ground state oxygen), the formation of a charge transfer (CT) complex between the polymer and oxygen (in minutes), as well as by photo-oxidation of the polymer (in hours)[55].

The fastest component of fluorescence quenching, which is due to collisional quenching, follows a Stern-Volmer behavior[42]:

$$FQ = \frac{F_0}{F} - 1 = K_{SV} \cdot [O_2](t) \qquad \textbf{Eq.37}$$

where F and F_0 are the fluorescence intensities with and without oxygen, respectively, $[O_2](t)$ is the time-dependent oxygen concentration and K_{SV} is the Stern-Volmer constant

$$K_{SV} = k_q \cdot \tau_0(S_1) \qquad \textbf{Eq.38}$$

where $\tau(S_1)$ is the unquenched singlet exciton life-time and

$$k_q = 4\pi N_A R_{eff}^{O_2} [D(S_1) + D(O_2)] \qquad \textbf{Eq.39}$$

is the quenching rate constant, containing Avogadro's number (N_A), the effective collision radius ($R_{eff}^{O_2}$, considering the possibility of finite quenching probability on the encounter of exciton and oxygen) and the sum of the diffusion coefficients of oxygen and the singlet exciton ($D(O_2)$ and $D(S_1)$, respectively). The facts that $FQ \propto [O_2]$ (from Eq. 37) and $D(S_1) >> D(O_2)$ [43, 44], allows the diffusion coefficient of oxygen in the P3HT film to be obtained by monitoring the temporal development of fluorescence quenching upon admission of oxygen into the evacuated sample chamber. At an oxygen pressure of 8 bar, the fluorescence of annealed P3HT films of several micrometers in thickness is quenched by a factor of about two within a few seconds. Fitting the

fluorescence quenching curves according to the diffusion model detailed in reference an oxygen diffusion coefficient of $D(O_2) = 3 \cdot 10^{-8}\, cm^2 \cdot s^{-1}$ is gained at 295 K, which is close to the value reported by others[20]. The diffusion coefficient turns out to be independent of the presence of water, both for diffusion of oxygen into as well as out of the film. Even samples which have been stored under oxygen at 100 % rel. humidity (295 K) for several hours show exactly the same rate of fluorescence recovery upon pumping of oxygen as do samples which have been stored under dry oxygen. In order to determine the activation energy of diffusion, the diffusion coefficient was determined in the temperature range from T = 293 K to T = 100 K. From the Arrhenius plot in Fig.18 b, the activation energy for oxygen diffusion of $E_A = 26.5 \pm 0.5\, kJ \cdot mol^{-1}$ is obtained, which is a typical value for the diffusion of oxygen in polymers below the glass transition temperature[45-47].

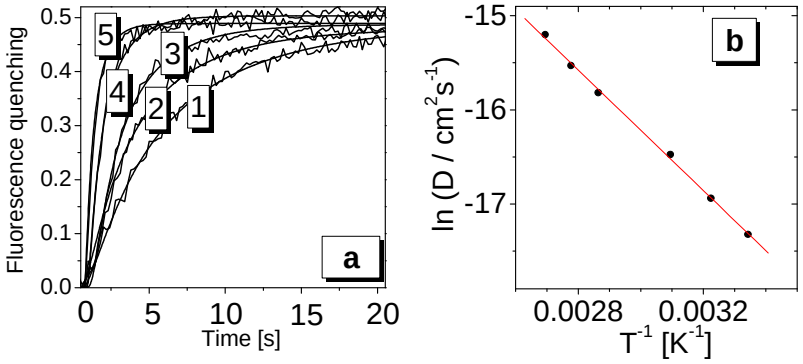

Fig.18 Temperature dependence of the diffusion of oxygen in annealed P3HT films. Panel a; Fluorescence quenching FQ in a 7 µm thick film of P3HT at different temperatures as a function of time after admission of oxygen (p = 8 bar) at different temperatures: Circles - experimental data. Smooth lines show fits according to Eq. 37. Panel b: Arrhenius plot of the diffusion coefficients extracted from panel a.

While the collisional component of fluorescence quenching (FQ) is completely reversible upon removal of oxygen[42], the slow component is only partially reversible. The reversible part of the slow FQ component is due to the light-assisted formation of a charge transfer complex between the polymer and oxygen[20, 48], whereas the irreversible part is due to photo-oxidation of the polymer[42] and is thus accompanied by a loss of absorbance. Obviously a small loss in absorbance (by about 2%) leads to substantial photoluminescence (PL) quenching (by about one third), see Tab. 4. This is due to the diffusion of excitons to the quenching centers which have been formed by photo-oxidation of the polymer[49]. Assuming that Stern-Volmer kinetics not only apply to the quenching of fluorescence by oxygen but also to FQ by photo-oxidatively created defects, an estimate for the concentration of quenching sites, $[Q]$, can be given by solving the Stern-Volmer equation:

$$[Q] = \frac{FQ}{4\pi N_A R_{eff}^{Q} D(S_1)\tau_0(S_1)} \qquad \textbf{Eq.40}$$

Inserting typical values of $R_{eff}^{Q} = 10^{-9}\ m$,[43,50] $D(S_1) = 10^{-7}\ m^2 \cdot s^{-1}$,[42,44] and $\tau_0(S_1) = 3.4 \cdot 10^{-10}\ s$ [42] for the collision radius of quenching site and exciton, exciton diffusion coefficient, and exciton life-time in the absence of quenchers, respectively, the quencher concentrations given in Tab. 4 are obtained. On the other hand, the concentration of thiophene rings which have been oxidized, $[P]$, is obtained from the loss of UV/Vis absorbance, $\Delta E_{\max}$, of a P3HT film of thickness d,

$$[P] = \frac{\Delta E_{\max}}{d \cdot \varepsilon_{\max}(T)} \qquad \textbf{Eq.41}$$

inserting a molar extinction coefficient per thiophene ring of $\varepsilon_{\max}(T) \approx 10^4\ M^{-1}cm^{-1}$. This proportionality of absorbance loss and the number of destroyed thiophene rings is valid in the early stages of degradation in good approximation, irrespective of the degradation mechanism, because for long chains of thiophene units (n > 10) the spectral position of the absorption maximum depends only weakly on the conjugation length[35]. Tab. 4 shows that the concentration of quenching sites increases monotonously with the progress of photo-oxidation. However, the absolute concentration of quenching sites as calculated from Eq.40 is only a fraction of the concentration of oxidized thiophene rings obtained from Eq. 41, indicating that the reaction products are, on average, not very efficient quenching centers. Whether this is due to small effective quenching radii of the products, R_{eff}^{Q}, or to small fractions of effective quenchers among the multitude of products, remains an open question.

Tab. 4 Absorbance loss and fluorescence quenching (FQ) of a P3HT film on glass after irradiation with the full spectrum of a 450 W Xe lamp under 10 bars of oxygen for different times t_{irr}. c_p and c_Q are the concentrations of photo-oxidized rings (as calculated from the absorption loss) and of fluorescence quenchers (as calculated from FQ), respectively. The films were excited at 550 nm, the fluorescence intensity was monitored at 700 nm (no spectral shift of the PL was observed during the measurement) and corrected for the intensity of the absorbed light.

t_{irr} / s	**Absorbance**	$[P]$ / **mM**	**FQ**	$[Q]$ / **mM**
0	1.200	0	0	0
600	1.193	39	0.26	1.0
2400	1.179	144	0.46	1.8

III.1.2 Oxygen induced energy level shifts of P3HT

Oxygen is well known to act as p-doping agent for organic semiconductors studied by electrical measurements using Field effect transistor (FET) structures. Quantitative information about the influence on the energy levels in the polymer film especially the concentration of oxygen in the thin film however is rarely available. In order to overcome this lack of information, photoelectron spectroscopy was used to simultaneously probe the effects of oxygen on the energy levels as well as the oxygen concentration in a polymer thin film. As these measurements are performed under ultra high vacuum conditions (~$3 \cdot 10^{-10}$ mbar) with the oxygen exposure realized in an attached closed chamber (Fig. 13) other factors than oxygen influencing the energy levels are excluded.

The core level spectra of pristine P3HT are shown in Fig. 19. The carbon C1s signal consists of a single broad peak with the maximum located at 285.3 eV. The energetic position of the signal is in good accordance to literature values for carbon in low oxidation states. Three chemically different carbon species are expected to contribute to this peak: C-C bonded carbon, representing the alkyl side chain, as well as C=C bonded and C-S bonded carbon of the thiophene ring. For a detailed discussion see e.g. reference[51]. The sulfur S2p signal consists of a single doublet which is due to spin orbit coupling. As the polymer layer was prepared under ex situ conditions and exposed to ambient atmosphere during the transport to the vacuum system a small amount of oxygen is already present in the pristine film, even after annealing under vacuum conditions. The molar ratio oxygen/sulfur, representing the number of oxygen atoms per monomer unit is smaller than 0.01 in the annealed film, as calculated from the corresponding peak areas and sensitivity factors (C1s 0.25, O1s 0.66, S2p 0.54) [39], see Fig. 19, bottom right. This oxygen concentration is close to the detection limit of the spectrometer.

When the sample is exposed to oxygen twice for 30 min in the dark, no significant changes in the position of the energy levels are observed. However, upon simultaneous exposure to white light (AM1.5 standard) and oxygen all core level peaks of the polymer shift towards lower binding energies (marked by the dotted lines). Upon thermal annealing of the sample, the observed shifts are reversible as will be discussed below in more detail. The exposure to light and oxygen for 105 min leads to only minor irreversible chemical degradation as concluded from the absence of significant amounts of oxidized products in the high binding energy region of the core levels.

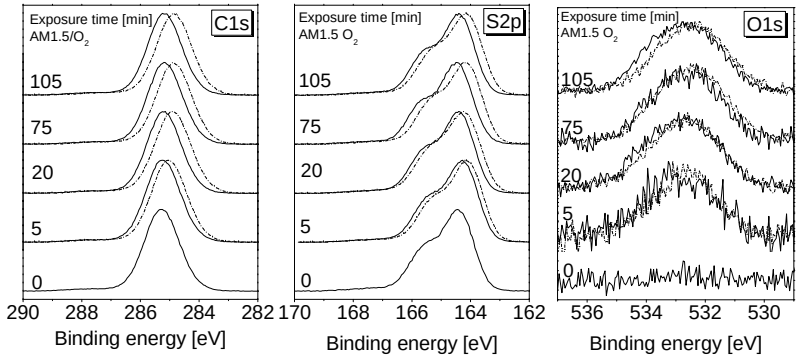

Fig. 19 Core level spectra of C1s, S2p, and O1s for P3HT films after different times of simultaneous exposure to light and oxygen (full lines) and subsequent annealing at 423K at 10^{-3} mbar for 10 min. Spectra were normalized to the peak maxima except for the pristine oxygen signal which was normalized to the same signal to noise ratio compared to the other O1s spectra.

The observed core level shifts in a second series of experiments without thermal annealing steps are accompanied by corresponding energetic shifts in the valence band region. Fig. 20 shows the dependence of the valence levels on the oxygen concentration in the film. The oxygen concentration, expressed as the oxygen to sulfur ratio, is calculated from the respective peak areas and the corresponding sensitivity factors. With increasing oxygen content, the HOMO level position, obtained from the low binding energy onset in UPS, shifts to lower binding energies, accompanied by an increase of the work function estimated from the high binding energy cutoff of the UPS spectrum. The binding energies of all the P3HT core levels decrease significantly with increasing O:S ratio. Even for the highest observed O:S ratio of 0.34, which correlates with an irreversible UV/VIS absorbance loss of less than 5%[25], neither C1s nor S2p spectra show any indication for the presence of chemically oxidized species. This is in line with results about the irreversible photo degradation which will be presented in section III.2.1.2 where it will be shown that photo oxidation products of P3HT in the core level spectra of C1s and S2p become visible only at O:S ratios larger than 1.3. This can be rationalized by considering that an O:S ratio of 0.34 corresponds to 34% of all 3-hexylthiophene units containing an oxygen atom. As carbon and sulfur are oxidized at about the same rate, this means that only about 3% of all carbon and sulfur atoms carry an oxygen atom. Although such a concentration might be detectable by XPS under favorable conditions, the signals of the oxidized species are located on the high binding energy side of the peaks of the unoxidized species and might thus be superimposed by the secondary electron background and possible energy loss satellites. Furthermore, the oxidized peak, depending on the oxidation state, can be located quite close or even within the main signal which makes its detection even more difficult.

The rigid shift of all core levels as well as of the valence band features together with the absence of significant spectral features of oxidized products indicates that physical interactions between the polymer and oxygen are responsible for the observed binding energy shifts, rather than chemical reactions. This interpretation is supported by the observation that while core level and HOMO binding energies decrease, the work function increases by approximately the same value (Fig. 20). Thus, the energetic distance between the HOMO and the vacuum level of the polymer, i.e. the ionization potential (IP), does not show a distinctive trend as a function of oxygen concentration, but seems to stay constant. Since IP is, in first approximation, a property of the material, this behavior also supports the statement that only minor chemical interactions are present.

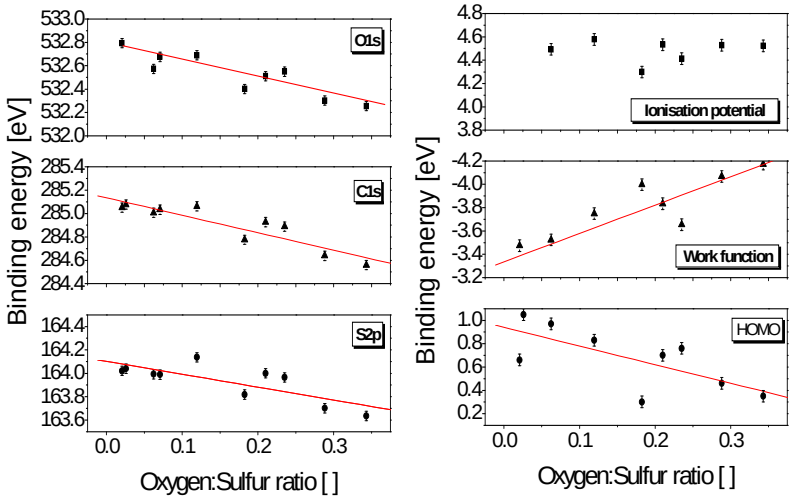

Fig. 20 Energy levels of a 100 nm thick P3HT film at different oxygen concentrations (O:S ratio) without annealing steps. Left panels: Core level binding energies of sulfur, carbon and oxygen. Right panels: HOMO energy and work function in reference to the Fermi energy. Additionally the ionization potential is shown.

Possible reasons for the systematic energetic shifts observed in Fig. 20 are either the p-doping of the organic semiconductor P3HT or, alternatively, the variation of the interface dipole between P3HT and the underlying substrate (interface doping)[52]. Both phenomena induce the Fermi level to shift towards the HOMO level position and thus all other occupied states. As the reference energy in photo electron spectroscopy is the Fermi level (E_F = 0eV binding energy), such a shift will reduce the binding energy of all occupied states (i.e. the energy difference between the considered state and E_F). In contrast, the work function, i.e., the energy difference between E_F and the vacuum level of the spectrometer, if the

Fermi level to shift towards the HOMO level position. From the fact that oxygen is homogeneously distributed over the polymer film, it can be concluded that p-doping of the polymer is more likely than interface doping. Further support for this interpretation may be derived from theoretical work[53] and experimental observations[54], both stating that P3HT itself is doped by oxygen. Strong evidence for the doping of the polymer is also provided by the fact that light promotes the doping effect significantly. Such light promoted doping effects have been reported for in situ prepared sexithiophene [55]and P3HT films[15,42,54,104].

In order to check the strength of the interaction between P3HT and oxygen, the reversibility of the observed effects was examined by thermally annealing the sample. Fig.21 shows the sulfur S2p and C1s binding energies after different annealing / oxygen exposure cycles (Fig.21 a), together with the corresponding O:S ratios (Fig.21 b) out of the experiment presented in Fig. 19. First, a pristine P3HT thin film is vacuum annealed twice in order to get rid of solvent residues and minimize effects caused by changes in the polymer morphology. This procedure also reduces the O:S ratio to less than 0.01. Subsequently, the polymer film is exposed to the light of a sun simulator and 970 mbar of oxygen for defined periods of time, which leads to a substantial decrease in the binding energies of the C1s and S2p core levels of roughly 0.3 eV and a concomitant increase of the O:S ratio of about 0.02.

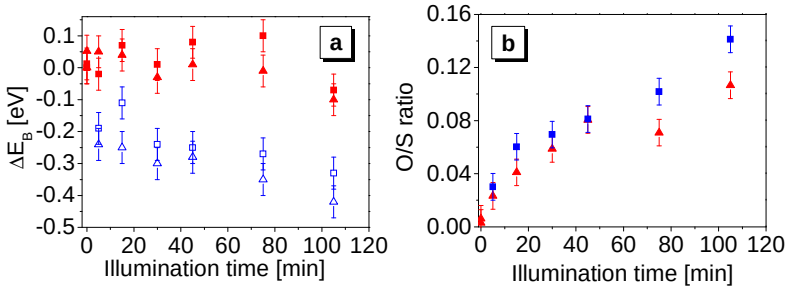

Fig.21 Panel a: Binding energies of annealed (S2p, full squares, C1s full triangles) and oxygen/light treated (S2p, open squares, C1s open triangles) P3HT film during several cycles of exposure to light and pure oxygen (970 mbar) under AM1.5 conditions and thermal annealing (15 min at 10^{-4} mbar and 170°C); Panel b: Corresponding O:S ratios after oxygen/light treatment (squares) and thermal annealing (triangles).

Upon annealing, the binding energies of the core levels return to their initial values they had before the exposure to oxygen and light, whereas the O:S ratio shows only little recovery. This holds true for repeated cycles of doping and annealing, throughout the duration of the experiment of almost two hours. Consequently, the core levels are switched between the constant binding energies of the "doped" and the initial "undoped" state. Only a slight trend towards smaller binding energies is

observed during the experiment. However, the O:S ratio constantly increases, resulting in a value of roughly 0.16 after two hours of illumination, which corresponds to an irreversible loss of UV/VIS absorption below 2%. These observations point to the presence of at least two oxygen species with significantly different binding energies to P3HT. The reversibly bound species is attributed to physisorbed oxygen, which probably forms a metastable charge transfer complex with the polymer upon photo excitation of the latter[104]. The irreversibly bound species is assigned to oxygen contained in photo oxidation products[25]. Unfortunately, the chemical nature of these species cannot be resolved as the peak shape of the O1s spectra in Fig. 19 does not change significantly upon oxygen/light and thermal treatment. Nevertheless, the above assignment explains why the reversibly bound oxygen species, which represents an only minor part of the total oxygen content of the film, leads to the shift of the core and valence levels, whereas the much more abundant, irreversibly bound oxygen species has a negligible effect on the electronic properties and only a weak effect on the optical properties of the film. The oxygen molecule bound to the π-system of the polymer in the CT complex traps an electron which leaves behind a mobile hole on the electronic π-system of the polymer. This leads to a shift of the Fermi level towards the HOMO level of the polymer. The oxygen species chemically bound in oxidation products is preferably located at molecular sites which are electronically isolated from the π– conjugated system (probably in the side chain position or in already destructed thiophene rings). Consequently, its interaction with electrons of the π-system is much weaker and therefore does not lead to substantial changes in the electronic structure of the polymer. Nevertheless, the irreversibly bound part of the oxygen population also presents a degradation pathway of the polymer because this oxygen species are most probably acting as quenching sites for excited states of P3HT as presented in the previous section about the oxygen induced fluorescence quenching[56].

III.2 Irreversible oxygen effects on P3HT

Under ambient conditions a broad parameter spectrum is participating in the decomposition of polymeric materials. However the basic pathways can be cut down to thermal, photo oxidative, hydrolytic and ozone degradation. In order to evaluate the importance of each of these pathways in terms of daily application and reaction mechanism, the photo oxidation and the ozone degradation of P3HT were investigated first with subsequent research about the influence of other environmental factors influencing photo oxidation under controlled atmospheric conditions.

III.2.1 Photo oxidation vs ozone degradation

The exposure of thin P3HT layers (nominal thickness of 100 nm) to either, ozone or photo oxidative conditions, results in the decay of the optical absorption in the range between 330-650nm (UV/VIS) as shown in Fig. 22.

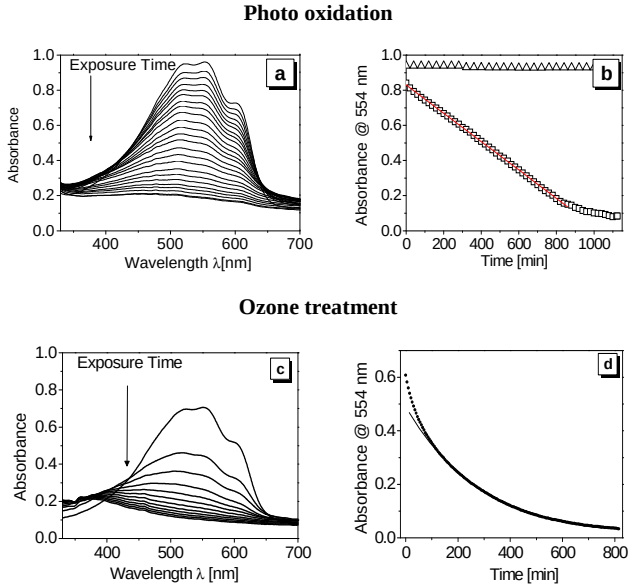

Fig. 22: Panel a: UV/VIS spectra of a thin film of P3HT after different periods (60 min steps) of exposure to 1 bar oxygen and 0.13 Wcm^{-2} Xenon light. Panel b: Dotted: time trace (20 min steps) of the absorption maximum at 554 nm corrected by the baseline value at 750 nm, Solid line: linear fit to the experimental data; Triangles: time trace in pure oxygen in the absence of light and ozone. Panel c: UV/VIS spectra after different periods (60 min steps) of exposure to ozone (20 ppm), Panel d) Dotted: Decay (5 min steps) of the absorbance at 554 nm (corrected by the baseline value at 1100 nm) as a function of ozone exposure time. Solid line: Exponential fit to the experimental data

The decay of the optical signals shows several distinctive differences between exposure to photo oxidative conditions and to ozone conditions. Under photo oxidative conditions, the time trace of the absorption maximum at 554 nm shows a fairly linear decay whereas an almost exponential decay is observed under ozone (Fig. 22 c and d). In the case of ozone treatment, the decrease in absorption is accompanied by a blue shift of the absorption maximum from 554 nm to 395 nm (Fig. 22 a and b)

starting at around 50% of the initial absorption whereas photo oxidation does not cause a significant shift before the final stages of degradation. In the absence of light and ozone, oxygen does not cause any significant degradation on the monitored time scale (Fig. 22a). The different decay kinetics and the differences with respect to spectral shifts suggest that photo-oxidation and ozonization follow different degradation mechanisms.

III.2.1.1 Ozonization rate vs. photo oxidation rate

In order to assess the relevance of ozonization and photo oxidation for practical purposes, the reaction rates of both degradation paths were determined experimentally. The reaction rate of photo-oxidation is obtained from the slope of the decay trace in the linear presentation (Fig. 22 b) whereas the reaction rate of ozonization in the dark is taken as the reciprocal of the natural life time of the exponential fit to the experimental decay curve (Fig. 22 d). The effect of ozone concentrations in the range from 0 to 6 ppm in pure oxygen on the degradation rate of P3HT films is shown in Fig.23.

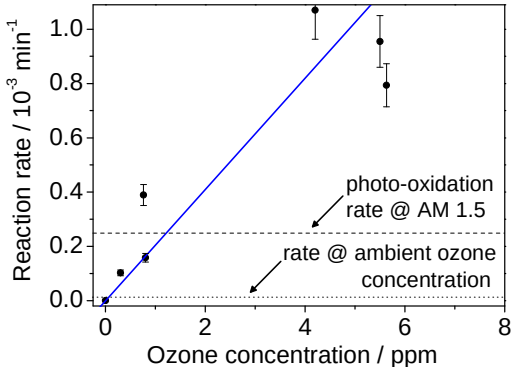

Fig.23 : P3HT degradation rate as a function of ozone concentration. Full dots: Experimental data. Full line: Linear fit to the data points. The dashed horizontal line represents the photo-oxidation rate observed at AM 1.5 conditions in dry air while the dotted horizontal line represents the degradation rate at 0.1 ppm ozone in dry oxygen in the dark.

The reaction rates of ozonization scale fairly linearly with the ozone level in the investigated range, with a slope of $m \approx 3.3 \times 10^{-6}$ s^{-1}ppm^{-1}. Based on this linear relationship it is possible to compare the rates of ozone degradation to those of photo oxidation under ambient conditions. Ambient ozone concentrations are below 0.2 ppm for natural environments [57] whereas peak values of up to 0.4 [58] ppm

are reported for urban regions. At ozone concentrations of 0.05 ppm, which is an average value for urban areas, the ozonization rate is expected to be $r_{oz} \approx 1.6 \times 10^{-7}\ s^{-1}$. Under normal laboratory conditions, where ozone concentrations of up to 10 ppb are encountered, the reaction rate is even smaller by a factor of 5 to 10. Under the standard solar illumination of Air Mass 1.5 (AM 1.5) conditions in synthetic air, the rate of photo oxidation is around $r_{po} = 4.2 \times 10^{-6}\ s^{-1}$, i.e., about two orders of magnitude faster than ozonization in a typical laboratory environment.

III.2.1.2 Photoelectron spectroscopic studies of degradation kinetics

In order to characterize the chemical changes of the P3HT film caused by degradation, the XPS signals of carbon C1s, sulfur S2p, and oxygen O1s were monitored during photo oxidation and ozone degradation at defined stages of degradation obtained via UV/VIS spectroscopy (Fig. 24). In both cases of oxidation, the spectra of carbon and sulfur develop spectral features at higher binding energies, i.e., of species in higher oxidation states (Fig. 24). The spectra recorded at a detection angle of 70°, i.e., providing an information depth of about 2 nm (Fig. 24 panel b,c,d dotted lines), are not significantly different from those recorded at normal emission with an information of approximately 10 nm, indicating the absence of any significant spatial reaction gradient in the films near the surface region. The signal of pristine, i.e., non-oxidized, carbon consists of a single broad peak with the maximum located at 285.0 eV (Fig. 24). Both, position and spectral shape of this signal are in good accordance to literature values for carbon in low oxidation states[51]. Three carbon species are contributing to this peak: C-C bonded carbon representing the alkyl side chain as well as C=C bonded and C-S bonded carbon of the thiophene ring. In the early stages of degradation (corresponding to 10-40% loss of optical absorption) the carbon peak shifts towards lower binding energies by up to 0.4 eV. Similar shifts have been observed for the valence band features of sexithiophene films upon exposure to oxygen and have been interpreted by p-type-doping[59] and a resulting change in the Fermi level position[59]. It is well-known that thiophene based oligomers and polymers are strongly p-doped upon interaction with either oxygen and light [54,60,61] or with ozone[62] as already discussed in chapter about oxygen induced doping of P3HT (section III.2.1**)**. Such a change in the Fermi level should lead to an identical shift of all XPS signals. Indeed, the same shift is also observed for the sulfur signals in the case of photo oxidation. However, neither a shift nor a broadening of the sulfur S2p signal is observed in the case of ozonization. This can be understood by taking into consideration that energetic shifts due to the change of the Fermi level position might be superimposed by chemical shifts caused by local chemical interactions. As example, such chemical interactions have been observed at an interface between an related molecule (4,7-bis(5-methylthiophen-2-yl)benzo[c][1,2,5]thiadiazole) and gold, resulting in energetic shifts in XPS of more than 3 eV [63]. In this case the expected shift towards lower

binding energies of the sulfur signal might be compensated by a decrease of the electron density at the sulfur.

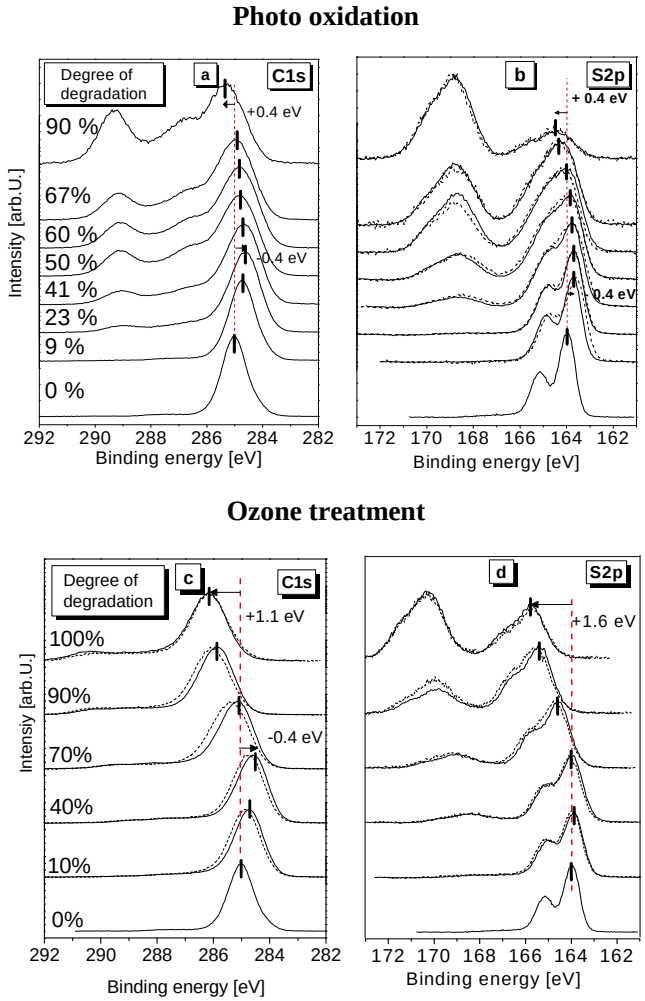

Fig. 24 XPS core level spectra of carbon C1s (left column) and S2p (right column) at different stages of degradation. Signals are normalized to the maximum peak. The position of the peak maximum is indicated with black bars. The degree of degradation is given by the loss of the UV/VIS absorption at 554 nm. Full lines represent bulk sensitive measurements (detection under 0° polar angle). Dotted lines show surface sensitive measurements (70° polar angle). Spectral shifts are indicated by vertical lines. The top row shows spectra upon photo oxidation. The bottom row shows spectra during ozone treatment.

At later stages of oxidation (UV/Vis absorption losses exceeding 40%), carbon and sulfur peaks shift back to higher binding energies. In the case of photo-oxidation, the carbon and sulphur spectra shift to binding energies which are by 0.4 eV higher than the ones for the pristine species. During ozone exposure, the carbon C1s signals shift to binding energies which are higher than those for pristine carbon by 1.1eV, accompanied by a significant broadening of the peaks. For sulfur S2p peaks this shift even amountsup to 1.6 eV. These shifts are interpreted in terms of charging effects due to the decreasing electrical conductivity of the films during oxidation. Interestingly, charging seems to be more pronounced under ozonization than for photo-oxidation, at the same degree of UV/Vis absorption loss. During photo-oxidation, additional peaks arise in the carbon region at 286.4 eV and 289.2 eV. The peak at 286.4 eV is ascribed to the formation of carbonyl groups while the peak at 289.2 eV is located in a region which is typical for carboxyl groups[64]. The ratio of oxidized to unoxidized carbon components can be roughly estimated by fitting the carbon C1s signal (Fig.25 a), assuming the same peak shape for the unoxidized component during degradation and the presence of 3 or 4 oxidized components. A slight variation of the peak widths and the number of oxidized species results in the error bars shown in Fig.25b. Plotting the fraction of unoxidized carbon as a function of loss of optical absorption (Fig.25 b) yields distinctly different decay curves for the two oxidation mechanisms. In the case of photo-oxidation, a more or less linear decay is observed, with a slightly smaller slope at the beginning of oxidation. The average slope is 0.75, corresponding to 75% of the carbon being oxidized at the moment of complete loss of absorbance.

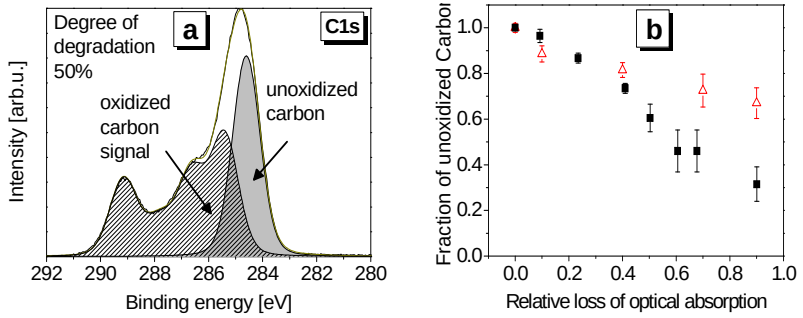

Fig.25 Panel a: Carbon C1s signal of a P3HT film degraded to 50% loss of its initial UV/Vis absorption. The contribution of the pristine component (dark grey) to the overall signal was calculated using the signal shape observed before the start of oxidation (Fig. 24 bottom). The fraction of oxidized products is represented by the hashed area. Panel b: Signal intensities of unoxidized carbon, calculated for both, photo-oxidation (squares) and degradation by ozone (triangles), as a function of loss of UV/VIS absorption.

In the case of degradation by ozone, a linear decay with an average slope of only 0.35 is obtained, with more than 60 % of the carbon atoms remaining unoxidized when the optical signal has vanished. The XPS signal of pristine sulfur (Fig. 24 b) and d)) shows a doublet with a spin orbit splitting of 1.2 eV. The $S2p^{3/2}$ signal for unoxidized P3HT is located at 164 eV, which is in good accordance to values reported in literature. A detailed analysis of the sulfur signals appearing during oxidation reveals at least 4 species which contribute to the overall signal, under both photo-oxidative conditions and ozone exposure (Fig. 26, panels a and c). The species at 164 eV is assigned to unoxidized sulfur while the signal at 168.7 eV is assigned to highly oxidized species, probably sulfonic acids[65] or peroxides[64,65,66]. The chemical nature of the species (Fig. 26, panels a and c) located at 164.3 eV and 167.3 eV (probably sulfoxides and sulfones[65]) cannot be assigned unambiguously.

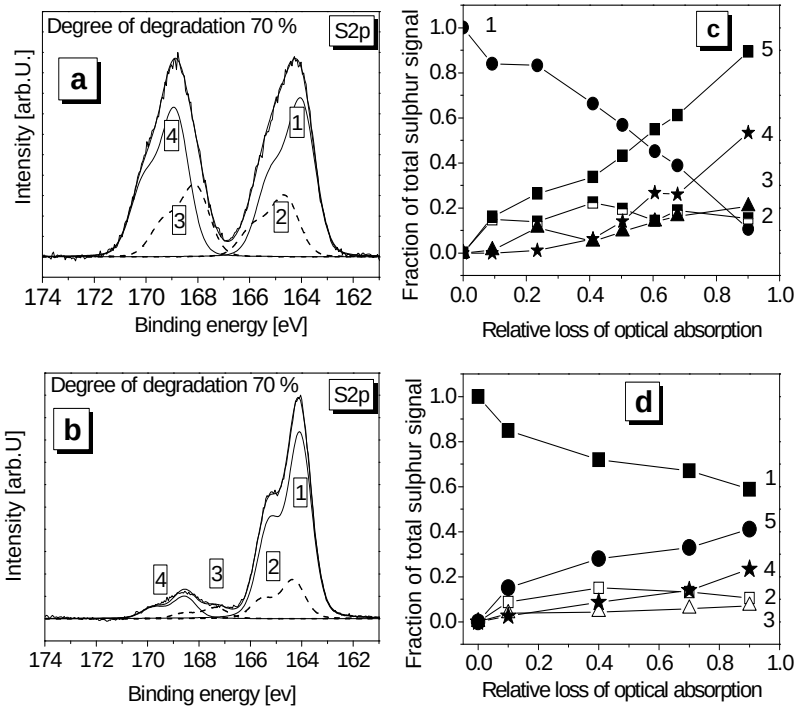

Fig. 26 Panel a and b: S2p XPS signal of degraded P3HT. Panel c and d: Changes of relative XPS intensities of the species in the left panel as a function of the relative loss of optical absorption during degradation. 1) Pristine sulfur, 2) and 3) slightly oxidized sulfur, 4) strongly oxidized sulfur, 5) sum of all oxidized species. The top row shows results upon photo oxidation. The bottom row shows the results for ozone treatment. The degree of degradation is given by the relative loss of the initial absorbance at 554 nm.

The comparison of the evolution of these species as a function of the loss in optical absorption gives valuable information about the mechanism of P3HT degradation (Fig. 26, panels b and d). In the case of photo oxidation, sulfur is completely oxidized by the time the optical absorption vanishes. The appearance of the highly oxidized sulfur species at 168.7 eV is strongly correlated with the loss of UV/Vis absorption, yielding an almost linear slope of around unity (Fig. 26). In the case of ozone degradation, even at complete loss of absorbance, 60% of the sulfur atoms remain unoxidized (Fig. 26.d). In both cases of degradation, the slightly oxidized species (species 2 and 3 in Fig. 26, panels c and d) remain in small concentrations, species 2 exhibiting a maximum at around 40% loss of absorption). The fraction of the most highly oxidized species (species 4 in Fig. 26, panels c and d) remains small initially and increases at later stages of degradation with growing rates. This hints to a consecutive reaction with species 2 and 3 being intermediate products and species 4 being the final product of degradation. Plotting the elemental composition of the film (O/S ratio, O/C ratio, C/S ratio) as a function of relative absorption loss, yields further insight into the respective degradation mechanisms (Fig.27).

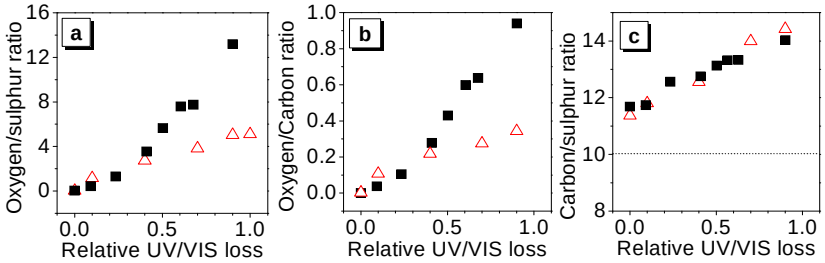

Fig.27 Elemental composition of a P3HT thin film as determined by XPS spectroscopy at different stages of photo oxidative and ozonic degradation. The degradation level is given by the relative loss of UV/VIS absorbance at 554 nm. Squares show photo oxidation measurements, triangles show ozone measurements. The molar ratio of oxygen/sulfur (panel a), oxygen/carbon (panel b) and carbon/sulfur (panel c) was calculated using the total intensity of the corresponding XPS peaks and the respective sensitivity factors.

Both, photo oxidation and ozone degradation, lead to an increase of the oxygen content in the polymer film as seen from the increasing ratios of oxygen to sulfur (O/S) and oxygen to carbon (O/C) (Fig.27 panels a and b). In the early stages of oxidation (UV/Vis absorption losses of less than approximately 35%), the relationships between O/C and O/S ratios on one hand and absorption loss on the other hand are very similar for the two oxidation conditions. In the case of photo oxidation, the plots of O/S and O/C against relative absorption loss yield steadily increasing curves with slightly larger slopes for absorption losses exceeding 35%. At total loss of absorption, the molar ratios are O/C ≈ 1 and O/S ≈ 15. In the case of ozone treatment, the slopes are more or less constant throughout the reaction,

yielding O/C ≈ 0.35 and O/S ≈ 5 at 100% absorption loss. Interestingly, for both oxidation pathways, the carbon to sulphur ratio (C/S) increases by 30% during the reaction together with the occurrence of the indium signal of the underlying ITO substrate upon the total loss of absorption. Both of these observations points to the loss of material by the decomposition of the polymer backbone.

III.2.2 Environmental factors influencing photo degradation of P3HT

In this chapter the influence of several environmental factors on the photo oxidative degradation of P3HT is discussed. Despite the effort spent on understanding the degradation of P3HT in the solid state there is still a lack of understanding of the details of the degradation mechanism. Literature reporting on the quantitative influence of illumination, temperature and atmospheric conditions is rarely available, although these are key factors in polymer aging. In this section the dependence of the photo-degradation kinetics of P3HT films on irradiation intensity, wavelength, oxygen partial pressure, temperature, and humidity is investigated quantitatively by infrared and UV/VIS absorption spectroscopy in order to obtain a broader data basis for the elucidation of the reaction pathways.

III.2.2.1 Variation of light intensity

In order to determine the dependence of degradation rate on light intensity, P3HT films of comparable thicknesses ($d \approx 100\ nm$) were irradiated with white light of different intensities in the range from I =0.08 Wcm^{-2} to 0.12 Wcm^{-2} (maximum power output) at 8 bar oxygen partial pressure. Both the spectral distribution of the light source and the temperature on the sample surface were kept constant (T = 298 K, ΔT<1 K) over the whole investigated intensity range. The degradation rate depends linearly on the intensity incident on the sample (Fig. 28) within the measured range. Degradation in the dark is negligible under our experimental conditions, as revealed by keeping films in the dark for 2 hours at elevated temperatures and high oxygen pressures (T = 373 K, p = 8 bar oxygen) (not shown here).

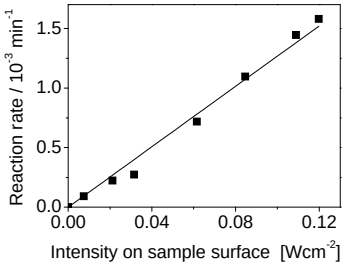

Fig. 28 Degradation rate (monitored by the loss of absorbance at $\lambda = 554\ nm$) of P3HT films by white light under 8 bar of dry oxygen as a function of light intensity (solid squares).

III.2.2.2 Wavelength Dependence of P3HT Photo Degradation

So far all the investigations have been performed by irradiation with a broad band white light source. In order to further evaluate the role of the spectral distribution of the incoming light on the photo oxidation kinetics wavelength resolved degradation experiments were performed. The wavelength dependence of the photo-oxidation rate is an important indication as to whether the polymer is destroyed by reacting with singlet oxygen which has been sensitized by the polymer itself or by a radical chain mechanism which is driven by the photo generation of radicals by the photolysis of precursors absorbing in the UV region. In order to obtain the activation spectrum of photo oxidation, polymer films were irradiated at different wavelengths, monitoring the decrease of UV/Vis absorbance on-line. The effectiveness of the P3HT photo oxidation presented in Fig. 29 which is obtained from Eq. 29 increases towards the UV region, being by about a factor of 50 larger at 334 nm than at the main absorption maximum of the polymer around 550 nm. It is thus clearly different from the absorption spectrum of P3HT. Interestingly, the wavelength dependence of the effectiveness is similar to the activation spectra which have been observed for polymers with saturated backbones, like PE, PP[67], PS[68] and PMMA[69] which are photo oxidized by radical chain mechanisms.

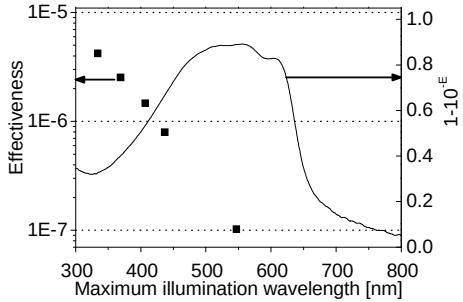

Fig. 29 Effectiveness (squares) of the photo degradation of a P3HT film as a function of irradiation wavelength. The absorption spectrum of P3HT is shown as a solid line. Degradation experiments were performed under constant oxygen flow of 0.1 $Lmin^{-1}$ at 970 mbar oxygen partial pressure.

In order to check whether under white light illumination the oxidation rates at different wavelengths add up linearly or different wavelengths have a synergistic effect, the reaction rate under white light conditions was calculated from the wavelength resolved data (Fig. 29). To this end, the spectral photon distribution of the illumination source (Xe high pressure lamp), $I_0(\lambda)$ was multiplied with a fit to the photochemical quantum efficiencies (with respect to the incident photon flux $I_0(\lambda)$), $\phi_{pc}(\lambda)$

, as obtained from the monochromatic experiments (Fig. 29). The integral of this function then yields the calculated reaction rate according to:

$$v_{pc,calc} = \frac{dE}{\varepsilon_T \cdot dt} = \int_{\lambda=0}^{\infty} \phi_{pc}(\lambda) \cdot I_0(\lambda) \cdot d\lambda \qquad \text{Eq.42}$$

where E is the absorbance of the film at the monitoring wavelength and ε_T the extinction coefficient of one thiophene unit at this wavelength. The reaction rate thus calculated and the experimental rate are in accordance within the error bars, thus showing that the rates at different illumination wavelengths add up linearly.

III.2.2.3 Thermal activation of P3HT photo degradation

Temperature is another crucial environmental factor which has to be considered in the degradation of polymeric materials and has therefore been studied. The reaction rate of the photo-oxidation of P3HT films increases exponentially with temperature in the range from T = 298 K to 393 K (Fig. 30 a). The activation energy obtained from the slope of the corresponding Arrhenius plot yields a value of E_A = 26 kJ/mol (Fig. 30 b). As this value is equal to the activation energy found for oxygen diffusion in the P3HT films (see section 3.2.1.), the question arises whether oxygen diffusion might be the rate limiting step in the photo-oxidation of P3HT. However, at the conditions under which the temperature dependence is investigated ($p_{O_2} = 6 bar$), the flux of oxygen into the film easily keeps up with the consumption of oxygen by the photo-oxidation. This becomes obvious when calculating the Deborah number $Z = L \cdot (D/k)^{-0.5} \approx 0.01$ from the thickness L of the film, the diffusion coefficient of oxygen $D = 3 \cdot 10^8 \ cm^2 \cdot s^{-1}$ (see section III.1.1) and the pseudo-first order rate constant $k = -[O_2]^{-1} \cdot \frac{d[O_2]}{dt} = -[O_2]^{-1} \cdot \frac{dA}{\varepsilon_{tr} \cdot dt}$ of the photo-oxidation reaction, assuming that the absorbance loss equivalent to one thiophene ring corresponds to the consumption of one oxygen molecule[25]. The value of Z = 0.01 obtained for the Deborah number for films of about 100 nm in thickness indicates that the reaction rate is not controlled by the rate of oxygen diffusion into the film (The case of diffusion limitation is expected for Z > 1). It also means that there should be no vertical gradient of product distribution, which has been shown to in section III.2.1.2 correlating surface sensitive XPS and bulk sensitive UV/VIS spectroscopy.

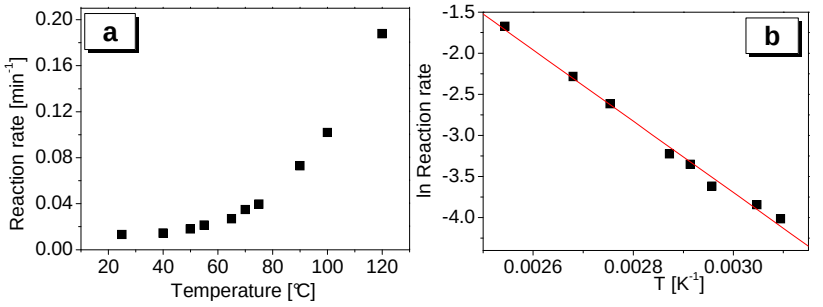

Fig. 30 Temperature dependence of the photo-oxidation rate of annealed films of rre-P3HT under 6 bars of dry oxygen and at an irradiation intensity of $I_0 = 0.13 \ W \cdot cm^{-2}$. Panel a: Reaction rate vs. temperature. Panel b Arrhenius plot of the photo oxidation rates extracted from the left panel.

III.2.2.4 Dependence of the photo degradation rate on oxygen partial pressure

The dependence of the photo-oxidation rate on oxygen pressure is shown in Fig. 31. For small oxygen partial pressures (p < 0.2 bar) the reaction rate increases steeply, whereas towards higher oxygen concentrations the rate asymptotically approaches a maximum value, which is about five times that of the value at the atmospheric oxygen partial pressure. Such a sublinear dependence of the degradation rate on oxygen partial pressure has been observed for several polymers, including LDPE[70] and dialkoxy-PPV[71]. It has been explained by different mechanisms, such as singlet oxygen sensitization[71, 72, 73] and radical chain mechanisms. For both mechanisms, the saturation of the rate for higher oxygen pressures is due to the depletion of a transient species by the reaction with oxygen or with an oxygen centred radical species. While in the singlet oxygen case the transient species is the triplet state of the polymer, it is a chain propagating radical (which reacts with an oxygen containing radical in the termination reaction) in the case of the radical mechanism. Both mechanistic considerations can be fitted to the experimental data according to Eq.27 for the singlet oxygen based degradation and Eq.24 for the radical based mechanism as presented in Fig. 31.

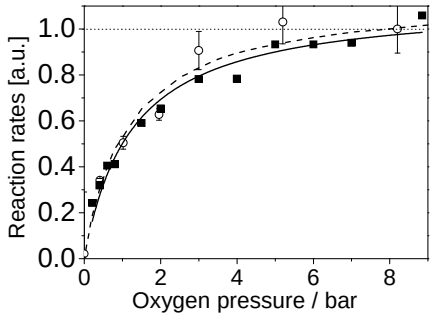

Fig. 31 Normalized reaction rates as function of oxygen pressure (the value of the reaction rate at 8 bar is set to 1). Values obtained from UV/VIS decay kinetics (554 nm, squares) and FTIR loss of carbon-carbon double bonds at 1509 cm^{-1} (circles) are shown. The full and dotted lines are fits to the experimental data corresponding to Eq. 27 (singlet oxygen mechanism) and 24 (radical mechanism), respectively.

As evident from the fit curves in Fig. 31, both functions describe the observed pressure dependence rather well, so that distinguishing between the two mechanisms on the basis of pressure dependence of the reaction rates is not possible.

III.2.2.5 Accelerated photo oxidation in the presence of humidity

Another environmental factor affecting the degradation rates is the ambient humidity (Fig. 32 a). The presence of humidity during the photo oxidation of P3HT increases the reaction rate significantly. Humidity in the absence of oxygen does not cause significant degradation, revealing that humidity itself is not responsible for the degradation of P3HT. The variation of relative humidity in the range from 0 to 100% (at 295 K) results in an increase of the reaction rate by a factor of up to 2.2 (Fig. 32 b). This value was consistently found for different oxygen partial pressures in the range from 0.2 bar to more than 3 bar.

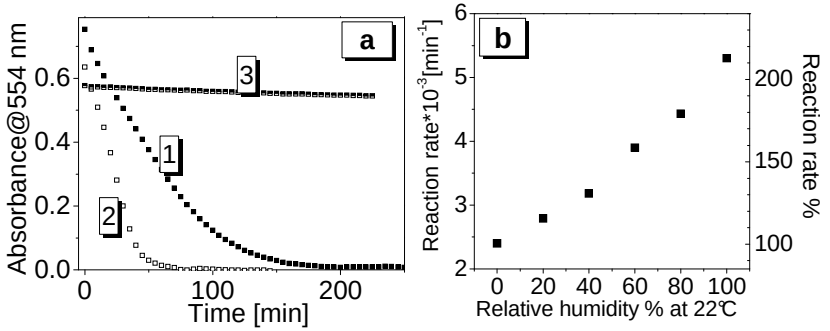

Fig. 32 Effect of humidity on the photo oxidation rate of annealed films of P3HT. Panel a: time trace of the P3HT absorption maximum during degradation under (1) oxygen, (2) humidified oxygen (100% rel. humidity) and (3) humidified nitrogen (100% rel .humidity).Panel b: Degradation rate as function of relative humidity at 295 K. Total pressure p = 1 bar in all experiments.

III.2.2.6 Structure of the polymer and morphology

Besides atmospheric conditions, the structure of the polymer has to be considered in order to state about the stability of the corresponding material. Both, the shape of the UV/VIS absorption band and the degradation rate of P3HT depend sensitively on the structure of the polymers. In the following the influence of the region-regularity on the photo degradation will be shown comparing P3HT thin films of highly regular and strongly irregular P3HT Fig. 33.

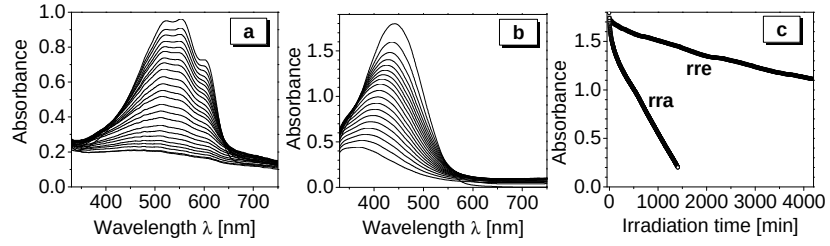

Fig. 33 UV/VIS spectra of regioregular (Panel a) and regiorandom (Panel b) P3HT thin films during photo oxidation. Panel c: Decay traces extracted from the UV/VIS spectra of regio-regular (rre, 554nm) and regio-random (rra, 442 nm) P3HT corrected by the baseline values at 800 nm.

While regio-regular P3HT (Fig. 33 a) absorbs with the maximum located at 554 nm and shows a shoulder at 600 nm which is indicative for the lamellar arrangement of the polymer chains, regio-random P3HT (Fig. 33 b) shows an unstructured absorption band peaking at 442 nm. Under identical degradation conditions, regio-random (rra-) P3HT is photo-oxidized much faster (by a factor of about five) than regio-regular (rre-) P3HT (Fig. 33 c). The peak maximum of the rra-P3HT shifts to lower wavelengths much faster than in the case of the rre polymer. In order to further investigate the accelerated degradation of the regiorandom polymer the wavelength resolved effectiveness was recorded. The action spectrum of the regio random isomer in Fig. 34 generally shows a higher reaction effectiveness compared to the regio regular isomer in Fig. 34 b. Whereas the effectiveness monotonously increases towards the UV region for the regular isomer the action spectrum of the random polymer seems to be closer to the absorption spectrum. This likely indicates that the polymer absorption is relevant in the degradation process of the random isomer but is of minor importance for the regio regular P3HT.

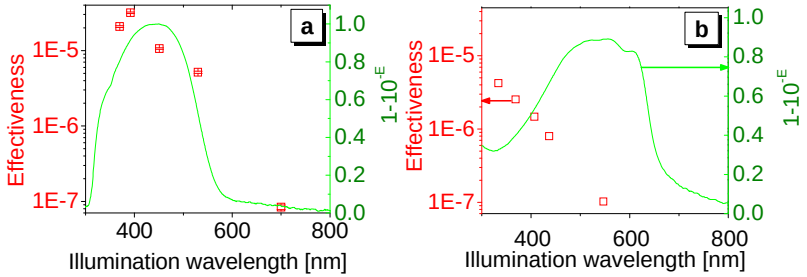

Fig. 34 Effectiveness of P3HT photo oxidation (full squares) as function of the illumination wavelength for regio random. Lines show the absorption of the corresponding polymer. Experiments were carried out under oxygen flow of 0.1l/min and ambient temperature. Panel a: Regio random P3HT. Panel b: Regio regular P3HT

In order to investigate a possible influence of the film morphology on the photo oxidation rate, thermally annealed P3HT (regio regular) were compared to non annealed films Fig. 35. Annealing films of P3HT of the same regio regularity (95%) does not have a measurable effect on the photo-oxidation rates (Fig. 35 a) although the films show clearly different absorption spectra, indicating that the annealed film has a significantly higher degree of crystallinity than the non-annealed film (Fig. 35 b). This is in good accordance with the results obtained in section III.2.1, thus ruling out an oxygen diffusion limitation and the absence of a spatial reaction gradient.

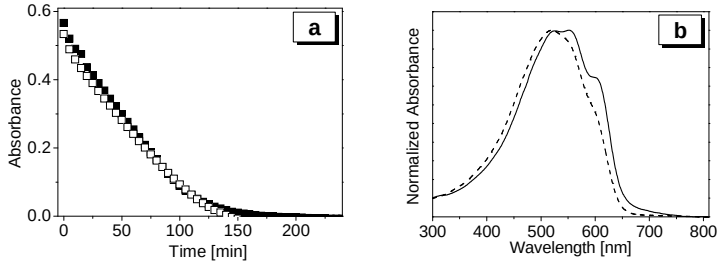

Fig. 35 Effect of crystallinity of films of rre-P3HT. Panel a: Degradation kinetics for highly crystalline P3HT at 554 nm (full squares) and P3HT of lower crystallinity at 520 nm (open squares). Panel b: UV/VIS spectra of highly crystalline P3HT (full line) and less crystalline P3HT (dotted line).

III.2.3 Product evolution under defined reaction conditions:

In this chapter, defined border cases of environmental conditions will be addressed in more detail concerning the product evolution during degradation. First of all the product evolution under monochromatic illumination conditions will be presented comparing samples irradiated with 365 nm and 525 nm since this turned out to significantly influence the reaction effectiveness, as described in section III.2.2.2. Subsequently, the product evolution under dry and humidified conditions will be investigated in order to account for the accelerating factor of humidity in the photo oxidation process. In both cases, UV/Vis and FTIR spectroscopy are employed to identify and quantify the reaction products.

III.2.3.1 Illumination with monochromatic light of 365 nm and 525 nm

The UV/VIS spectra of P3HT thin films during the degradation process are presented in Fig. 36. Irradiation with both UV light of 365 nm (Fig. 36 panel a) and visible light of 525 nm (panel b), leads to the reduction of the optical absorption due to damage of the π-conjugated system[25]. The UV/VIS decay kinetics of both experiments are presented in Fig. 36 panel c as a function of the incoming photon dose. Using UV light of 365 nm (full circles) leads to the decay of the optical signal which is approximately 30 times faster than the decay under 525 nm illumination (open squares). These results are in line with the enhanced reaction effectiveness already presented in section III.2.2.2.

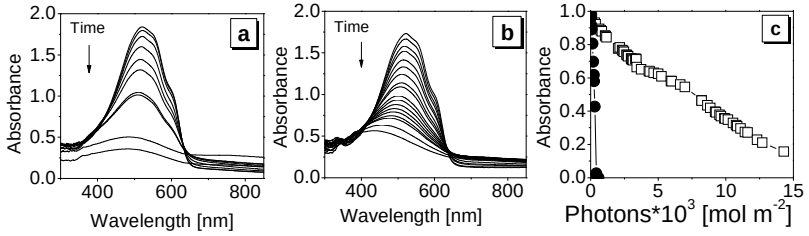

Fig. 36 UV/VIS spectra of P3HT during photo degradation under dry synthetic air. Panel a: Degradation carried out with UV light (365nm) with an incoming photon flux density of $6.77x10^{-4}$ mol photons $m^{-2}s^{-1}$, Panel b: Degradation carried out using visible light (525nm) with an incoming photon flux density of $3x10^{-3}$ mol photons $m^{-2}s^{-1}$. Panel c: Time trace of the absorption maximum at 520 as function of the incoming photons dose at 365 nm (full circles) and 525 nm (open squares).

In order to further investigate the accelerated degradation in the presence of UV light, FTIR spectroscopy was used to study the product evolution during degradation. The FTIR spectrum of pristine P3HT (Fig. 37 bottom spectra) in the range from 4000 to 1000 cm^{-1} consists of a weak aromatic C-H stretching mode at 3054 cm^{-1} , aliphatic C-H stretching modes from the hexyl side chain consisting of methyl vibrations at 2955 (asym.), and 2870 (sym.) cm^{-1} , and methylene vibrations at 2925 (asym.), and 2855 (sym) cm^{-1}. Furthermore, ring stretching modes at 1563 cm^{-1} , and 1509 cm^{-1} as well as a ring stretching mode overlapping with a methyl / methylene deformation located at 1456 cm^{-1} are observed. The mode at 1377 cm^{-1} is assigned to a symmetric methyl deformation[26]. The assignment of all signals is summarized in Tab. 5.

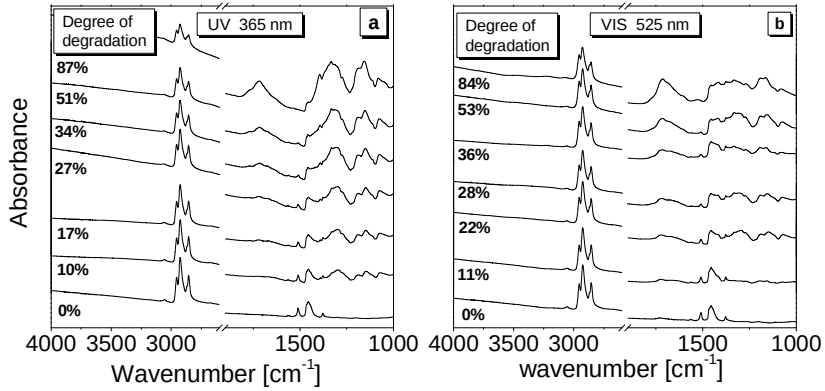

Fig. 37 FTIR absorption spectra of P3HT during degradation under dry synthetic air with UV light of 365 nm (panel a) and Visible light of 525 nm (panel b). The degree of degradation is given by the loss of optical absorption at 520 nm in the UV/VIS.

The fingerprint region below 1400 cm^{-1} exhibits a number of rising bands during the degradation. Interestingly, their peak shape is initially quite similar for both illumination conditions. With ongoing degradation however the signal intensity remains constant under VIS conditions whereas some of the bands increase under UV conditions. The constant signal intensity under VIS conditions suggests that these bands might originate from an intermediate species with a low steady state concentration rather than from final reaction products. The increasing bands under UV illumination however might present final products which rise during degradation. However their detailed nature cannot be unambiguously identified due to the large number overlapping signals in the region. Literature reports that sulfur oxidized species are typically located in this region[11,26].

Tab. 5 FTIR signals $\tilde{\upsilon}$ of a pristine P3HT thin film and the assignment to the corresponding molecular vibrations[24,26].

$\tilde{\upsilon}$ [cm^{-1}]	Assignment	$\tilde{\upsilon}$ [cm^{-1}]	Assignment
3054	Aromatic ring CH stretching	1563	C=C-Ring stretching
2955	Asym. side chain CH_2 stretching	1509	C=C-Ring stretching
2870	Sym. side chain CH_2 stretching	1456	CH_3 /CH_2 deformation
2925	Asym. side chain CH_3 stretching	1377	CH_3 deformation
2855	Sym. side chain CH_3 stretching		

Hydroxyl stretching vibrations in the range from 3700-3200 cm^{-1} are not observed for both illumination wavelengths until the latest stages of degradation, revealing the absence of significant amounts of alcohol functions, carboxylic acids and sulfonic acids during the entire degradation process. Furthermore, this indicates that the steady state concentrations of hydroperoxides R-OOH, which are known to be active species in the degradation of polymers are way below the detection limit of the spectrometer.

In the following, the detail spectra of polymer and product species will be discussed. During degradation under both illumination conditions, the loss of optical absorption is accompanied by the decrease of absorption in the polymer C=C double bond region of the FTIR spectra (Fig.38 panel a and b) representing the destruction of the π-conjugated system. Interestingly a new feature around 1530 cm^{-1} rises in the C=C region under illumination with 525 nm. However the assignment to a new C=C species cannot be unambiguously made as this band may also derive from the bending vibration of water which might be a reaction product of the degradation process.

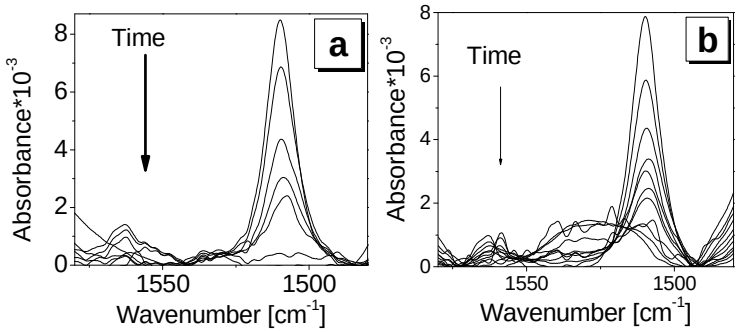

Fig.38 C=C double bond stretching region of the FTIR spectra of P3HT during degradation. The spectra were extracted from Fig. 37. Panel a: Degradation carried out using irradiation at 365nm. Panel b: degradation carried out under 525 nm illumination.

Concomitant with the loss of polymer absorption several distinctive bands in the carbonyl region of the FTIR spectrum start to rise with the spectral shape being similar for both of the illumination conditions (Fig. 39 panel a,b). Furthermore the carbonyl products are not too different from those observed under white light conditions observed in literature[11,20,26]. According to literature these carbonyl species can be attributed to ester or anhydride functions (1775 cm^{-1}), aliphatic ketones (1715cm^{-1}), aromatic ketones (1670cm^{-1}) and an unidentified species at 1620 cm^{-1}. The reliability of this assignment will be discussed below.

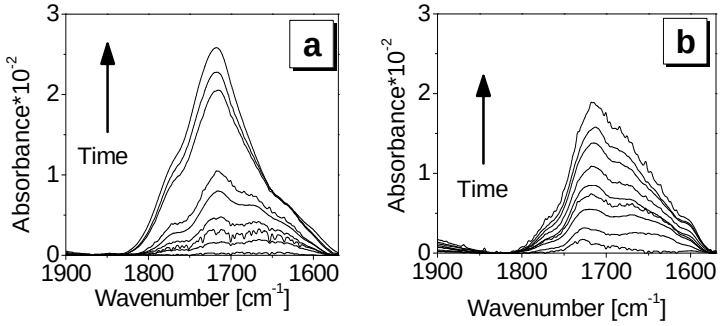

Fig. 39 Carbonyl C=O double bond stretching region of the FTIR spectra of P3HT during degradation under illumination with UV light (a) and green light (b). The spectra were extracted from the complete spectra in Fig.37.

Although these species are monitored under both conditions, the spectral shape of the overall carbonyl signal is different depending on whether the degradation is carried out under UV or VIS conditions. It seems that the band at 1775 cm^{-1} remains lower in intensity during degradation with 525 nm illumination. Furthermore the relative intensity of the 1670 cm^{-1} band compared to the signal at 1715cm^{-1} is higher. In order to further evaluate the number and the behaviour of the single carbonyl compounds during degradation, the carbonyl spectra were fitted assuming the presence of 4 species described by Voigt profiles of the same FWHM of 48±8 cm^{-1} (Fig. 40 a). Subsequently the carbonyl surface concentration was calculated according to Eq.30 using the single peak heights and a molar absorption coefficient of 300 mmol cm^{-2} which represents a typical value for carbonyl species[74,85].

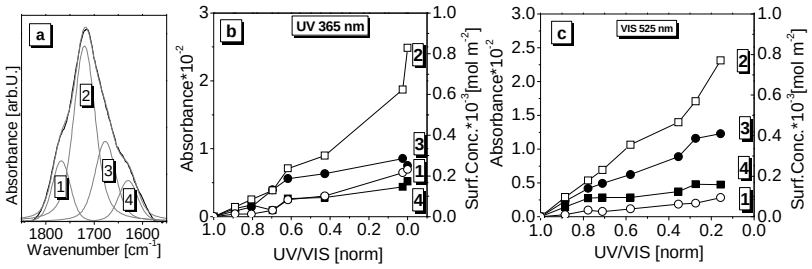

Fig. 40 Panel a: Carbonyl signal during 365 nm illumination (black line) with peak fit assuming 4 carbonyl species with same FWHM of 48±8cm^{-1}. The temporal evolution of the single carbonyl species (peak heights) as function of the UV/VIS loss at 520nm is given in panel b for 365 nm degradation and in panel c for 525 nm illumination.

The observed carbonyl spectra are well described by the presence of 4 carbonyl species as presented in Fig. 40 panel a. The temporal evolution of the four species obtained by this fitting procedure reveals that the carbonyl product at 1715 cm^{-1} is generally the main contribution of the evolving carbon species(Fig. 40 panel a and b trace 2). Under 525 nm illumination, this species rises steadily whereas its evolution accelerates under UV light of 365 nm. The bands at 1620 cm^{-1} and 1775 cm^{-1} (Fig. 40 panel a, b trace 1 and 4) remain in minor concentrations with only little differences between UV and VIS degradation. Contrary to this, the signal at 1670 cm^{-1} tends to saturate in the UV case, see Fig. 40 panel b, whereas it steadily increases under illumination with 525 nm light.

The small, saturating concentrations of species 1, 3 and 4 in the UV case (Fig. 40 panel b) and the increasing slope of species 2 suggest that under these conditions a consecutive reaction may be present with species 2 representing the final product. Under Vis conditions the evolution of the different species seems to be independent of each other.

A major difference in the decomposition under UV and VIS degradation is recognized by comparing the FTIR spectra of the C-H stretching vibration. Under irradiation with UV light the complete C-H region (Fig. 41 panel a) strongly decays whereas visible light of 525 nm only slightly affects the side chain signal (Fig. 41 panel b).

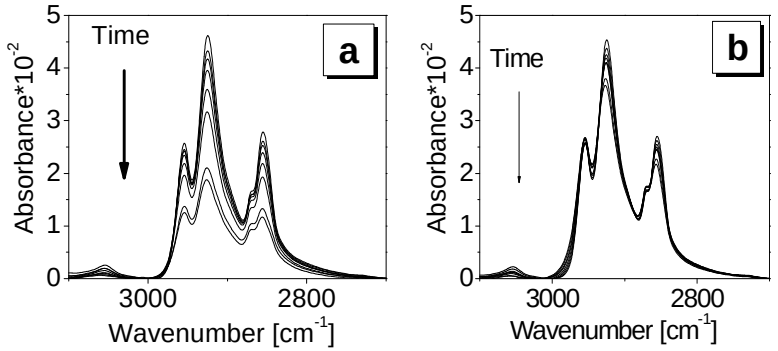

Fig. 41 C-H stretching vibration region of the FTIR spectra of P3HT during degradation. The spectra were extracted from Fig.37. Panel a: degradation carried out using irradiation at 365nm. Panel b: degradation carried out under 525 nm illumination.

This suggests that under UV light the side chain is either completely oxidized or detached from the molecule and lost to the gas phase. These two cases can be discussed comparing the concentration of reaction products during the degradation under both illumination conditions. In order to do so, the extracted reaction kinetics of both, UV/VIS and FTIR signals, are summarized in Fig. 42 presenting the surface concentration of all species (educts and products) during degradation. The surface concentration of thiophene rings is calculated according to Eq.30 out of the UV/VIS Data yielding an initial value of 1.6 to 1.7 mmol m^{-2}. The integrated C=C area out of FTIR at time t = 0 was normalized to the same value. The integrated C-H region at time t = 0 was normalized to the six fold value as 6 side chain groups are present per thiophene ring. The carbonyl concentration is calculated according to Eq.30 using the sum of single peak heights in Fig. 40 and a molar absorption coefficient of 300 mmol cm^{-2} typical for carbonyl species[75,85].

Both illumination conditions lead to the simultaneous decay of the UV/VIS absorbance at 520 nm and the C=C double bond vibration in the IR range. Interestingly, the decay under UV conditions seems to be rather linear, whereas a deceleration is observed under visible light (Fig. 42 panel a and b) of 525 nm. The evolution of the carbonyl concentration shows an induction period and then strongly rises under UV light whereas the opposite is obtained under VIS conditions. Here the carbonyl signal first rises very fast and shows a constant slope towards the end of degradation. In the first case this might

further support the presence of a consecutive reaction as proposed above whereas the carbonyl groups seem to be formed during the first oxidation step under VIS conditions..

Although the shapes of the carbonyl kinetics are different, the same surface concentration is reached at the end of the degradation process suggesting that quite similar amounts of carbonyl products are present under both illumination conditions.

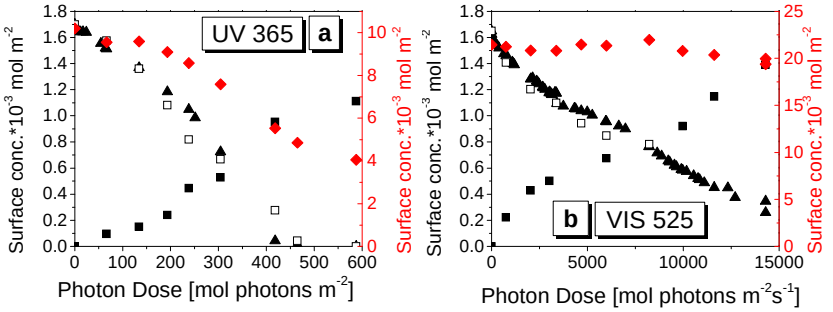

Fig. 42 Surface concentrations during photo oxidation under dry synthetic air vs. light dose incident on the polymer film. Panel a: Illumination with 365 nm. Panel b: Illumination with 525 nm. Concentrations: Thiophene rings out of UV/VIS data (full triangles), thiophene rings out of the integrated FTIR C=C region (open squares), side chain groups out of the integrated FTIR C-H region (full diamonds), carbonyl groups out of FTIR (full squares).

The wavelength dependence of the degradation process becomes even more prominent concerning the side chain signal. The concentration of the side chain groups steadily decreases under UV light. Interestingly the relative decay is minor compared to the loss of the C=C signal in both the IR and the UV/VIS region (Fig. 42 a). This effect becomes even more pronounced upon 525 nm illumination where the surface concentration of the side chain is hardly affected (Fig. 42 b). Together, the facts that same concentrations of carbonyl products are formed under UV and VIS illumination, the absence of other carbonic products, and the completely different behavior of the side chain groups observed for the two illumination conditions have some mechanistic implications. The side chain is not strongly oxidized under UV light but detached from the thiophene ring and removed from the sample as the product evolution does not depend on the presence or the absence of the side chain. This detachment is strongly suppressed under visible light. Consequently the carbonyl groups are mainly created on the thiophene ring itself. In order to further support this interpretation the correlation between the UV/VIS and the carbonyl surface signal is presented in Fig. 43. The carbonyl and thiophene ring surface concentrations presented in Fig. 43 correlate linearly with a slope of approximately 0.8. This value reveals that roughly one carbonyl function is created upon the loss of a single thiophene ring.

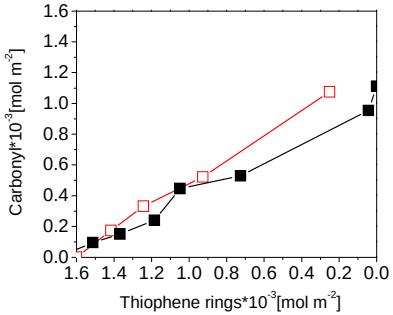

Fig. 43 Carbonyl surface concentration as a function of the thiophene ring surface concentration extracted out of the UV/VIS data for UV illumination (full squares) and VIS illumination (open squares). Data were extracted from Fig. 42.

As the side chain is not detached under illumination with light of 525 nm, these conditions offer the opportunity to further study the behavior of the hexyl side chain during degradation. Here the alpha methylene unit is of tremendous interest, as this position is reported to be the weak point of the polymer which initiates the photo degradation of P3HT in the solid state[24,26] leading to radical based reaction pathway. In order to clearly probe this position, P3HT with deuterated α-methylene groups was degraded using 525 nm and directly compared to regular P3HT[76]. Deuteration of this groups leads to the occurrence of the C-D stretching vibration in the range between 2300 cm^{-1} to 2000cm^{-1} with the rest of the spectrum remaining unaffected which is also valid for the UV/VIS spectra[76].

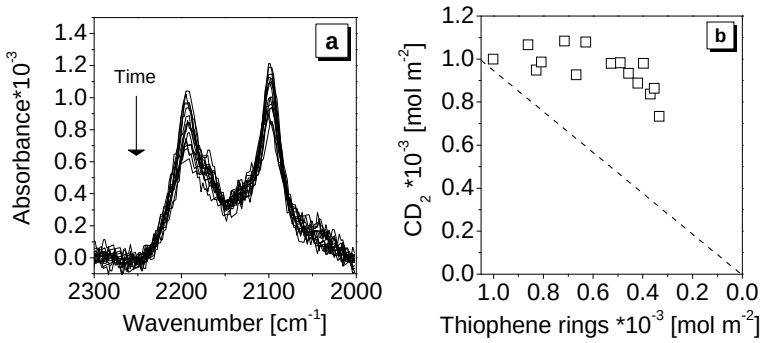

Fig. 44 Panel a: FTIR spectra of the C-D stretching vibration of deuterated P3HT during degradation using 525 nm light and ambient air, asymmetric vibration (2193 cm^{-1}), symmetric vibration (2097 cm^{-1}) Panel b: CD_2 surface concentration as a function of the thiophene ring surface concentration (open squares).

Under green light the reaction rate is generally lowered by approximately 5-10% upon deuteration of the material. Typically the reaction rate upon deuteration is lowered by 75-85% in the presence of a primary kinetic isotopic effect[77,78,79]. Therefore it is not clear whether the reduced reaction is due to the isotopic labeling or other factors e.g. different purity levels of the materials. The more evident probe here is the intensity of the CD_2 group itself during degradation. The spectra of the C-D stretching vibration are hardly affected during the degradation process as presented in Fig. 44 panel a. The surface concentration of CD_2 groups during degradation (Fig. 45 panel b) remains constant until approximately 50% of all thiophene rings are degraded and then only slightly decays. In other words, the decay of the CD_2 groups is not correlated to the decay of thiophene rings, thus ruling out that the alpha methylene group is the starting point of degradation for individual rings. In order to elucidate the nature of the active oxygen species generated photo chemically by the polymer, several samples with different content (0% - 20% mass content) of the singlet oxygen quenching agent DABCO were degraded under 365 nm and 525nm illumination. The resulting decay kinetics and extracted reaction rate are shown in Fig. 45.

Illumination wavelength 525 nm

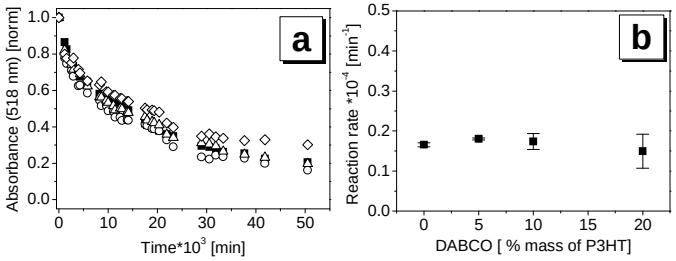

Illumination wavelength 365 nm

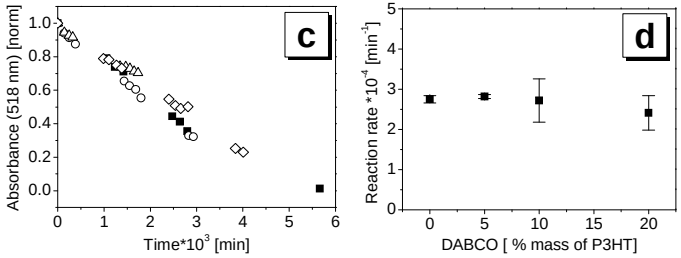

Fig. 45 Left column: UV/VIS decay kinetics of P3HT thin films at 520nm under 525 nm illumination (panel a) and 365 nm illumination (panel c), for pure P3HT (full squares), with addition of 5% DABCO (open circles), with 10% DABCO (open triangles), and with 20% DABCO (open diamond). Right column: Reaction rate extracted via linear regression from panel a (from 6000 to 30000 min) and panel c (complete range).

The time traces presented in Fig. 45 panel a and c show once more the difference in the decay kinetics of samples degraded under 365 nm illumination, where a linear decay is observed, and the more exponential decay under 525 nm irradiation. In general the presence of DABCO does not seem to affect the shape or the slope of the extracted decay kinetics. In order to clearly state this, the reaction rates were extracted from the decay kinetics (Fig. 45 panel b and d). Here the reaction rate does not show significant differences between the presence and the absence of DABCO. Although this strongly suggests that singlet oxygen is not the photo chemically created active oxygen species under monochromatic illumination this may not be unambiguously stated. The efficiency of a stabilizer in the solid state may strongly depend on the diffusion of the reactive species as the stabilizer molecule, here DABCO, are strongly localized. Assuming that singlet oxygen is formed in the vicinity of a thiophene ring and may subsequently degrade the same ring, the diffusion length of singlet oxygen is rather small. Consequently singlet oxygen may not reach any DACBO molecule within its lifetime. Therefore DABCO would not show any stabilizing effect although singlet oxygen is present.

In summary, both 365 nm and 525 nm illumination lead to the occurrence of the same concentration of at least 4 carbonyl species which are mainly located on the thiophene ring. Other oxidized carbon species are not observed. It seems that illumination at 525 nm only degrades the π-conjugated system respectively the thiophene ring itself, with the side chain being only slightly affected. In contrast, UV light additionally leads to the detachment of the hexyl side chain, most probably in a consecutive reaction and therefore the disruption of the polymer backbone.

The alpha methylene group of the side chain is hardly affected during degradation as evident by isotopic labeling with deuterium. Thus it is ruled out, that this position is the starting point of degradation at least under illumination at 525 nm. The presence of singlet oxygen was investigated using the singlet oxygen quenching agent DABCO. Although the experimental results state that singlet oxygen is not present this cannot be unambiguously stated due to the considerations above.

III.2.3.2 White light illumination under dry and humidified conditions

1. Accelerated photo oxidation in the presence of humidity

The absorption spectra of P3HT thin films during photo-oxidation are shown in Fig.46 for degradation experiments carried under dry and humidified conditions (D_2O and $H_2{}^{18}O$ not shown). The comparison of the reaction spectra under dry and humid conditions indicates that there are no significant differences in the fragmentation behavior of the π-conjugated system during degradation under the two different conditions.

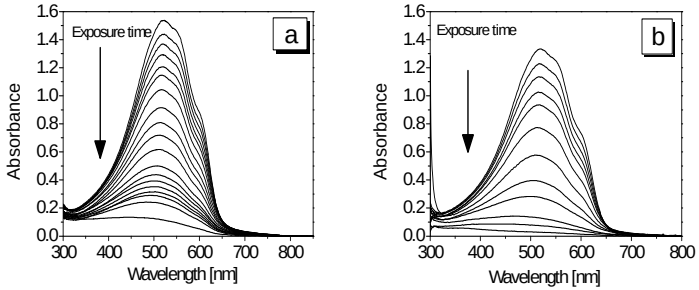

Fig.46 Panel a) UV/VIS spectra of a P3HT thin film during photo degradation in dry synthetic air; Panel b) Degradation in H2O humidified synthetic air (100% rel.hum. at 22°C),

However, comparing the temporal evolution of the absorbance at 520 nm reveals that the decay kinetics significantly changes in the presence of humidity (Fig.47). Under dry conditions a linear decay is observed with an exponential tail observed towards the end of the reaction. In the presence of humidity the reaction accelerates first and decelerates to the very end of the degradation. Generally humidity leads to the acceleration of the photo oxidation by a factor of about 3 compared to the dry case. This becomes evident from the illumination time required for complete bleaching of the main UV/Vis absorption band. Although Fig.47 (panel a) suggests that there are differences between humidified conditions of H_2O, D_2O and $H_2{}^{18}O$, the deviation is within the error bars of the experiment, see Fig.47 panel b. Therefore similar acceleration factors are observed for H_2O, D_2O and $H_2{}^{18}O$ indicating the absence of a significant isotopic effect on the degradation process, as it is observed, for example in the case of polyglycolide degradation[80]. In the following the product evolution during the degradation process in the presence and in the absence of humidity will be discussed according to FTIR spectroscopy.

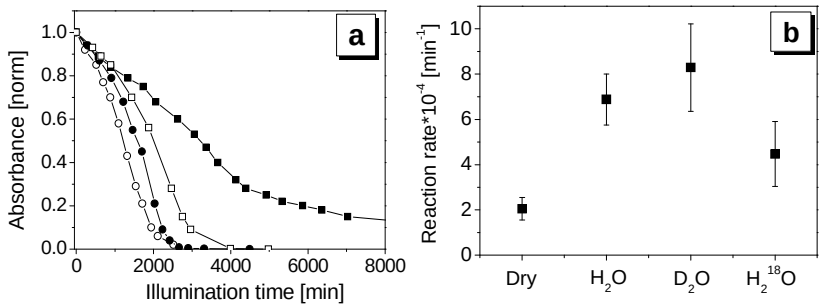

Fig.47 Time trace of the absorbance band at 520 nm during photo oxidation under dry synthetic air (full squares), synthetic air/H_2O (open circles), synthetic air/D_2O (full circles), synthetic air/$H_2{}^{18}O$ (open squares) normalized to the corresponding absorbance at t = 0. Panel b: reaction rates extracted from panel a via linear regression.

2. Product evolution in the presence and in the absence of humidity

In order to evaluate the product evolution during photo oxidation, FT-IR spectroscopy was employed at defined stages of degradation given by the loss of the UV/VIS main absorption at 520nm. In the following, the differences in the IR-spectra will be described for each spectral region. It will also be attempted to elucidate the chemical nature of the reaction products by chemical derivatization. The assignment of the FTIR signals in the pristine P3HT film was already presented in section III.2.3.1.

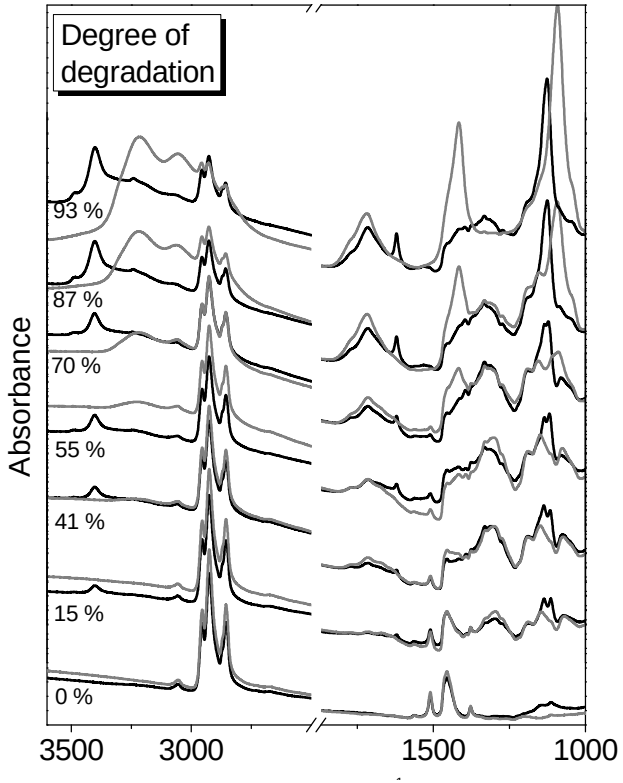

Fig.48 FTIR spectra of the P3HT photo-oxidation carried out under dry (grey lines) and humidified conditions (black, H_2O, 100% rel.hum 22°C). Data were recorded in the same experiment as shown in Figure 1. Additionally, the loss of the main UV/VIS absorption band at 520nm is given.

Product evolution in the carbonyl range (1800-1600 cm^{-1})

In the region of carbonyl stretching vibrations a broad band appears during degradation for both dry and humidified conditions. This band seems to consist of at least four species located at 1775 cm^{-1}, 1715cm^{-1} and 1670cm^{-1} and 1620cm^{-1} as presented in Fig. 49. The spectral shape under both dry and humidified conditions is quite similar except for a strong and narrow absorption band at 1620 cm^{-1} in the presence of humidity (Fig. 49 panel b).

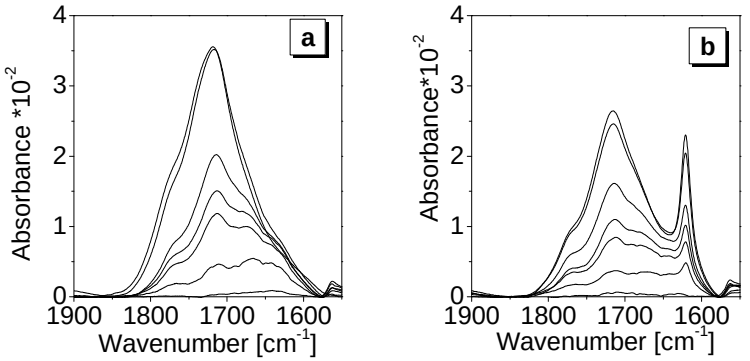

Fig. 49 FTIR carbonyl detail spectra during degradation extracted from Fig.48 Panel a: Degradation carried out under dry synthetic air conditions, Panel b: Degradation carried out under synthetic air with 100% rel.hum. at 22°C.

In order to make clear statements about the chemical nature of the carbonyl species the presence of ketone, aldehyde, anhydride, ester and carboxylic acid functions has to be considered. Due to the fact that the polymer under consideration contains a thiophene ring, additionally the presence of thiolesters has to be regarded. According to the identification methods by chemical derivatization described in section I.3.4, P3HT thin films degraded under dry conditions were exposed to water and NH_3 vapour to check for anhydrides, esters and carboxyl functions Fig.50. The exposure of a degraded P3HT thin film to water vapour leads to the formation of an additional feature at 1588 cm^{-1} (Fig.50 panel a) which is reversible upon thermal annealing. Therefore this species is attributed to the bending vibration of absorbed water. The carbonyl region does not exhibit remarkable changes pointing to the absence of large amounts of anhydrides as these would rapidly decompose. Furthermore no other spectral changes are observed, suggesting that generally no species are present which are sensitive to hydrolysis. As a consequence, the presence of thiolesters is rather unlikely as they are very sensitive to hydrolysis.

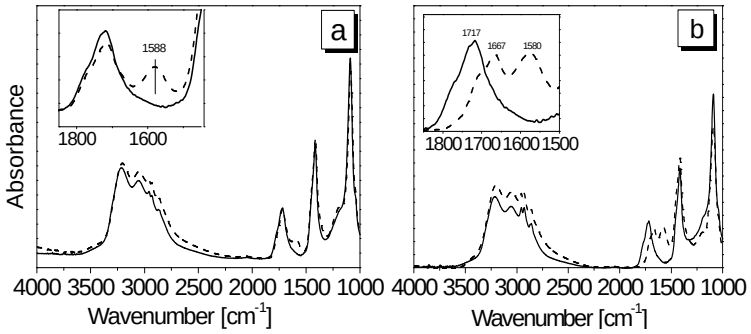

Fig.50 FTIR spectra of P3HT thin films degraded under dry synthetic air (full lines) with subsequent derivatisation (dotted lines) with water (panel a) and NH_3 (panel b).

Derivatization with NH_3 strongly affects the carbonyl range. The signal at 1775 cm^{-1} strongly decreases upon NH_3 treatment together with the occurrence of signals at 1667 cm^{-1} and 1588 cm^{-1}. Whereas the first one can be assigned to an amide function, the latter most probably originates from adsorbed water as discussed above. Based on these results the species at 1775 cm^{-1} can be clearly assigned to an ester function whereas the assignment to anhydride species is ruled out. Further support of this interpretation comes from an increased absorption in the hydroxyl range (3500-3100cm^{1}) upon NH_3 treatment which is expected upon the reaction of an ester with NH_3 (see section I.3.4). The increased hydroxyl absorption additionally points to the absence of carboxylic acids as these would be consumed in the reaction with NH_3 consequently leading to a lowered hydroxyl absorption. The band at 1715cm^{-1} is assigned to an aliphatic ketone[11,26] which does not show significant reactivity towards derivatization with NH3 or humidity.

Tab. 6 Assignment of carbonyl species created during degradation of P3HT and the used derivatization technique.

$\tilde{\upsilon}$ [cm^{-1}]	Assignment	Derivatization
1775	Ester	Reacts with NH_3, yielding amide and H_2O No reaction with H_2O
1715	Aliphatic ketone	Literature[11].No reaction with NH_3 and H_2O
1670	Conjugated carbonyl Probably α,β-unsaturated	Spectral position, no reaction with water and NH_3
1620	**C=C**-C=X, X =C, O	

The 1620cm^{-1} signal is strongly pronounced in the presence of humidity. Interestingly the peak is rather sharp compared to the other carbonyl moieties. In order to quantify this observation, peak fitting using Voigt profiles was employed revealing that the FWHM of the carbonyl species is roughly 45 cm^{-1}. The FWHM for the sharp 1620cm^{-1} signal is about 14cm^{-1}. Therefore it seems that this peak is an additional feature created in the presence of humidity and is superimposed to a carbonyl species in the same region. Interestingly the FWHM of 14 cm^{-1} is also observed for the thiophene double bond signal at 1510cm^{-1} at t = 0. These observations suggest that this feature may arise from isolated double bonds which are created during the degradation process. The assignment to the bending vibration of adsorbed water is rather unlikely as this signal is not sensitive to D_2O derivatization (Fig.51) where a spectral red shift of several hundred wave numbers is expected due to a hydrogen deuterium exchange. Furthermore this band is only slightly affected by thermal annealing (Fig. 52).

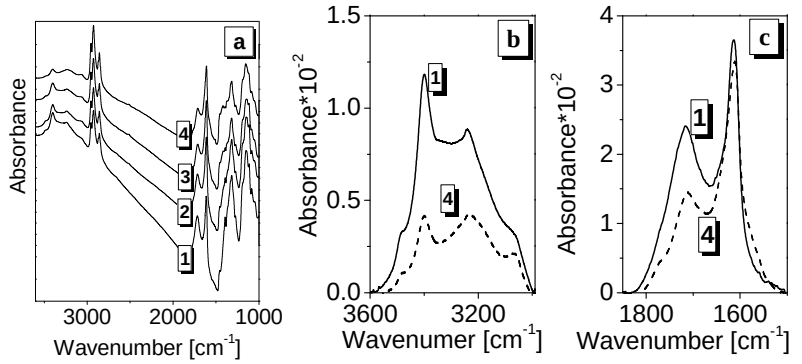

Fig.51 FTIR spectra of P3HT thin films degraded under humidified synthetic air with subsequent derivatization. Panel a: (1) as degraded, (2-4) subsequent exposure to D_2O vapor in the dark for 17 h, 65h, and 137 h, respectively. Panel b: Hydroxyl range extracted from panel a. Panel c: Carbonyl range extracted from panel a.

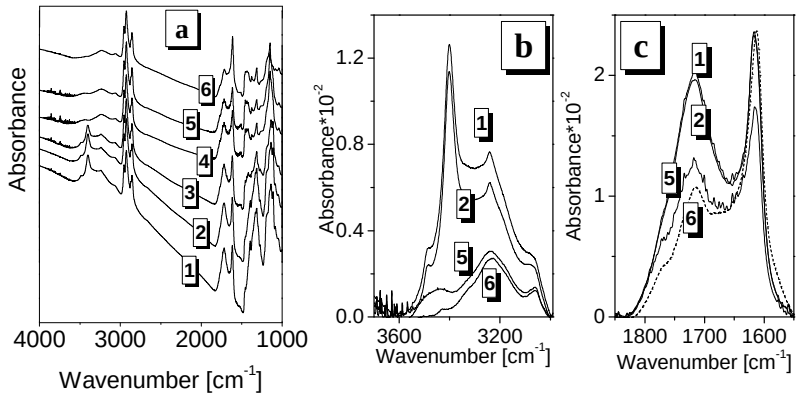

Fig. 52 FTIR spectra of P3HT thin films degraded under humidified synthetic air with subsequent derivatization Panel a: (1) as degraded, (2) after 12h at 1mbar and T=293K, (3) after 30 min at 1 mbar and T = 413K, (4) after 90 min at 1mbar and T =413K, (5) after 150 min at 1mbar and T=413K, (6) after 15h in water vapor and darkness at 293 K, subsequent to thermal annealing in vacuum. Panel b: Hydroxyl range extracted from panel a. Panel c: Carbonyl range extracted from panel a.

Product evolution in the hydroxyl stretching range (3500 cm^{-1}-3100 cm^{-1})

In the range of OH stretching vibrations the degradation of P3HT leads to the appearance of several broad bands. For the degradation carried out in the absence of humidity two dominant features are observed with maxima at 3060 cm^{-1} and 3215 cm^{-1}. Interestingly these bands are strongly suppressed in the presence of humidity with an additional sharper OH feature evolving at 3400 cm^{-1} (Fig.48). The difference in the half widths of the signals observed under dry and humidified conditions already points to the presence of strong hydrogen bonds under dry conditions which lead to a spectral broadening and to a red shift of the signal. For a detailed chemical analysis several OH containing groups have to be considered, namely adsorbed water (H_2O ads.), alcohol functions (R-OH), carboxylic hydroxyl functions (RCOOH), and hydroperoxide groups (ROOH). Before the detailed chemical analysis will be presented the presence of adsorbed humidity (H_2O) is discussed. During degradation water can either originate from the ambient humidity or from water generated in a chemical reaction. The spectral shape of the hydroxyl absorption band strongly depends on the polymer water interaction, with both broad unstructured[81] and structured[82] bands observed in literature. In order to check for a simple adsorption process of the polymer itself a pristine P3HT thin film was

exposed to humidified air for the timescale of the photo degradation experiments. No hydroxyl species were observed as a consequence of the treatment, revealing that the polymer itself does not significantly adsorb water[83,84]. However the film properties strongly change during the degradation process as evident from the rising carbonyl products which probably cause enhanced hydrophilicity. Interestingly the species at 3060 cm^{-1} and 3215 cm^{-1} are strongly present upon degradation under dry synthetic air but are hardly visible in the presence of humidified air. This makes the assignment to absorbed humidity from the ambient air unlikely. Further support comes from drying experiments which reveal that these bands vanish upon thermal annealing but do not recover upon subsequent exposure to humidified air. This behavior upon thermal annealing is also observed for the 3400 cm^{-1} band in the presence of humidity (Fig. 52). Here the assignment to adsorbed water was additionally checked by exposing a degraded sample to D_2O vapor (Fig.51). Upon the presence of adsorbed humidity an isotopic exchange is expected which would lead to a redshift of the signal. However this was not observed, thus further supporting that this species is not due to adsorbed moisture.

The assignment of the observed hydroxyl species to any kind of adsorbed water is therefore rather unlikely for samples degraded both in the presence and in the absence of humidity in the ambient air. As the absence of significant amounts of adsorbed water is eliminated, the question remains whether the observed hydroxyl functions can be assigned to carboxylic (ROOH) or alcoholic (ROH) species. In the first case derivatization using NH_3 should result in a rapid decline of the hydroxyl absorption due to the deprotonation of the acidic function. However the contrary, an increased hydroxyl absorption, is observed for sample degraded under dry conditions (Fig.50 b). On the one hand, this points to the absence of significant amounts of carboxylic acids and on the other hand this indicates the presence of R-OH, formed the aminolysis of the ester function identified in the previous section. In order to prove the presence of alcoholic R-OH species, derivatization using TFAA was employed. Here the hydroxyl absorption (3500cm^{-1}-3000cm^{-1}) partially declines, a new feature in the carbonyl region at 1786 cm^{-1} appears, the signal at 1414 cm^{-1} decreases whereas the absorption at 1089cm^{-1} seems to shift to 1163cm^{-1}(Fig. 53). These findings are in line with the expected reaction products of ROH groups with TFAA where ROH is consumed and a new carbonyl is created. Furthermore these observations allow to assign the C-O stretching vibration of the alcoholic ROH group to the band at 1089cm^{-1} which is transformed into the C-O function of the TFA-ester at 1163 cm^{-1}. The signal at 1414 cm^{-1} is assigned to the bending vibrations of the alcoholic ROH groups which also decrease. In the case of degradation carried out in the presence of humidity the band at 3400 cm^{-1} is insensitive against treatment with NH_3 and TFAA revealing that this species does not originate from any acidic or alcoholic functions. Finally the question remains whether this species can be attributed to the presence of hydroperoxides (ROOH). Hydroperoxides in polymer degradation are known to be thermally labile at 120°C [85]. Interestingly the species at 3400 cm^{-1} completely disappears upon thermal annealing at 120°C and 1 mbar within only 90 min. In contrast the identified alcohol function formed under dry conditions takes more than 30 hours to decompose. These observations suggest that the vibration at 3400 cm^{-1}

might be assigned to a hydroperoxide species. The assignment of hydroxyl functions is summarized in Tab. 7.

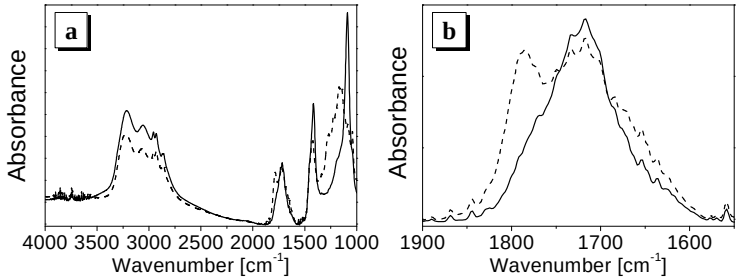

Fig. 53 Panel a: FTIR spectra of P3HT thin films degraded under dry synthetic air (full lines) with subsequent derivatization (dotted line) with TFAA. Panel b: Carbonyl region extracted from panel a.

Tab. 7 Assignment of hydroxyl species created during degradation of P3HT and the used derivatization technique.

$\tilde{\upsilon}$ [cm^{-1}]	Assignment	Derivatization
3060	R-OH	Esterification with TFAA No reaction with NH_3 Disappears upon drying, no recovery upon humidification
3215	R-OH	Esterification with TFAA No reaction with NH_3 Disappears upon drying, no recovery upon humidification
3460	R-OOH	Disappears upon thermolysis No reaction with TFAA No reaction with NH_3 Disappears upon drying, no recovery upon humidification No H/D-exchange

Product evolution in the fingerprint range (<1400 cm^{-1})

In the region below 1400 cm^{-1} a large number of overlapping signals evolve during the degradation process. It is therefore not possible to unambiguously identify all of them although it is known from literature that oxidized sulphur species (e.g. sulphones or sulphates) absorb in this region. However it is a useful approach to assign the most prominent signals. In the case of degradation carried out under dry conditions there are two species located at 1414 cm^{-1} and 1089cm^{-1}. Based on the derivatization experiments with TFAA described in the previous section these bands are assigned to the OH bending and the C-O stretching vibration of an alcohol.

Degradation under humidified conditions leads to the formation of a prominent feature at 1126 cm^{-1} which might also be assigned to a C-O stretching vibration most probably from the assigned hydroperoxides species at 3400 cm^{-1}.

Tab. 8 Assignment of species created during degradation of P3HT and the used derivatization technique.

Frequency / cm^{-1}	Assignment	Derivatization
1414	Alcoholic OH-bending	Disappears upon esterification with TFAA
1126	Hydroperoxide C-O stretching	Disappears upon thermolysis Appears upon degradation under humid conditions
1089	Alcoholic C-O-stretching	Shifts to 1163 cm^{-1} upon esterification with TFAA Appears upon degradation under dry conditions

3. Isotopic labeling with D_2O and $H_2{}^{18}O$

In order to further evaluate the role of humidity during the photo oxidation of P3HT isotopic labeling experiments with D_2O and $H_2{}^{18}O$ were carried out. Although it is obvious from the product evolution above that water does influence the photo oxidation process it is so far not clear whether this originates from water acting as promoter for a single reaction step and or water being a reactant which is consumed during the chemical reaction. The question whether hydrogen or oxygen originating from the water molecule is incorporated into the reaction products during the degradation can be answered using isotopic labeling with D_2O and $H_2{}^{18}O$. In the following, the product evolution of P3HT thin films degraded under humidified conditions with D_2O (Fig.54) and $H_2{}^{18}O$ (Fig.55) will be compared separately to the data recorded under humidified conditions with regular $H_2{}^{16}O$ as presented in the previous section.

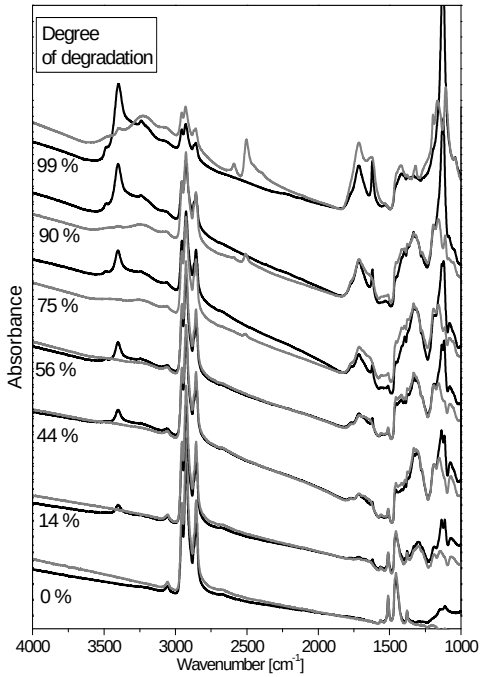

Fig.54 FTIR reaction spectra of the P3HT photo oxidation carried out under H_2O (black lines) and D_2O (gray lines), 100% rel.hum 22°C. Additionally, the loss of the main UV/VIS absorption band at 520nm is given.

Comparing the spectral evolution of P3HT during degradation under H_2O and D_2O humidified conditions shows mostly the same product distribution (Fig.54). However, two features evolves at 2500cm^{-1} and 2591 cm^{-1} with the same spectral shape as the hydroxyl vibration at 3400 cm^{-1} and the shoulder at 3486 cm^{-1} in the presence of H_2O. Taking into account the change in the reduced mass between OH and OD the observed shift is in good accordance with Eq.17 which predicts an isotopic shift from 3400cm^{-1} to 2475cm^{-1}. This strongly supports the idea that deuterium of the heavy water molecule is chemically reacting during the degradation process. This interpretation is further confirmed by the fact that a sample degraded under humidified conditions with subsequent exposure to D_2O for twice the time of the complete degradation process does not show the observed spectral shifts of the hydroxyl signals Therefore the presence of a hydrogen/deuterium exchange and thus the assignment to adsorbed water can be ruled out (Fig.51 a). The band located at 1620 cm^{-1} (Fig.54) is broadened but not strongly shifted by isotopic labeling with deuterium as observed for the hydroxyl vibrations at 3400 cm^{-1}. This further supports the statement that this band cannot originate from any vibration of adsorbed water. Taken together these results strongly suggest that the hydrogen atom out of the water molecule is incorporated into reaction products of the photo oxidation process.

Isotopic labelling using $H_2{}^{18}O$ (Fig.55) reveals some strong differences compared to the product distribution observed under humidified conditions. First, the influence on the carbonyl products (1800cm^{-1}-1550 cm^{-1}) will be discussed. According to Eq.17, the exchange of ^{16}O to ^{18}O in a carbonyl group leads to a spectral red shift of roughly 40 cm^{-1} which should be visible in the FTIR spectra. Indeed the carbonyl band is strongly broadened when switching from H_2O to $H_2{}^{18}O$ during degradation, pointing to the presence of $C^{18}O$ products. This clearly reveals that oxygen of the $H_2{}^{18}O$ water molecule is incorporated into reaction products of the photo degradation. Furthermore, the spectral broadening reveals that both ^{16}O of $^{16}O_2$ gas and ^{18}O of the $H_2{}^{18}O$ are present in roughly the same concentration. Otherwise no broadening but a red shift would be observed upon complete exchange to ^{18}O. Interestingly the bands located at 3056 and 3215 cm^{-1} are strongly suppressed until the latest stages of degradation but then rise. This suggests that other isotopic effects are present in the photo reaction. However their nature remains an open question here.

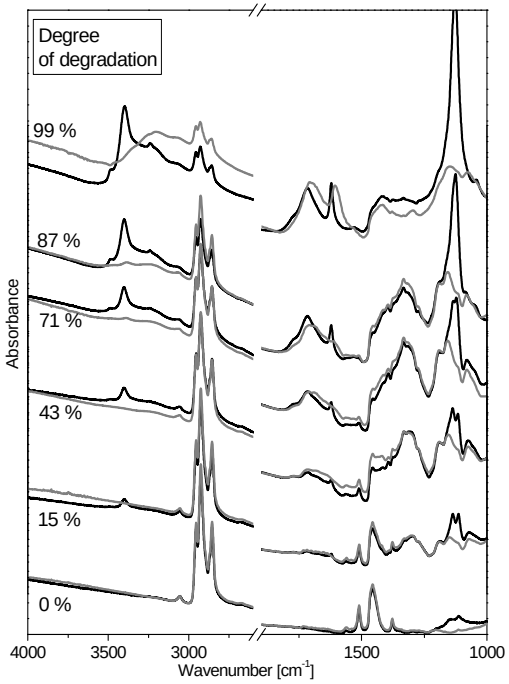

Fig.55 FTIR spectra of the P3HT photo oxidation carried out under H_2O (black lines) and $H_2{}^{18}O$ (gray lines), 100% rel.hum 22°C. Additionally, the loss of the main UV/VIS absorption band at 520nm is given.

4. Decay kinetics of the photo oxidation in the presence and absence of humidity

In order to get further insight into the role of humidity in the degradation process the temporal evolution of the surface concentrations was extracted from the single UV/VIS and FTIR spectra in as reported in the previous section III.2.2.6. As now hydroxyl functions are present the surface concentration of these species was calculated using the absorption at 3215 cm^{-1} under dry conditions respectively at 3400 cm^{-1} under humidified conditions and a molar absorption coefficient of 80 mmol cm^{-2} which is a typical value for hydroxyl species[86].

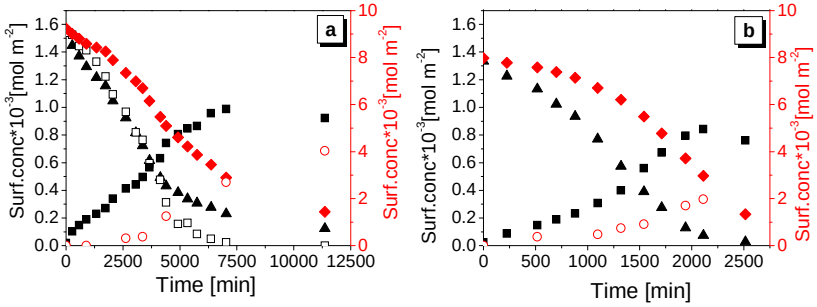

Fig. 56 Surface concentrations during photo oxidation under white light in synthetic air extracted from Fig.48. Panel a) degradation carried out under dry synthetic air, panel b) data obtained under humidified conditions (100% rel.hum at 22°C, H_2O). Concentrations: Thiophene rings out of UV/VIS data (full triangles), thiophene rings out of the FTIR C=C peak height at 1510 cm^{-1} (open squares), side chain groups out of the integrated FTIR C-H region (full diamonds), carbonyl groups out of FTIR (full squares), hydroxyl groups (open circles).

Under dry conditions (Fig. 56 a) the time traces of UV/VIS and C=C signals at first decrease almost linearly with an exponential part starting at roughly 80% loss. The fact that the thiophene ring concentration extracted from the UV/VIS signal (closed triangles) and the C=C signal of the FTIR (open squares) show the same decay kinetics confirms that the absorbance at 520 nm is a good measure for the quantification of the degradation process of P3HT as discussed in section III.2.1.2. While the signals of the polymer decrease with time, the carbonyl signal rises with a constant slope until the polymer is completely oxidized. Later the signal tends to decline, revealing that the carbonyls are not the final products. This is in good accordance with section III.2.1.1 regarding the formation of volatile species during the degradation process. At this point it has to be mentioned that the evolution of volatile species could not be monitored in these studies but has to be considered in order to discuss a possible mechanism properly.

In the case of humidified conditions the situation changes. The optical signal (closed triangles) and shows an increasing slope with prolonged degradation. The kinetics of the C=C signal in the FTIR cannot not be presented due to the presence of an evolving species at 1534 cm^{-1} which cannot be easily assigned or subtracted from the polymer signal. Even more interesting is the observation that the rate of carbonyl formation strongly increases at roughly 40% degradation indicated by the increased slope in the carbonyl evolution. The question now arises about the absolute concentration of the carbonyl species in the film. Interestingly, the same surface concentration is reached under dry and humidified conditions revealing that the concentration of carbonyls created within the film is the same under both conditions and furthermore equal to the concentrations observed in the single wavelength experiments presented in the previous section. The decay kinetics obtained for the isotopic labeling experiments show basically the same behavior of the polymer signals decaying. However a major difference was observed concerning the evolution of the carbonyl signals (Fig. 57).

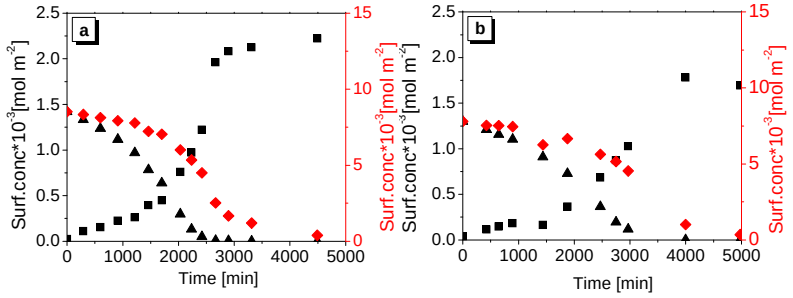

Fig. 57 Surface concentrations during photo oxidation under d synthetic air extracted from Fig.54 and Fig.55. Panel a) degradation carried out under D_2O humidified conditions, panel b) data obtained under $H_2{}^{18}O$ humidified conditions. Concentrations: Thiophene rings out of UV/VIS data (closed triangles), side chain groups out of the integrated FTIR C-H region (closed diamonds), carbonyl groups out of FTIR (closed squares).

First of all it seems that the relative carbonyl concentration is increased by roughly a factor of 3 compared to the experiment carried out in the absence of isotopic labeling (Fig. 56). Furthermore the slope of the carbonyl time trace strongly increases at the time when the thiophene signal calculated from the UV/VIS signal is almost completely down. As pointed out above the presence of isotopic labeling might influence several reaction pathways. However a detailed explanation for this behavior cannot be given with the experimental data at hand.

In summary the presence of humidity during the photo oxidation accelerates the degradation process by roughly a factor of 3. This factor does not depend on the presence of different isotopes within the water molecules suggesting that the splitting of the water molecule is not responsible for the

acceleration. The FTIR reaction spectra in the presence and absence of humidity reveal that the product distribution is strongly affected by the presence of moisture (see summary in Tab. 9). This is most prominent in the presence of different hydroxyl species. The question whether humidity acts as catalyst or as reactant being consumed during the degradation is answered using isotopic labeling. Here it turned out that both oxygen and hydrogen of the water molecule are incorporated into the reaction products as evident from spectral shifts in the presence of D_2O and $H_2{}^{18}O$. Therefore it can be clearly stated that water does directly participate in the photo oxidation process and is consumed during the reaction. However, other effects like water additionally acting as solvent stabilizing reactive intermediates cannot be ruled out. The assignment of all product species occurring during the degradation process is summarized in Tab. 9.

Tab. 9 Summary of the obtained product species of P3HT photo oxidation in the absence and in the presence of humidity.

ν [cm^{-1}]	Conditions		Assignment	Isotopic shift
	Dry	Humidified		
3400	--	X	R-OOH, OH stretching, hydroperoxides	with D_2O
3215	X	--	R-OH, OH stretching, alcohol	with D_2O
3060	X	--	R-OH, OH stretching, alcohol	with D_2O
1775	X	X	ROOR, C=O stretching, ester	With $H_2{}^{18}O$
1715	X	X	RCOR, C=O stretching, ketone	With $H_2{}^{18}O$
1670	X	X	C=O,	With $H_2{}^{18}O$
1620	X	X	C=O,	With $H_2{}^{18}O$
1620	-	X	C=C, sharp feature	--
1414	X	--	R-OH, OH bending, alcohol	--
1126	--	X	R-OH, C-O stretching, alcohol	--
1089	X	--	R-OH, C-O stretching, alcohol	--

III.3 Modeling of polymer photo degradation

III.3.1 Theory and function of the algorithm

Understanding the experimentally obtained reaction kinetics is a major step in the elucidation of the chemical mechanism of polymer degradation. In order to obtain a deeper insight into the degradation process upon photochemical decomposition of P3HT a numerical simulation was established using a Matlab program. The simulation attempts to describe the photo-induced destruction of the π-conjugated system of P3HT in the solid state and the resulting UV/VIS data (reaction spectra) on the basis of simple mechanistic considerations concerning:

1.) The absorption of mono- or polychromatic light.

2.) The mobility of the reactive center after the absorption process.

3.) The fragmentation pattern of the pi-conjugated system of the polymer.

4.) The thickness of the polymer film.

The detailed description of the algorithm is presented in Appendix A. In solid state photochemistry, the consideration of Lambert-Beer's law is of major importance due to the fact that the degradation process is light initiated and the reaction rate thus depends on the intensity of the light absorbed by the reacting species. In contrast to the homogeneous case like well-stirred solutions, regions close to the surface are exposed to higher photon densities than regions which are more remote from the illuminated surface (Fig. 59 left). This gradient in the photon density might lead to the occurrence of reaction gradients in the thin film. In order to quantitatively account for this behavior, the simulation is performed with monochromatic light for which both the incoming intensity and the extinction coefficient of the film are known. White light illumination is approximated by polychromatic illumination with up to 8 wavelengths. The layer thickness can be increased in nanometer steps starting at 1 nm without an upper limit. The Lambert Beer law is applied by dividing the complete polymer in sublayers j (Fig. 59 left) and calculating the number of absorbed photons in each sublayer j according to the present concentration of thiophene rings and the length distribution of intact thiophene chains. The consideration of the chain lengths is of major importance because it has a significant effect on the change of the polymer absorption, e.g. the absorption characteristics of oligothiophenes critically depend on the chain length for N<10 thiophene units as presented inFig. 58

assuming Gaussian functions for the absorption (the details of the Gaussian function are presented in the Appendix A).

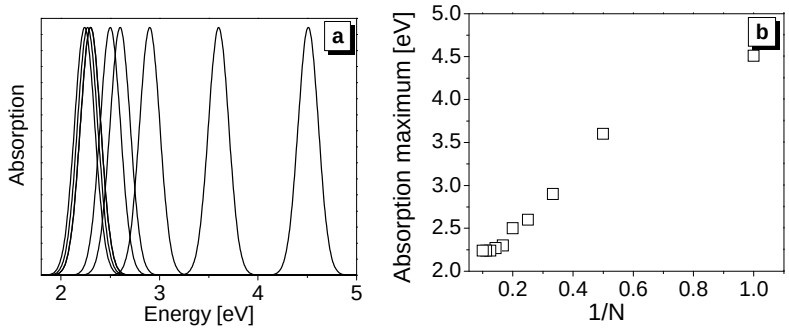

Fig. 58 Panel a: Absorption of oligothiophenes used in this work. Panel b: Absorption maximum position of the used oligomers as function of the reciprocal chain length 1/N extracted from panel a.

After the absorption of light single thiophene rings are destructed with a defined quantum efficiency, leading to the fragmentation of the initial po lymer chain. Consequently the fragmentation pattern of the π-conjugated system of the polymer has to be considered during the degradation process. In the following only the fragmentation of the π-conjugated system is considered. Statements about the disruption of the polymer σ-backbone are not part of this simulation. So far two border cases of the chain fragmentation pattern have been discussed in the field of polymer degradation[87,88] (Fig. 59 right). Whereas end chain breaking[89] assumes that the polymer chain is decomposed by destroying exclusively the terminal monomer units, random chain breaking assumes that the position of a destroyed thiophene ring is completely random. In the first case the π-conjugated system is shortened step by step with short oligomers with n < 10 thiophene units occurring only towards the very end of the decomposition process whereas in the latter case significant amounts of small oligomers appear at every stage of the degradation process. As the absorption maximum of oligothiophenes depends strongly[35]on the number of conjugated thiophene rings for n < 10 thiophene units, the occurrence of smaller fragments will lead to a spectral shift of the UV/VIS absorption spectra towards shorter wavelengths. These oligomers are also considered to react according to their absorption properties.

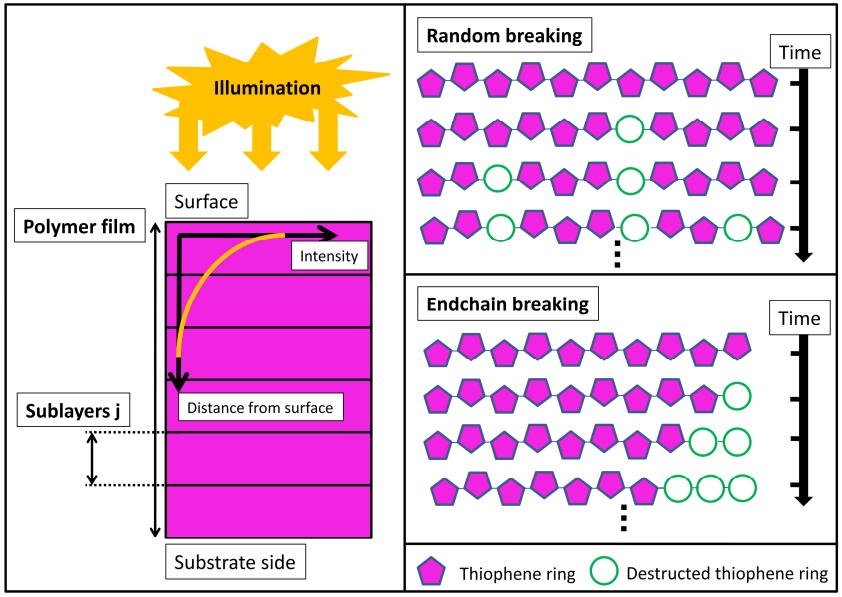

Fig. 59 Scheme of the basic concepts considered in the numerical simulation of P3HT thin film decomposition. Left: Polymer film divided in sub layers and illumination from the surface side. Right: Random (top) and end chain (bottom) fragmentation of a polymer as a function of time

Besides the absorption of light and the chain fragmentation pattern of the polymer the mobility of the reactive center created after the absorption process remains an important issue as mentioned above. Under classical photochemical conditions in solution the chemical reaction is localized on the molecule which is involved in the absorption process. However this is not necessarily the case in the solid state, as mobile reactive centers might be created after the absorption process. Well-known examples for mobile reactive centers are diffusing excitons created by the absorption process or radical species formed during the reaction. The detailed physical or chemical nature of the active species is not considered in the algorithm. The simulation approaches these considerations using two limiting cases for the nature of the reactive center created by the absorption of photons. The first mechanism is dealing with a strongly localized reactive center (classical photochemical case) which remains on the absorbing polymer fragment (Fig. 60 left). Here the polymer fragment i absorbs, the reactive centre remains on fragment i resulting in the destruction of a thiophene ring on the fragment i.

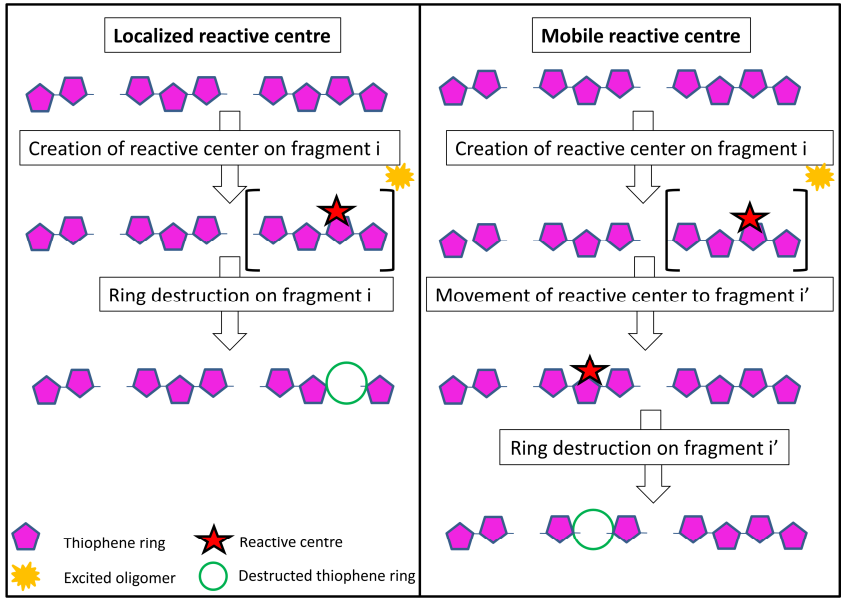

Fig. 60 Scheme of reaction mechanism in the classical photochemical approach (left) and radical like reaction (right) of polymer chains (pink). The excited fragment is marked in brackets with yellow star, the reactive center is indicated as red star, whereas the destructed thiophene ring is indicated as green open circle.

The second mechanism allows the created reactive center to be transferred to polymer fragments which were not involved in the absorption process (Fig. 60 right). Here the fragment i absorbs with subsequent transfer of the reactive centre to the fragment i´ in the same or any other sublayer j. Afterwards a thiophene ring is destroyed on the fragment i´. In this case the reactive centers are free to move within the complete polymer film. The diffusion of oxygen is not taken into account as the reaction has been shown not to be limited by oxygen diffusion (section III.2.2.3). Furthermore the occurrence of chemical substituents located at intact thiophene rings which may affect the spectral position of smaller oligomers is not considered at the moment.

The time counter of the simulation is given by the incoming photon flux. Therefore each time step in the simulation represents an illumination of the polymer for one second with a constant, incoming photon flux I_0 which can be varied.

III.3.2 Simulation results

In the following the results of the simulation will be presented. Here the attempt is made to simulate experiments which were presented in the previous sections using monochromatic or polychromatic illumination. First the classical photochemical case with localized reactive centers will be discussed. Here the influence of the light absorption and the fragmentation pattern of the polymer will be addressed. The consequences for the thin film properties will be discussed (e.g. spectral shifts and surface enhanced degradation). This gives valuable information about the expected degradation behaviour of thin films in the solid state upon the presence of a simple photo reaction. Subsequently deviations from the classical photochemical behaviour will be presented assuming the presence of a reactive mobile centre. Finally white light conditions under AM1.5 conditions will be adressed using polychromatic light. The following data were calculated assuming an initial polythiophene chain length of 300 thiophene rings which is an average value for commercially available P3HT used in the experimental section.

III.3.2.1 Influence of light absorption on photo-degradation under classical conditions

The simulated reaction spectra of a 100 nm P3HT thin film are presented in Fig. 61 for monochromatic illumination with 365nm (panel a) and 547 nm light (panel b), assuming end chain breaking and classical photochemical conditions. The end chain scission mechanism is applied here because spectral shifts are expected to be absent during the major part of the degradation process. Both 365nm and 547 nm illumination lead to the decay of the polymer absorption without significant spectral changes until the latest stages of degradation. Towards the very end of the reaction (Fig. 61 insets) the reaction spectra show strong differences between 365 and 547 nm conditions. Whereas the absorption decays without spectral modifications under 365 nm illumination, a shift towards shorter wavelengths is observed in the 547 nm case. These observations can be explained by the end chain scission of the polymer. Smaller oligomers absorbing at shorter wavelengths are only present in the latest stages of degradation. Due to their spectral absorption position these oligomers are decomposed under 365nm illumination but remain inactive under 547 nm as they do not longer absorb photons. Therefore these fragments accumulate and lead to the observed spectral shift observed.

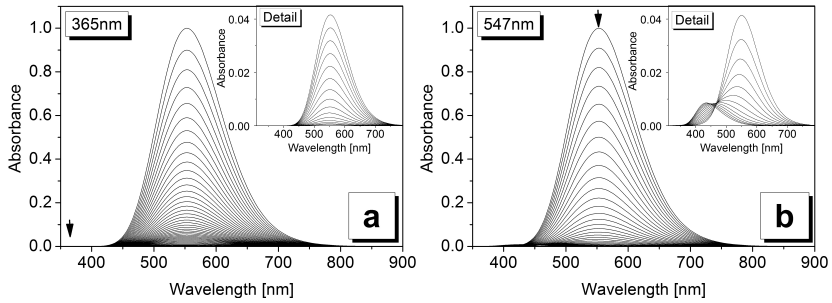

Fig. 61 Simulated UV/VIS spectra assuming classic photochemical conditions end chain breaking. Monochromatic illumination with 365 nm, 10^{-1}mol photons cm^{-2} (panel a) respectively 547 nm, 10^{-7}mol photons cm^{-2} (panel b) is used. Insets show the spectra towards the very end of degradation. The presented spectra represent a time interval of 100 seconds on the timescale of the simulation. The initial chain length was set to 300 thiophene units.

Although the wavelength used for the degradation causes only minor differences in the reaction spectra, it has prominent effects on the thin film properties during degradation.

In the case of 365nm illumination the polymer absorption is very weak with the penetration depth of the incoming light being larger than the film thickness ($d_{pen.} >> d_{film}$). Thus, the intensity profile does not show a significant gradient throughout the complete polymer film in (Fig. 62 a, open squares). Consequently the photo reaction rate is constant within the polymer film, resulting in a homogeneous decay of the polymer concentration over the complete 100 nm film thickness (Fig. 62 b).

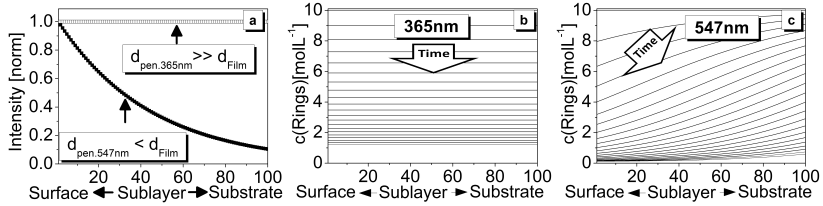

Fig. 62 Panel a: Light attenuation at 365 nm and 547 nm at t=0 for a 100 nm thin film of P3HT. Panel b: Time dependent concentration profile of thiophene rings at 365 nm illumination in a 100 nm P3HT film. Panel c: Time dependent concentration profile of thiophene rings at 547 nm illumination in a 100 nm P3HT film.

The situation changes using light of 547 nm which is strongly absorbed by the polymer with ($d_{pen.} < d_{film}$) . Here a strong gradient of the light intensity is observed (Fig. 62 a, full squares) resulting in a

higher photo reaction rate close to the surface. For this reason the concentration profiles under 547 nm illumination reveal a gradient during the degradation process with enhanced degradation at the surface (Fig. 62 panel c).

The temporal evolution of the gradient is demonstrated in Fig. 63 a where the average thiophene ring concentration of the complete film (trace 1), the surface region of 10 nm below the surface (trace 2) and the difference of both (trace 3) are shown. This comparison was chosen as these values represent the typical experimental conditions of UV/VIS or FTIR (both bulk sensitive) on one hand and XPS spectroscopy (surface sensitive) on the other hand. The shape of the observed kinetics will be discussed later on. During degradation the surface signal initially decays faster than the bulk signal. The difference of both signals (Fig. 63 panel a trace 3) reaches a maximum of 0.25 at the time index 500 meaning that the surface signal shows at maximum 25% more degradation than the bulk signal.

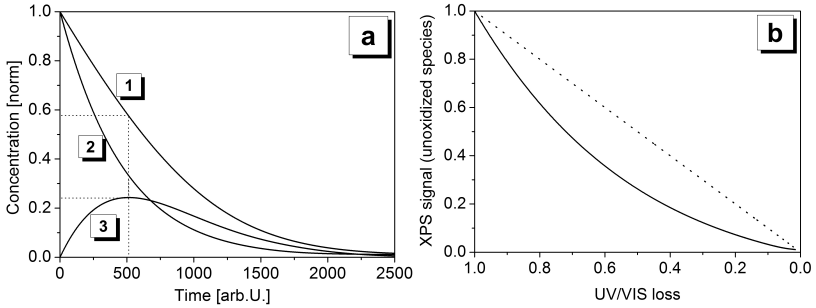

Fig. 63 Panel a: Time trace of the thiophene concentration in a 100 nm thin film. (1) Bulk signal of the complete polymer film, (2) Surface signal of the first 10 nm below the surface, (3) difference between surface and bulk signal with marked maximum (dotted lines). Data were extracted from Fig. 62 panel c. Panel b: Surface signal as a function of the bulk signal, data were extracted from panel a.

Plotting the surface signal as function of the bulk signal (Fig. 63 panel b) reveals the expected correlation between an XPS and UV/VIS transmission signal in the presence of a surface enhanced degradation. Upon the absence of a reaction gradient a linear correlation with a unit slope is expected (Fig. 63 panel b, dotted line). The reaction gradient will become more and more prominent by reducing the ratio between the penetration depth of the incoming light d_{pen} and the overall film thickness d_{film}. The presence of an enhanced reaction at the surface does also affect the observed degradation kinetics. The simulated decay kinetics of several polymer films of different initial film thickness and constant penetration depth of the incoming light are presented in Fig. 64.

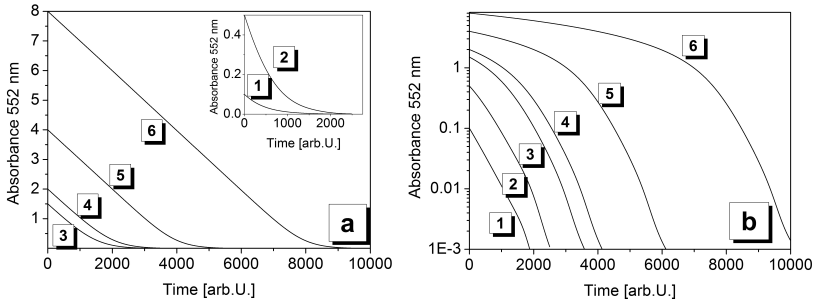

Fig. 64 Panel a: UV/VIS degradation kinetics at 552 nm of P3HT thin films under 547 nm illumination with initial thicknesses of 10 nm (1), 50 nm (2), 150 nm (3), 200 nm (4), 400 nm (5), 800 nm (6). Panel b: Same data as in panel a on semi logarithmic scale. Monochromatic illumination with 547 nm, 10^{-7}mol photons cm^{-2} is used. The initial chain length is set to 300 thiophene units. The penetration depth of the incoming light is d_{pen} = 50 nm, as extracted from the light attenuation according to Lambert Beer in the calculated films, Fig. 62 a.

Whereas a polymer film with initial thickness of 10 nm reveals an exponential decay (Fig. 64 panel b, trace 1) a more linear decay becomes prominent for thicker films. This can be understood taking into account the penetration depth of the incoming light of $d_{penetrate}$= 50nm. For polymer films thinner than this value, the attenuation of the incoming light I_0 is rather low resulting in an essentially homogeneous degradation of the complete film. In this case the number of absorbed photons I_{abs} declines during the degradation process according to:

$$I_{abs} = I_0\left(1-10^{-E}\right) \approx I_0 \cdot E = I_0 \cdot \varepsilon \cdot c_{surface}$$

with the absorbance E, the molar absorption coefficient ε, the surface concentration $c_{surface}$ and the quantum efficiency Φ, thus leading to an exponentially decreasing reaction rate.

$$-\frac{dc_{surface}}{dt} = I_{abs} \cdot \phi \approx I_0 \cdot \varepsilon \cdot c_{surface} \cdot \phi$$

For polymer films with $d_{film} >> d_{penetrate}$ this is not the case. Here the incoming light is completely absorbed in regions close to the surface. Although the polymer concentration decreases in this topmost area the absorption of photons is hardly affected as the remaining film thickness is still sufficient to lead to total absorption of the incident light (Fig. 62). Therefore the reaction rate remains constant

$$-\frac{dc_{surface}}{dt} = I_{abs} \cdot \phi \approx I_0 \cdot \phi = const$$

until the latest stages of degradation when the deviation from total absorption becomes significant.

Finally, the correlation of the UV/VIS signal at the absorption maximum and the concentration of thiophene rings in the polymer film has to be considered. Due to the fact that spectral shifts are observed only towards the very end of the degradation, the UV/VIS signal and the thiophene ring concentration correlate with a slope of 1 as will be shown below in Fig. 67.

In summary, the effect of the light absorption on the degradation process was demonstrated in this chapter using the end chain scission model. The end chain breaking has been chosen here because spectral shifts do not significantly occur until the latest stages of degradation. Furthermore the spectral shape of the UV/VIS reaction spectra does not depend on the wavelength of the incoming light until the very end of the reaction. In the final stages of degradation the reaction spectra depend on the incoming wavelength. Whereas 547 nm leads to a spectral shift originating from accumulation of shorter oligomers, these fragments are decomposed under UV light resulting in the absence of a significant blue shift. Furthermore it turned out that the ratio between the overall film thickness and the penetration depth of the incoming photochemical active light strongly affects the degradation process. For $d_{penetrate} >> d_{film}$ which typically is the case for UV light, due to the small extinction coefficient of polymers in this spectral region, a homogenous reaction within the complete polymer film is observed resulting in an exponential decay of the polymer concentration. In the case of $d_{penetrate} << d_{film}$ which corresponds to visible light close to the absorption maximum, a reaction gradient is observed within the film. This is due to the fact that surface near region exhibit higher photons flux densities than deeper regions of the polymer film. Here the decay kinetics are more linear. The observed reaction kinetics therefore strongly depend on the ratio $d_{penetrate} / d_{film}$, although the general mechanism is not changed.

III.3.2.2 Effect of π-system fragmentation pattern on the degradation process

In this chapter the influence of the random chain scission on the reaction spectra and the thin film properties during degradation is presented. As pointed out in the previous section this mechanism leads to the formation of smaller oligomers throughout the complete degradation process. These fragments absorb at shorter wavelengths as presented in Fig. 58. In order to investigate the consequences of this effect on the degradation process the UV/VIS reaction spectra were simulated first for different illumination wavelengths as presented in Fig. 65.

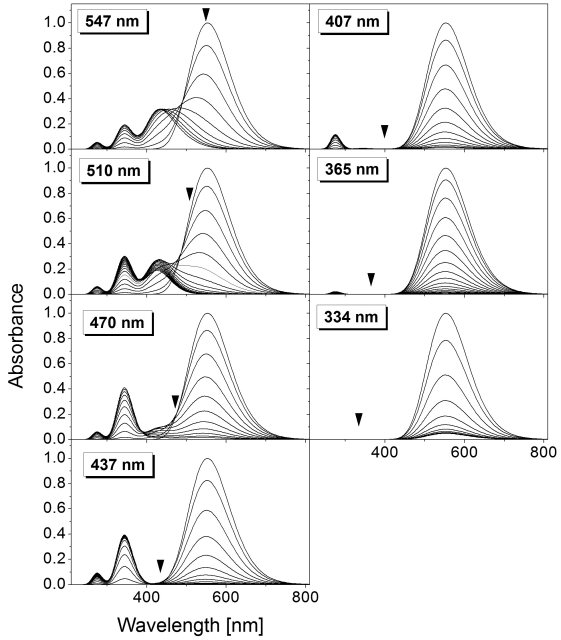

Fig. 65 Simulated UV/VIS reaction spectra of a 100 nm P3HT thin film according to the random chain scission mechanism using several single wavelengths as given in the panels. The spectral position of the incoming light is additionally marked by a black triangle. The initial chain length is set to 300 thiophene units.

The simulated illumination generally leads to the decay of the polymer absorption. However there are remarkable differences between the different illumination wavelengths. Light of 547 nm leads to the blue shift of the spectrum during degradation together with the evolution of absorption features at shorter wavelengths. Here, maxima at 425 nm (ter-thiophene), 342 nm (bi-thiophene) and 274 nm

(mono-thiophene) are visible which is in line with the formation of shorter polymer fragments. As the absorption of these species does not match the wavelength of the incoming light of 547 nm, they do not absorb light and thus do not decompose. In other words, the reaction stops at a defined stage and shorter oligomers accumulate. Reducing the wavelength of the incoming light leads to the reduction of absorption in the shorter wavelength range together with the diminution of the spectral blue shift of the complete spectrum (Fig. 65). This behavior originates from the fact that smaller oligomers created due to the random chain mechanism are capable of absorbing incoming photons in the near UV range. Therefore these oligomers are decomposed and do not longer accumulate. In the extreme case of illumination with 334 nm the oligomers of all lengths may absorb light. Therefore the steady state concentration of these species is rather low. Hence, no spectral shift is observed, with the reaction spectra being quite similar to those observed for the end chain scission of the polymer. The concentration profiles obtained under illumination at 365 nm and 547 nm further demonstrate this effect. In the case of illumination at 547 nm the reaction stops, although more than 50% of the initial thiophene ring concentration is left (Fig. 66 panel b).

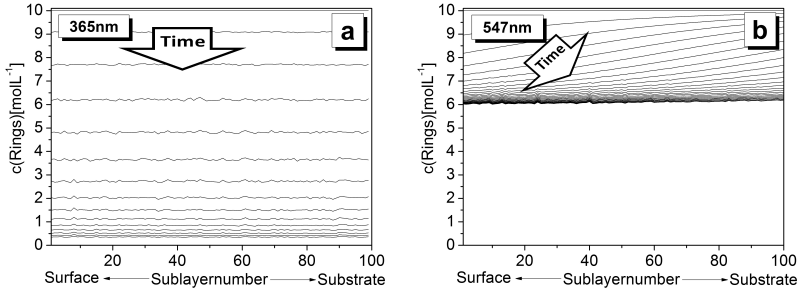

Fig. 66 Panel a: Time dependent concentration profile of thiophene rings at 365 nm illumination in a 100 nm P3HT film. Panel c: Time dependent concentration profile of thiophene rings at 547 nm illumination in a 100 nm P3HT film. The simulation was performed assuming random chain scission.

These thiophene rings belong to oligomers, which are to short to absorb photons of the incoming wavelength. In contrast, illumination with 365 nm light leads to the homogeneous decrease of the thiophene ring concentration (Fig. 66 panel a).

Due to the observed spectral shifts it is interesting to compare the decay kinetics extracted from the UV/VIS spectra with the decay of the thiophene ring concentration in the film (Fig. 67). In the case of end chain scission the UV/VIS signal and the thiophene ring concentration decay with the same slope. This is observed under both, 365nm and 547 nm illumination (Fig. 67, panels a and c). The shape of the decay kinetics assuming the end chain scission mechanism is influenced by the used irradiation wavelength which is explained by the different ratios of light penetration depth and film thickness

presented in the previous section. For an increasing ratio of $d_{Film}/d_{Penetrate}$ the kinetics become more and more linear.

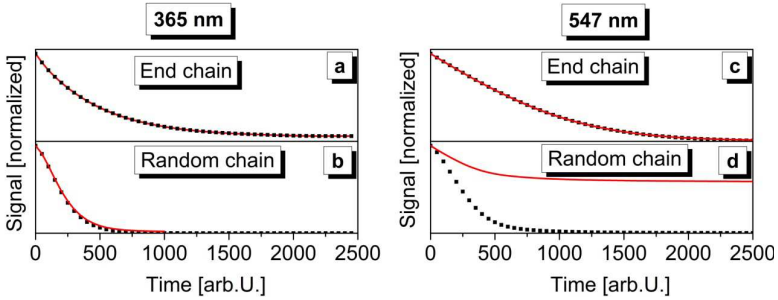

Fig. 67 Decay kinetics of a 100nm P3HT film under 365nm and 547 nm illumination. Black dots show the time trace extracted from the UV/VIS reaction spectra at 552 nm. Full red lines show the average concentration of thiophene rings in the complete film. Panel a) 365nm end chain scission, panel b) 365 nm random scission, panel c) 547 nm end chain scission, panel d) 547 nm random scission. The initial chain length is set to 300 thiophene units.

In the case of the random chain mechanism there are some differences concerning the shape of the decay kinetics and the correlation between UV/VIS signal and thiophene ring concentration. First of all the UV/VIS decay, both under 365nm and 547 nm illumination, is strongly accelerated compared to the end chain scission. Furthermore the shape of the UV/VIS kinetics is quite similar between 365 nm and 547 nm (Fig. 67 panel b and d).

The most striking difference is obtained in the case of 547 nm illumination (Fig. 67 panel d) where the UV/VIS signal completely decays, but the thiophene ring concentration stabilizes at roughly 80 % of the initial value. The acceleration of the polymer degradation in the UV/VIS upon the random chain scission mechanism with respect to end chain breaking can be understood by the creation of smaller oligomers absorbing at shorter wavelengths. Therefore the polymer signal at a given wavelength is reduced not only by the direct destruction of thiophene rings but also by the resulting spectral shift of the spectrum as presented in Fig. 65 (the fastest decay of UV/Vis absorption would be observed if always the central ring of all oligomers were destructed). In the case of 547 nm illumination shorter oligomers with blue-shifted absorption maxima accumulate, leading to the difference between thiophene ring concentration and the UV/VIS signal at 552 nm (Fig. 67 d). In contrast, illumination at 365 nm also decomposes shorter oligomers. Therefore the decay kinetics of thiophene concentration and UV/VIS signal show the same behavior (Fig. 67 c).

In summary, the fragmentation pattern of the π-conjugated system may strongly affect the observed reaction spectra in the UV/VIS and the observed decay kinetics. The random chain scission mechanism generally leads to the presence of shorter oligomers and therefore a spectral blue shift of the spectrum during degradation. The steady state of these oligomers and therefore the shape of the reaction spectra critically depend on the wavelength of the incoming light. Under irradiation with visible light random and terminal scission mechanisms of the π-conjugated system can be clearly separated according to a strong blue shift in the case of random chain scission. In contrast, the reaction spectra simulated under UV light are very similar for the two scission mechanisms. Generally the degradation of the polymer in the UV is strongly accelerated in the presence of the random chain scission compared to the end chain scission. As stated above, this originates from the spectral blue shift of the spectrum, due to the formation of shorter oligomers during the degradation process. Experimentally the two scission mechanism might be discriminated with respect to the observed decay kinetics, the spectral blue shift and especially comparing the UV/VIS signal and the concentration of thiophene rings which can be studied by FTIR.

The spectral information from the simulation may be compared to the experimental data obtained under monochromatic illumination. In section III.2.3.1 different reaction spectra were observed in the presence of visible or UV light. A spectral blue shift of roughly 100 nm was observed during degradation with light at 525 nm which is on the same order of magnitude as for the simulated reaction spectra (Fig. 65). However the general concentration of shorter oligomers seems to be lower in the experiment compared to the simulation. During experiments with 365 nm illumination a minor blue shift of 40 nm was observed mainly towards the end of the degradation process which is not obtained in the simulation. These observations suggest that at least in the presence of visible light the π-conjugated system is destructed partially by the random chain scission.

III.3.2.2 Effect of mobile reactive centre on degradation

So far, classical photochemical conditions were discussed. In this case molecules react from their excited state, i.e. only molecules which absorb photons undergo chemical reaction. The reactive center is therefore localized on the molecule participating in the absorption process. In the following this will be changed assuming the presence of a mobile reactive centre. After the absorption process this centre can shift to other oligomers of the entire film which were not involved in the absorption process (Fig. 60) with subsequent degradation of thiophene rings in these fragments. Chemically this mechanism may describe e.g. the presence of mobile radicals or mobile excitons. In the following the simulated reaction spectra will be presented for the extreme case of reactive centers which react with the same probability in the complete film. This case represents the presence of species which may cover a distance of multiple times the film thickness of the polymer. This may not be explained by the diffusion of excitons (~10nm), but by the presence of radicals with low reactivity.

For the end chain scission of the polymer the presence of mobile reactive centers does not significantly influence the obtained reaction spectra and decay kinetics (not shown here). However, the reaction spectra and the decay kinetics are strongly influenced in the case of the random chain scission (Fig. 68).

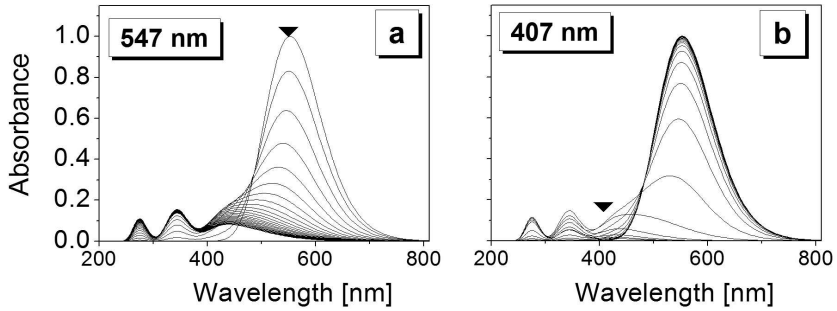

Fig. 68 Simulated reaction spectra of 100 nm P3HT thin films according to the random chain scission mechanism and the presence of mobile reactive centers. Panel a: 547 nm illumination, panel b: 407 nm illumination. The spectral position of the incoming light is additionally marked by black triangles. The initial chain length is set to 300 thiophene units.

The two examples shown in Fig. 68 present the decay of the polymer absorption together with a blue shift of the spectrum. Interestingly, the reaction spectra are quite similar for illumination by 547 nm light and to 407 nm light (Fig. 68 panel a, b). This represents a major difference compared to the data

presented in the previous section (localized reactive centers) where the reaction spectra were strongly dependent on the incoming wavelength. This is explained by the fact that the mobile reactive centers created are distributed over all oligomers of the complete film, independently of the incident wavelength. The decay kinetics in the presence of localized and mobile reactive centers are presented in Fig. 69 for both illumination at 407 nm and 547 nm. In the case of 407 nm illumination the presence of mobile reactive centers leads to a strongly accelerated degradation compared to presence of localized reactive centers. Illumination with light of 547 nm leads to the deceleration of the UV/VIS decay and the slight acceleration of the thiophene concentration decay.

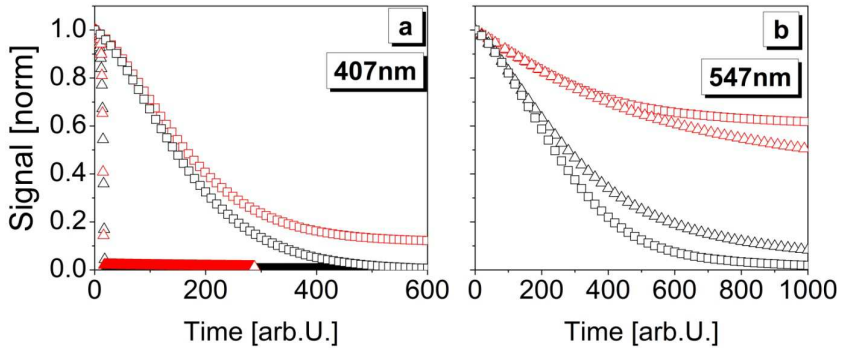

Fig. 69 Decay kinetics of 100 nm P3HT films in the presence of localized reaction centers (open squares) and mobile reactive centers (open triangles). Black symbols: UV/VIS absorbance at 552nm. Red symbols: Average thiophene ring concentration in the polymer film. Panel a: 365 nm illumination, panel b) 547 nm illumination. Signals were normalized to their value at time t = 0. The initial chain length is set to 300 thiophene units.

This behavior is explained by the nature of the mobile reactive centers. Under 547 nm illumination only longer fragments absorb, with the major fraction of reactive centers remaining on these fragments. During degradation the concentration of longer fragment declines, thus they transfer reactive center to shorter oligomers only towards the end of the degradation. These oligomers do not affect the polymer absorption, therefore the reaction rate out of of the UV/Vis signal declines. In the case of 407 nm illumination, also shorter oligomers created by random scission absorb light, but only a minor fraction of reactive centers remains on these fragments. Therefore, they are hardly degraded. The major part is transferred to longer oligomers which are then decomposed. In other words, shorter oligomers absorbing in the UV range act as photosensitizers for the degradation of the complete polymer although they are weakly degraded themselves.This accelerating effect is demonstrated in Fig. 70 where the reaction effectiveness for the random chain scission mechanism is presented as simulated for different photochemical conditions.

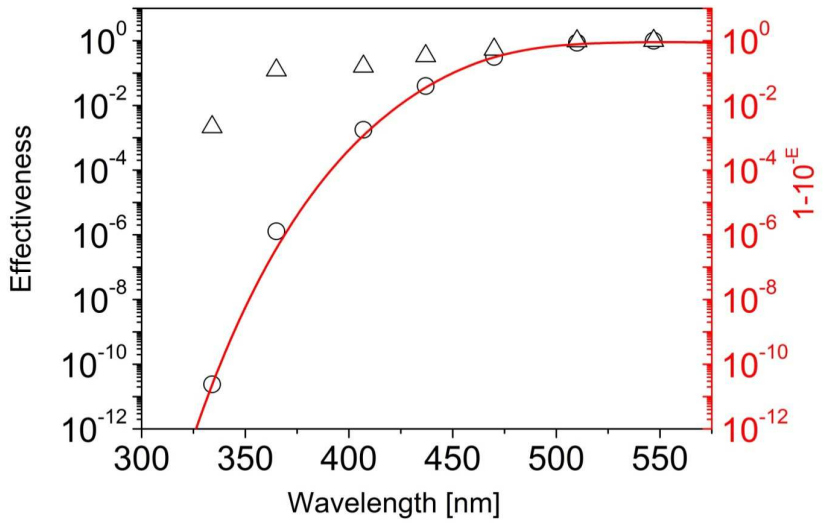

Fig. 70 Normalized effectiveness of P3HT degradation as function of the irradiation wavelength for the random chain scission. Localized reactive centers (open circles), mobile centers (open triangles), absorption of the polymer at time t = 0 (red line).

In the classical photochemical case with localized reactive centers (Fig. 70 open circles) the effectiveness strongly declines towards the UV range and follows the polymer absorption. The presence of mobile reactive centers (Fig. 70 open triangles) leads to the enhancement of the effectiveness towards the UV range.

In summary the presence of mobile reactive centers leads to the independence of the reaction spectra of illumination wavelength. Furthermore, the reaction effectiveness is strongly enhanced in the UV range compared to the classical mechanism with localized reactive centers. This enhancement originates from the UV absorption of shorter oligomers sensitizing the degradation process for oligomers of all lengths. Experimentally the effectiveness is increasing by a factor of 50 towards the UV region (see section III.2.2.2). As shown here in the simulation, this cannot originate from a classical photo reaction based on the polymer absorption itself. The results of the simulation suggests that the presence of a transient species absorbing in the UV (here short oligomers) increase the effectiveness to a certain extent. Whether these species are thiophene oligomers or any other reaction product occurring during the degradation cannot be stated.

III.3.2.4 White light conditions

So far the effect of different mechanistic assumptions on the degradation process of P3HT was discussed in order to establish a theoretical basis for the discussion of the experimental data observed in this work. Finally the question remains what is expected for the degradation of P3HT carried out under white light conditions. In order to do so the AM1.5 photon spectrum was used to determine the relative photon distribution of the different wavelengths used in the simulation. Subsequently the white light spectrum AM1.5 was approximated using the relative intensity distribution of the spectral line positions indicated in Fig.71. Additionally the polymer absorption of a simulated 100 nm P3HT thin film is shown.

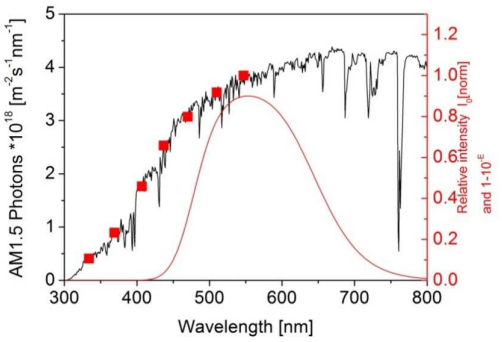

Fig.71 Full black line: AM1.5 photon spectrum. Red squares: Relative intensities used to approach white light conditions. Full red line: Absorbed in intensity at t = 0 for a simulated P3HT thin film of 100 nm thickness.

Using the relative intensities of the AM1.5 spectrum marked in Fig.71 leads to the reaction spectra presented in Fig 72. According to the algorithm, these spectra present the linear superposition of the single wavelength data presented in the previous sections. For details see appendix A. Here the spectra in the presence of both, localized and mobile reactive centers are presented together with the different chain scission mechanisms. Generally the spectra obtained for the end chain scission do not show any differences upon switching from classical (localized reactive species) to radical based (delocalized reactive species) conditions. The spectra do not show any spectral shift until the very end of degradation but simply decrease during degradation as observed under monochromatic illumination. Contrary to this, the random chain scission mechanism generally leads to a spectral blue shift and the appearance of shorter oligomers as presented by the rising absorption in the shorter wavelength range. Only a minor effect of the photochemical conditions (localized or mobile reactive centers) on the reaction spectra is observed. The presence of mobile reactive centres leads to a slightly reduced

absorption at 342 nm compared to the presence of localized ones. However this difference is certainly not significant under our experimental conditions. Generally, the presence of significant amounts of oligomers absorption suggest the degradation carried out under white light conditions is mainly due to the absorption of longer wavelengths by the polymer and not due to the absorption of UV light by smaller oligomers.

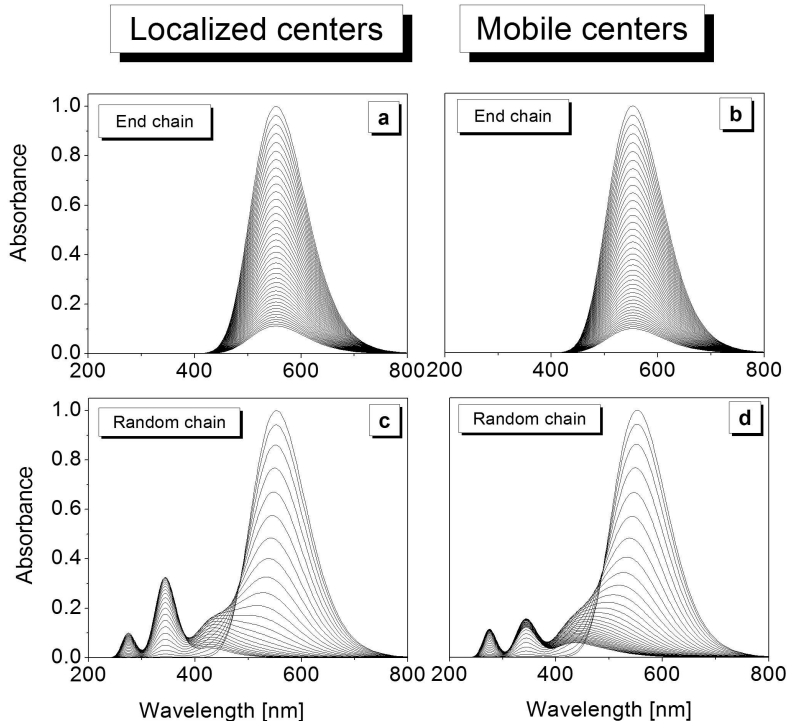

Fig 72 Reaction spectra of a 100 nm P3HT thin film under simulated white light conditions according to AM1.5 presented in Fig.71. Left column: localized reactive centers. Right column: mobile reactive centers. Top row: end chain scission. Bottom row: random scission. The initial chain length is set to 300 thiophene units.

Compared to the results of the simulation, the experimentally obtained reaction spectra under white light conditions reveal only a weak evolution of unstructured absorption in the UV range. This may be either explained by the idea that mostly the end chain scission mechanism is present or by a higher reaction quantum efficiency of smaller oligomers in the random chain scission case. With the experimental data at hand this cannot be unambiguously concluded.

The applied white light conditions may also influence the presence or the absence of a reaction gradient within the polymer film due to the fact that the penetration depth of the incoming light is different for the used single wavelengths. In the case of mobile reactive centres which are free to diffuse along the complete polymer film a gradient is intrinsically absent. In the case of localized reactive centers a gradient is observed for both, the end chain and the random chain scission mechanism, Fig 73. The gradient observed here in the end chain case is approximately 20% and therefore very similar to the one observed under monochromatic conditions in Fig. 63.

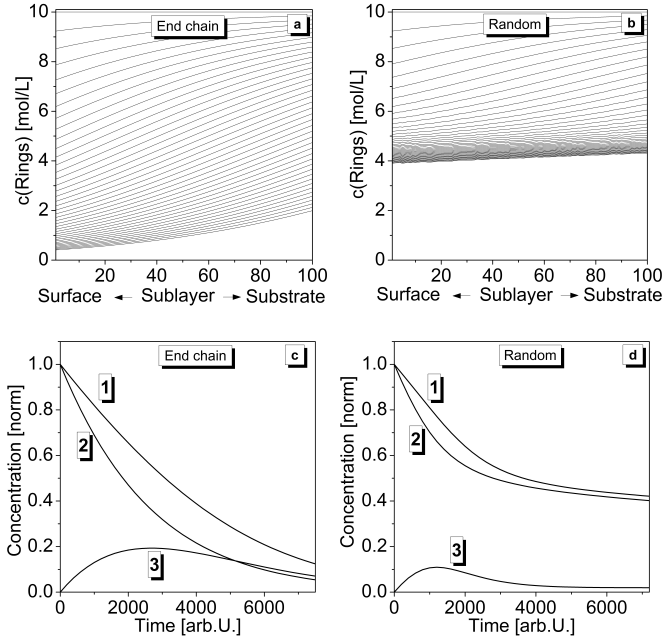

Fig 73 Concentration profiles of 100 nm P3HT thin films during degradation under white light assuming localized reactive centers. Panel a: End chain scission mechanism. Panel b: Random chain scission mechanism. Panel c: Time trace of the thiophene concentration in a 100 nm thin film for end chain scission extracted from panel a. Panel d: Time trace of the thiophene concentration in a 100 nm thin film for random scission extracted from panel b. (1) Bulk signal of the complete polymer film, (2) Surface signal of the first 10 nm below the surface, (3) difference between surface and bulk signal.

In the case of random scission the gradient becomes smaller with a maximum value of 10%. Interestingly such a gradient was not observed under experimental white light conditions combining surface sensitive XPS and bulk sensitive UV/VIS data. This strongly supports the idea that the white light degradation under experimental conditions is not due a classical photo chemical reaction of the

polymer itself. Furthermore this supports that the reaction may be controlled by the presence of a homogeneously distributed transient species leading to the degradation of the polymer.

The decay kinetics simulated under white light conditions remains a last issue to be compared to the experimental data. The results are presented in Fig. 74. In the case of end chain scission the decay kinetics of P3HT are very similar in the presence of localized and mobile reactive centers (Fig. 74 panel a,c). As observed under monochromatic illumination both the UV/VIS signal and the concentration of thiophene rings decay with the same slope. The shape of the decay kinetics is strongly influenced by the ratio of film thickness and penetration depth of the incoming light as discussed in a previous section. Generally the slope the degradation rate decreases during the complete degradation process as evident by the decreasing slope. In the presence of the random scission mechanism (Fig. 74 panel b,c) several differences are observed. First of all the UV/Vis signal and the average thiophene ring concentration do not longer show the same slope. This originates from the spectral blue shift of the spectrum as discussed in the monochromatic case. In general it seems that the degradation carried out under white light conditions and a localized reactive center is very similar to the monochromatic case of 547 nm illumination. Switching to mobile reactive centers does only slight affect the decay kinetics, whereas it leads to the disappearance of a reaction gradient.

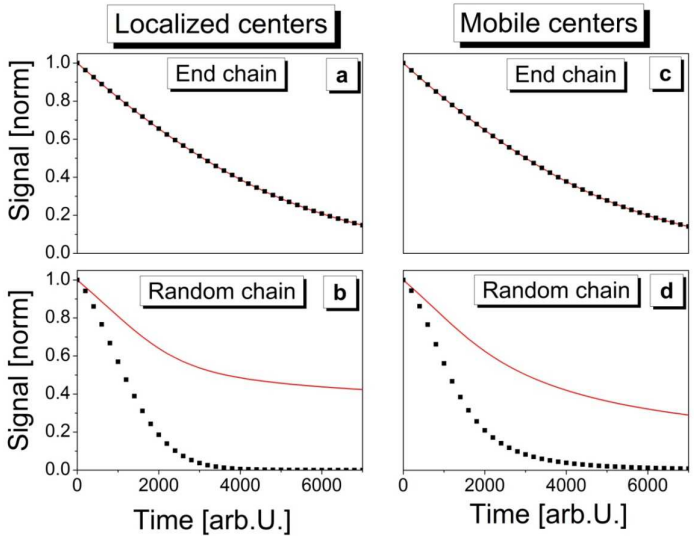

Fig. 74 Decay kinetics of 100 nm P3HT thin films during simulated degradation with white light in the presence of localized reactive centers (panel a, b) and mobile reactive centers (panel c ,d). Both the end chain and the random chain scission mechanism are presented. Full squares: UV/VIS decay at 552 nm, red lines: Average thiophene ring concentration in the film. The initial chain length is set to 300 thiophene units.

Comparing these results to the experimentally observed degradation kinetics under white light conditions reveal some strong differences. Neither a strong blue shift in the UV/VIS reaction spectra nor the occurrence of significant concentration of intact thiophene rings in the FTIR was observed experimentally upon the complete loss of the UV/VIS absorption. As stated above, this suggests that either the degradation of P3HT proceeds mainly via the end chain scission mechanism, or that smaller oligomers are more reactive in the degradation process.

IV Discussion

In this chapter the single results of the degradation studies will be discussed all close together in order to present a most completely picture of the degradation process under ambient conditions. Before the photo oxidation process of P3HT will be discussed in detail, the ozone degradation of the polymer is explained separately as this pathway is not dominating under ambient conditions.

IV.1 Ozone degradation of P3HT

The exposure to ozone cause the degradation of P3HT, leading to the loss of the UV/Vis absorption band in the range of 300 to 800 nm and to the occurrence of highly oxidized states of carbon and sulphur obtained via photo electron spectroscopy (XPS). During the initial stages of degradation, the polymer is p-doped, leading to a stabilization of the Fermi level, whereas towards the end of oxidation, the loss of electrical conductivity causes charging effects during photoelectron spectroscopy. The details of doping will be discussed in section IV.2 about the photo degradation of P3HT.

Throughout the degradation process, no significant dependence of the composition of the film on the distance from the surface is observed by angle dependent XPS measurements. This is an indication for the absence of a reaction gradient in the polymer film on the accessible depth scale (~10nm), in accordance with the results of XPS[90] investigations on the ozone treatment of P3HT and other polymeric systems. Obviously, the reaction rate of ozone with P3HT is slow compared to the diffusion rate of ozone into the film, even at the highest ozone concentration (6ppm) used in this work. This is supported by the observation that other gases of similar molecular size as ozone homogeneously penetrate a 100 nm thick P3HT film in less than one second[55].

The oxidative character of degradation via ozone becomes evident from the observation of the oxygen uptake by the film and by the appearance of oxidized carbon and sulfur species in the photoelectron spectra. Concluding from the electron binding energies observed, several oxidized carbon species of different oxidation states evolve, which comprise carbonyls, carboxyls, and probably also alcohols, peroxides, as well as ozonides. Interestingly the amount of carboxyl groups remains in relatively small fractions.

A detailed inspection of the sulfur XPS signals reveals the presence of four different oxidation states in the film. The time traces of these species suggest a consecutive oxidation mechanism 1→2, 3→4, with species 2 and 3, i.e., probably sulfoxides and sulfones, as intermediate products, while species 4, probably a sulfonate, seems to be formed in a subsequent step from the intermediate sulfur species. This kinetic scheme is similar to the one proposed on the basis of FTIR studies of the photo-oxidation

of P3HT[11], where sulfoxides and sulfones were identified as the intermediate products and sulfinate esters as the final. Although species 4 is the final product observed by XPS, it is not necessarily the final product in this sequence of oxidation reactions: the increase of the carbon to sulfur ratio by 30% during the reaction indicates the generation of volatile oxidized sulfuric species [91]. The loss of material during the reactions is further supported by the appearance of the XPS signal of Indium, which is part of the substrate material ITO, at later stages of degradation. During the further discussion of degradation kinetics it has thus to be kept in mind that the elemental composition of the film is not really constant and that final products of oxidation might not be detectable by methods such as XPS, UV/Vis, and FTIR, which only probe the solid film.

The analysis of the ratio of oxidized to non-oxidized species of sulfur and carbon yields further insight into the degradation mechanism. In the case of degradation by ozone, the slope of the O:C ratio vs. the optical loss is only around 0.4, which means that even after complete destruction of the π-conjugated system, 60% of the sulfur atoms have not been oxidized. This suggests that sulfur is not involved in the primary step of the reaction which leads to the bleaching of P3HT, but that the oxidation of sulfur is rather part of subsequent reactions. The increase of the O/S ratio with growing absorption loss, showing an average slope of approximately 4, indicates that between one and two ozone molecules per thiophene unit are consumed during the destruction of the π-conjugated system, in accordance with what has been observed for thiophenes in solution[92]. Further insight comes from the evolution of the fraction of oxidized carbon species, showing a slope of 0.4 when plotted against absorption loss. The resulting fraction of 40% of oxidized carbon at complete loss of optical absorption matches the number of carbon atoms in the ring structure. This is an indication that the primary reaction step consists in the electrophilic addition of ozone to the double bonds of the thiophene unit, in accordance with the generally accepted mechanism of the ozone treatment of unsaturated organic materials[93,94] and of other conductive polymers like polypyrole and polyaniline[95].

The attack of ozone at the alkyl side chain is unlikely, due to the generally slow reaction rate of ozone with aliphatic C-H bonds [93] and actually has not been observed in FTIR studies of the ozonization of polythiophene[62]. After the addition of ozone to the double bond, subsequent reactions cause the cleavage of the C=C bond [93,96] via carbonyl formation, which finally leads to the opening of the thiophene ring with possible subsequent sulfur oxidation by a further ozone molecule [92]. The low oxygen to carbon ratio of O/C ~ 4 at the end of the bleaching reaction, which matches the fraction of oxidized carbons and the absence of a strong carboxyl signal in the carbon spectrum of ozone treated P3HT, further supports the assumption of a mechanism comprising an electrophilic attack of ozone at the thiophene ring as initial step of degradation. Radical mechanisms, either as side reactions or as subsequent reaction steps seem to play only a minor role, consistent with the low hydroperoxide concentrations observed in the ozonization of unsaturated polymers[96].

More detailed information about the degradation mechanism can be gained from the blue shift of the UV/VIS absorption during degradation. Under exposure to ozone, a significant blue shift is observed during the reaction, starting at around 60 to 70% of the total UV/Vis absorption loss. Therefore, fragments shorter than n = 10 thiophene rings need to exist in considerable amount. This hints to ozone attacking the π-conjugated system at random positions. The resulting random distribution of fragments during the whole process of ozonization is consistent with the 1st order kinetics of UV/Vis absorption loss Such a random attack of ozone has been observed for both saturated [97] and unsaturated polymers.

Regarding the relevance of ozone degradation in the decomposition of the polymer under ambient conditions the rates of ozone degradation in the dark and photo oxidation were compared. Under irradiation at AM 1.5 conditions in synthetic air, the rate of photo oxidation is about two orders of magnitude higher than ozonization in a typical laboratory environment (10 ppb) and roughly one order of magnitude higher than under high urban concentrations of 0.05 ppm. Ozone degradation of P3HT[98] therefore seems not to play major role in the lifetime of the polymer. However this investigation is helpful concerning the possible presence of local, higher concentrations of ozone in the large scale production of organic electronic devices. In daily application however the photo induced degradation seems to play the major role, therefore the photo induced degradation effects will be discussed in the following.

IV.2 Photo degradation of P3HT

The exposure of P3HT thin films to light and oxygen leads to the occurrence of several degradation effects which take place on significantly different time scales. However these effects all contribute to the overall degradation of the polymer and will be therefore discussed all close together. A mutual basis for all of the observed effects is the simultaneous presence of present light and oxygen as revealed in section III.2.2.1 and III.2.2.4. In the following these effects will be discussed according to their occurrence on the different time regimes with special attention to possible correlations.

IV.2.1 Reversible, oxygen induced quenching of excited states

Upon exposure to oxygen a thin film of P3HT (~100nm) is homogeneously penetrated by the gas within the first milliseconds which leads to the partial quenching of excited states via collisional quenching and therefore a loss in fluorescence intensity[55].This phenomenon is fully reversible upon switching to inert atmosphere or vacuum. Parallel to the collisional quenching the formation of a charge transfer complex between the polymeric donor and oxygen as acceptor rises within minutes, also quenching the excited polymer state. This component is reversible upon thermal annealing under nitrogen or vacuum conditions.

The third component of fluorescence loss is given by the photo oxidation of the polymer itself yielding irreversible defects. Interestingly the complete loss of polymer emission is accompanied by minor losses in the UV/VIS absorbance of approximately 3% as presented in section III.1.1.The nature of these defect states remains an open question as their concentration is way below the detection limit of standard spectroscopic techniques like FTIR, NMR or XPS. Although a direct proof cannot be given it may be concluded that these quenching sites are due to the formation of carbonyl functions created during the complete degradation process as obtained in section III.2.3. As these species present a major part of the reaction products as will be discussed below. Further support of this interpretation comes from the observation that carbonyls show high electron affinities which facilitate a pathway for the quenching of the emissive polymer state[99,100].

IV.2.2 Reversible, oxygen induced doping of P3HT

Upon exposure to light and oxygen the energy levels of P3HT show a reversible shift together with the occurrence of a weakly adsorbed oxygen species which is removed upon thermal annealing at 150°C and a strongly, irreversibly bound species remaining in the polymer upon thermal annealing as presented in section III.1.2. As oxygen is known to act as p-dopant for organic semiconductors two possible reasons for the systematic energetic shifts can be discussed.

First a p-doping of the organic semiconductor P3HT or, alternatively, a variation of the interface dipole between P3HT and the underlying substrate (interface doping) can be considered. Both phenomena may induce the Fermi level to shift towards the HOMO level position. As the reference energy in photo electron spectroscopy is the Fermi level, such a shift will decrease the binding energy of all occupied states and increase the work function presented by the energy difference of E_F and the vacuum level, as observed. Oxygen induced p-doping of the polymer is more likely than interface doping due to the fact, that oxygen is homogeneously distributed over the polymer film as concluded from the large oxygen diffusion coefficient and the present film thickness of the polymer film of roughly 100 nm as presented in III.1.1. Further support for this interpretation may be derived from theoretical work[101] and experimental observations[54], both stating that P3HT itself may become doped by oxygen. Such doping effects were already reported several years ago for in situ prepared sexithiophene thin films[59]. However, the possibility of interface doping and the influence of light or different oxygen species were not discussed there.

Because the P3HT film was prepared ex situ in this work, the influence of oxygen during the preparation cannot be fully excluded. However, with XPS the oxygen amount in the polymer film can be quantified. Statistically there is one oxygen atom on every 200th thiophene ring in the pristine film. Assuming a density of 1.1 $g \cdot cm^{-3}$ for P3HT[102,103]this yields an oxygen concentration of $2x10^{-19}$ oxygen atoms per cm^3 in the pristine polymer film.

Whereas the effect of doping of P3HT by oxygen is clear, the influence of light or the estimation of the oxygen content in the polymer film which is actually responsible for the doping remains an open question. In particular, in view to applications of these materials in organic solar cells, the question arises whether or not light does affect the interaction between P3HT and oxygen. Therefore, the P3HT thin film was exposed to oxygen twice for 30 min in dark without significant changes in the position of the energy levels. In other words, the presence of light promotes doping effects significantly which is in good accordance with the observed minor oxygen effects in the dark[104] and the enhanced rates of oxygen doping under light[54] .Interestingly the occurrence of two different oxygen species was monitored via XPS; a weakly adsorbed one which can be removed upon thermal annealing and a

strongly bound species which cannot be removed. These observations point to the presence of at least two oxygen species with significantly different binding energies to P3HT.

The reversibly bound species is attributed to physisorbed oxygen which probably forms a metastable charge transfer complex with the polymer upon photo excitation of the latter[15]. The irreversibly bound species is assigned to oxygen contained in photo–oxidation products.

Unfortunately the chemical nature of these species cannot be resolved as the peak shape of the oxygen O1s spectra does not change significantly upon oxygen/light and thermal treatment. Most probably these irreversible oxygen species originate from the presence of carbonyl functions as presented in section III.2.3 about the product evolution studied via FTIR. Nevertheless, the assignment above explains why the reversibly bound oxygen species, which represents an only minor part of the total oxygen content of the film, leads to the shift of the core and valence levels, whereas the much more abundant, irreversibly bound oxygen species has a negligible effect on the electronic properties and only a weak effect on the optical properties of the film.

The oxygen molecule bound to the π-system of the polymer in the CT complex traps an electron which leaves behind a mobile hole on the electronic π-system of the polymer. This leads to a shift of the Fermi level towards the HOMO level of the polymer. Interestingly the concentration of the reversible oxygen component during repeated doping cycles is between c(rev. oxygen) = $2.7x10^{19}$-$1.2x10^{20}$ oxygen atoms per cm^3. Comparing these numbers to the free charge carrier density c(CC) = 10^{17}- 10^{18} cm^{-3} in oxygen doped P3HT thin films[104] suggests that equilibrium constant of charge carrier formation K = c(CC)/c(oxygen) ~ 0.01-0.1 is rather low at a given dopant level.

The oxygen species chemically bound in oxidation products is preferably located at molecular sites which are electronically isolated from the π- conjugated system (probably in the side chain position or in already destructed thiophene rings). Consequently, its interaction with electrons of the π-system is much weaker and thus does not lead to substantial changes in the electronic structure of the polymer. Although the electronic structure is affected, the irreversibly bound part of the oxygen population also presents a degradation pathway of the polymer. Most probably these oxygen species are the ones acting as quenching sites for excited states of P3HT as discussed in the previous section about the irreversible, oxygen fluorescence quenching of P3HT. The above considerations about the p-doping mechanism and the two different oxygen species are summarized graphically in Fig.75.

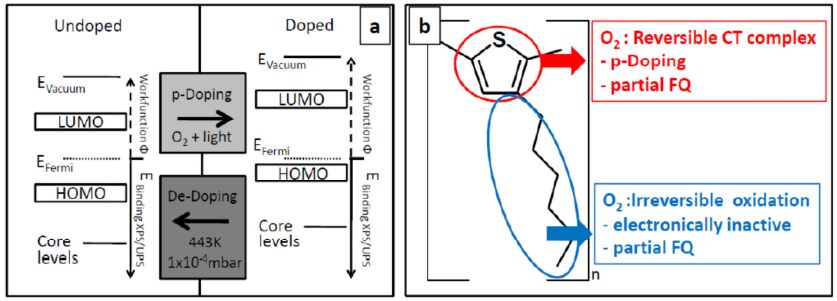

Fig.75 Panel a: Energy level sketch of pristine undoped and oxygen doped P3HT summarizing the oxygen induced doping originating from the weakly absorbed oxygen species. Panel b: Model of the different oxygen species and their effect respectively position on the polymer.

Finally the timescale of the different phenomena has to be discussed. The oxygen induced doping presented here occurs on the time scale of minutes under AM1.5 illumination, whereas the complete photo bleaching of the polymer requires roughly 1 week under these conditions. Therefore the formation of the CT state respectively the doping of the polymer presents a reaction pathway in the very early stages of degradation where the polymer is bleached by less than 3%.

IV.2.3 Irreversible photo oxidation of P3HT

In order to further approach the degradation mechanism of P3HT in the solid state the influence of several environmental factors on the stability of the polymer under was investigated in section III.2. Thermolysis of P3HT at moderate temperatures ($T < 400K$) under air in the dark, is negligible as compared to the photo-oxidative degradation of P3HT, even at low light levels[23]. Similarly, photolysis in the absence of oxygen[105] takes place on the time scale of years. Furthermore the degradation by ozone is negligible under ambient conditions as presented in section III.2.1.1.

Thus the dominating reaction pathway leading to the irreversible degradation of P3HT under ambient conditions is the photo induced oxidation of the material. Therefore the discussion will concentrate solely on the kinetics of the photo oxidation process and the elucidation of the reaction mechanism.

During the degradation under white light and constant oxygen partial pressure, the decay rate monitored via UV/VIS is constant. In other words, the reaction rate does neither decrease with the absorbance of the film nor with the rapid decay of luminescence intensity discussed in the previous

section about the irreversible photo oxidation. The linear dependence on light intensity indicates that the steady state concentration of the active species is proportional to the rate of absorbed photons i.e the reaction is at least photo initiated.

However, this active species does not originate from excited states of the (intact) polymer or any reactive species sensitized by the polymer, as this would neither be in accordance with the observed zeroth order kinetics, the fast irreversible fluorescence quenching, nor would it agree with the activation spectrum of photo oxidation which will be discussed below. It also excludes that the bimolecular recombination of possibly photo generated radicals plays an important role in the overall reaction scheme. The observed pressure dependence of the P3HT photo oxidation is consistent with both mechanisms under discussion, the singlet oxygen path (Eq. 27) and the radical based pathway (Eq. 24). The pressure dependence of the degradation rate indicates that oxygen or an oxygen centred intermediate species depletes a transient species involved in the rate limiting step of the reaction. This transient species may be either an excited state or a chain propagating radical species. The linear decay kinetics may originate from several factors:

1.) Surface enhanced reaction:

First of all, the photo-oxidation can be a surface reaction. This requires at least one of the reactants, i.e., either the excited polymer or oxygen, to be restricted to the surface. This is not very likely, as the penetration depth of incoming light is approximately 50 nm at the absorption maximum of the polymer and even larger for shorter wavelengths (Fig. 62). Therefore the penetration depth of light and the film thickness of 100 nm are on the same order of magnitude. The simulation of the P3HT photo degradation under white light conditions in section III.3.2.4 reveals that, if at all only a minor reaction gradient of 10-20% at maximum is expected under white light in a classical photo reaction. This does not lead to linear decay kinetics for a film thickness of 100 nm. The reaction is furthermore not limited by the diffusion of oxygen into the bulk (section III.2.2.3) as the diffusion of oxygen can easily keep up with the oxygen consumption of the chemical reaction in the film. Direct experimental evidence for the absence of a significant reaction gradient is given the equal photo oxidation rate obtained for bulk sensitive UV/VIS (100 nm information depth) and surface sensitive XPS (10 nm information depth) in section III.2.1.2. In summary both the simulation and the experimental results reveal the absence of a significant reaction gradient and thus rule out that this explanation for the observed linear kinetics.

2.) Fragmentation pattern of the conjugated system

Secondly, the fragmentation pattern of the π-conjugated system might explain the observed linear decay kinetics. During degradation the destruction of double bonds leads to a decrease of the absorption cross section in the visible of about 10^4 cm^2mmol^{-1} per thiophene ring. Concomitantly, the effective π-conjugation length is reduced, which causes the position of the absorption maximum of polythiophene to shift to the blue as soon as there are significant amount of pi system fragments with the number of conjugated thiophene rings below $n \approx 10$ [35]. Assuming that only the terminal thiophene rings are starting points for degradation (end chain breaking) this means that the polymer chain is degraded step by step with the number of reactive centers remaining constant over the complete degradation process supporting the linear decay kinetics. Furthermore this model may explain the absence of a strong spectral blue shift during the photo oxidation of P3HT as the critical limit of $n<10$ leading to significant spectral shifts is reached at the very end of the degradation (~10% remaining absorbance) assuming an initial chain length of 200 units estimated from the molecular mass of the polymer.

3.) Intermediate species

A further possible reason for the linear decay kinetics is that the rate limiting step of the reaction involves an indestructible impurity or an intermediate species, whose concentration is constant during most of the reaction.

With the experimental results at hand it cannot be decided what is actually the reason for the observed linear kinetics of the photo degradation under white light. Nevertheless, the linear decay kinetics, i.e., the independence of the reaction rate on the absorbance of the polymer, is fully in accordance with the dependence of the effectiveness $\Im$ on the wavelength of the incident photons, i.e., the activation spectrum of photo-oxidation presented in section III.2.2.2. Both of these observations strongly suggest that the degradation of P3HT does not follow a classic photochemical reaction sensitized by P3HT itself.

The activation spectrum of photo degradation increases continuously towards the UV region of the spectrum and is thus clearly different from the absorption spectrum of the P3HT film. Assuming a classical photochemical reaction of P3HT the effectiveness should follow the absorption spectrum of the polymer as presented in the simulation section III.3.2.2. Although the activation spectrum cannot be assigned to any specific chemical species it further excludes the sensitization of singlet oxygen or of any other reative species by the polymer as the rate limiting step of the photo-oxidation.

Consequently, a photoinduced radical-based pathway is the more likely degradation mechanism of P3HT under light and oxygen. This has already been suggested by Abdou and Holdcroft[23], who identified radical induced crosslinking of the polymer chains as a major reaction pathway. More recent investigations[22] confirm this picture by showing that P3HT films are not attacked by singlet oxygen under white light conditions[22]. These results are supported by the stabilizer experiments presented in section II.2.3.1 suggesting that neither light of 365 nm nor of 525 nm illumination generates significant amounts of singlet oxygen which could be quenched by the DABCO stabilizer. At this point however it has to be considered that the efficiency of a stabilizer molecule in the solid state might be generally hindered by the diffusion length of the reactive active species. If the diffusion length is very small, the reactive centre may not reach any stabilizer molecules within its lifetime.

In order to derive a more detailed explanation for the observed wavelength dependence of the photo oxidation the product evolution was studied via FTIR. Here the two limiting cases of UV (365nm) and Vis (525nm) photo oxidation were investigated.

Illumination into the absorption maximum of the polymer at 525 nm leads to the degradation of the π-conjugated system by the formation of carbonyl species on the thiophene rings (polymer backbone) as studied by FTIR (section III.2.3.1). The aliphatic side chain is hardly affected. Together with the decreasing reaction rate during degradation this suggests that the reaction in this case might be due to reactive species which are sensitized by the polymer itself. Further support of this interpretation comes from the theoretical model presented in section III.3.2.1 revealing that the reaction rate for P3HT films of the used thickness used in the present experiments (~100nm) should decrease during degradation upon the presence of a photo reaction sensitized by the polymer. This represents a major difference to the linear decay kinetics observed under white light as now the reaction rate depends on the absorbance of the polymer film.

As illumination with 525 nm only excites the polymer itself, this gives the unique possibility to consider the nature of the reactive oxygen species. Generally, two reactive oxygen species have to be considered which may be sensitized by the polymer. On the one hand this might be singlet oxygen sensitized by the polymer triplet state, on the other hand this might be a superoxide radical created out of the polymer-oxygen charge transfer complex.

1.) Superoxide ion mechanism:

The presence of superoxide ions was supposed in the recent literature[106]. Superoxide is rather alkaline and should rapidly abstract a hydrogen cation from the nearest C-H groups which is the alpha methylene unit as presented in Fig.76. A possible mechanism is presented in Fig.76.

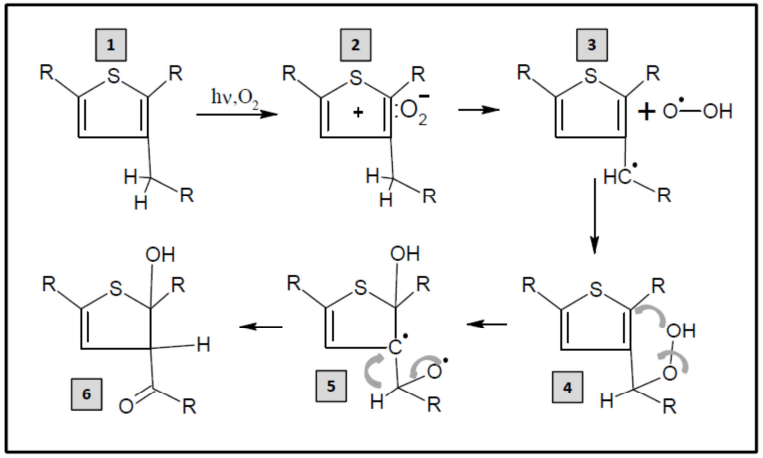

Fig.76 Reaction scheme for the initial degradation process assuming the formation of a superoxide anion sensitized by the polymer under 525 nm illumination. (1) Ground state P3HT, (2) Charge transfer complex, (3) P3HT and hydroperoxyl radical, (4) P3HT with hydroperoxide function on the alpha side chain position, (5) Reaction intermediate, (6) Reaction product after initial degradation.

Upon illumination of P3HT in the presence of oxygen a metastable polymer charge transfer complex (2) is formed. Subsequently a proton may be abstracted by the superoxide ion O_2^- from the alpha methylene unit of the side chain resulting in a neutral polymer radical and a hydroperoxyl radical (3). The proton abstraction at the alpha methylene unit is rather likely considering that this position is located close to the thiophene ring where the superoxide ion is created and furthermore that this group is rather acidic compared to the rest of the side chain groups. The created hydroperoxyl radical in (3) may abstract a hydrogen atom from an adjacent thiophene ring whereas the polymer radical may add an oxygen molecule. Both of these steps will lead to the chain propagation of the reaction. However these steps do not represent the destruction of the π-conjugated system. Therefore another possibility is the recombination of both radical species to form the polymer hydroperoxide species (4) which is so far discussed to be present in the initial stages of P3HT photo degradation[11,26]. This peroxide is thermally labile and is known to decompose into a hydroxyl radical (·OH) and a peroxy radical (CO·). Subsequently the hydroxyl radical most probably attacks the thiophene ring in the 2 or 5 position[107] resulting in the intermediate (5). This intermediate then relaxes by a hydrogen shift into the product (6). Here it has to be mentioned that each reaction step involving a radical species may lead to the further uptake of an oxygen molecule and thus to the propagation of the chain reaction. Species (6) represents the reduction of the π-conjugated system and consequently a loss in the UV/VIS absorption of the polymer. However it has to be stated that this is certainly not the final product as both remaining

double bonds and significant amounts of hydroxyl functions are not observed under these conditions. Here it is a safe assumption that in the presence of radical species these groups will certainly decompose in follow up reactions[108] leading to carbonyl species. According to the obtained FTIR data the oxidation behaviour of the thiophene sulfur remains an open question here.

The considered mechanism may explain the observation that the aliphatic side chain is hardly attacked under illumination with green light of 525nm. Furthermore it may even explain the observed decreasing reaction rate under these conditions. However the presence of the proposed superoxide mechanism is rather unlikely due to the fact that the α-methylene groups is not attacked as concluded from isotopic labeling experiments of this position (deuterated P3HT) in section III.2.3.1. Thus any mechanism assuming the alpha side chain position to be the starting point is rather unlikely although this has been suggested in literature[24,26].

2.) Singlet oxygen:

The presence of singlet oxygen is controversially discussed in the recent literature about the solid state degradation of P3HT[22,109]. Here it has to be pointed out that the degradation mechanism might change upon different environmental conditions, especially under white light compared to degradation carried out under monochromatic illumination conditions as secondary reactions may occur. The degradation carried out under green light conditions where only the polymer absorbs, supports the idea of singlet oxygen being present as this species does preferentially attack the double bonds of the π-conjugated system. This preferential reaction of the double bonds is actually observed under green light. In contrast, the side chain is only slightly degraded during the entire degradation process which is also expected in the presence of singlet oxygen. Furthermore the decreasing reaction rate is explained by the presence of singlet oxygen sensitized by the polymer. Therefore the presence of a singlet oxygen based mechanism is rather likely, at least under green light conditions.

The presence of UV light at 365 nm does not only increase the reaction effectiveness by a factor of approximately 30, but results in strongly linear decay kinetics and a modified product evolution. According to the simulations presented in sectionIII.3.2.1 a first order kinetics is expected under weakly absorbed UV light in presence of a degradation mechanism sensitized by the polymer. The unexpected linear decay kinetics already suggest the presence of a complex mechanism. The destruction of the π-conjugated system using UV light leads to the same concentration of carbonyl functions on the thiophene ring as observed under green light conditions. Other reaction products like hydroxyl species are not observed. In contrast to green light conditions, the side chain signal decreases during degradation. Taken together, these results suggest that the concentration of reaction products

does not depend on the presence or the absence of the side chain. Therefore the side chain is rather detached from the molecule instead of being oxidized. Together, these observations suggest that the detachment of the side chain is an additional photo-induced step, whereas the first reaction steps are the same as observed under 525 nm. Further support of this assumption comes from the observed carbonyl kinetics in section III.2.3.1 Fig. 42 showing the shape of a typical consecutive reaction. The fact that this additional pathway is present under UV conditions strongly suggests that the detachment of the side chain is due to the presence of a Norrish type I reaction taking place after the formation of initial carbonyl species on the thiophene ring. Interestingly the assumption of a Norrish type I reaction not only explains the detachment of the side chain but also gives a reasonable explanation for the enhanced effectiveness in the UV range. The Norrish type I reaction intrinsically produces free radicals[110,111] which in turn may add additional oxygen, thus promoting the formation of hydroperoxides species. These species are highly reactive upon UV illumination with kinetic chain lengths in the range of 10^2-10^3 [112] leading to the enhanced reaction effectiveness. Furthermore the proposed mechanism is in line with the observed linear degradation kinetics which may be explained by the rapid appearance of a steady state concentration of radicals in the film. In general it seems that the photo degradation of P3HT under UV light is not due to the absorption of the polymer itself but to the presence of carbonyl and hydroperoxide species which are highly reactive upon UV illumination. The above considerations are summarized in Fig. 77

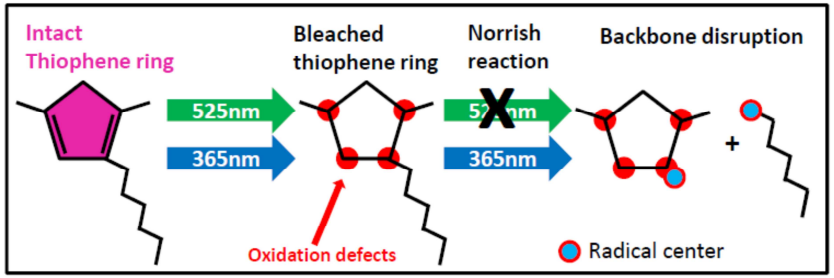

Fig. 77 Schematic pathways of polythiophene photo oxidation under illumination with 525 nm and 365 nm light.

Both UV light of 365 nm and visible light of 525 nm lead to the initial formation of oxidation defects on the polymer backbone. Subsequently, only UV light is capable of disrupting the sigma framework.

Under white light conditions the formation of carbonyl species is not significantly different from that obtained under monochromatic conditions (both UV and VIS degradation). Again the formation of carbonyl species (ketones, esters, conjugated carbonyls) is strongly correlated to the decay of both the optical signal and the loss of C=C double bond absorption in the FTIR. This suggests that also under

these conditions the carbonyl products are created mainly on the thiophene ring positions. The strong decay of the hexyl side chain again points to the detachment of the complete side chain which is likely to originate from the presence of a Norrish type I reaction. This side chain loss is very similar to the degradation obtained under UV light. The disruption of the sigma framework and the formation of volatile species under white light becomes even more evident by the increasing C: S ratio and the occurrence of substrate signals in the XPS spectra after the total loss of UV/VIS absorbance in section III.2.1.2. Interestingly the detachment of the hexyl side chain obtained via FTIR would essentially decrease the C:S ratio during the degradation process whereas an increase is observed in the XPS spectra. These observations strongly suggest that beside the detachment of the side chain several other pathways for the disruption of the backbone are present which may finally lead to the formation of volatile species including significant amounts of sulfur. In other words, the sigma framework is not only disrupted by the detachment of the hexyl side chain but also by the cleavage of bonds in the thiophene ring. Therefore the complete molecule is disrupted.

The formation of sulfur oxidation products could not be addressed on the basis of the FTIR data because they appear in the finger print region, but becomes evident from the XPS data presented in section III.2.1.2. A detailed inspection of the sulfur XPS signals reveals the presence of four different oxidation states in the film during the degradation under white light. The time traces of these species suggest a consecutive oxidation mechanism 1→2, 3→4, with species 2 and 3, i.e., probably sulfoxides and sulfones, as intermediate products, while species 4, probably a sulfonate, seems to be formed in a subsequent step from the intermediate sulfur species. This kinetic scheme is similar to the one proposed on the basis of FTIR studies of the photo-oxidation of P3HT, where sulfoxides and sulfones were identified as the intermediate products and sulfinate esters as the final product[11]. However these species could not be quantified in the FTIR investigations of this work due to the strong overlap of signals in the respective region. Although species 4 is the final product observed by XPS, it is not necessarily the final product in this sequence of oxidation as the formation and disappearance of volatile species was deduced from the occurrence of the substrate signal at the latest stages of degradation in the XPS spectra. The overall sulfur oxidation linearly correlates with the loss of the optical signal in the UV/VIS (see section III.2.1.2Fig. 26). At the same time the FTIR data in section III.2.3.2 Fig. 56 reveals that the loss of double bonds is also strongly correlated to the optical loss but not to the decay of the side chain. Therefore it seems that the destruction of double bonds and the oxidation of the sulfur position are also correlated further supporting the idea of a singlet oxygen based mechanism.

In contrast to the product evolution under monochromatic illumination with VIS and UV light, the presence of significant amounts of alcohol functions was observed via FTIR under white light conditions in section III.2.3.2. As all experimental conditions despite the illumination were constant this points to the presence of further photo induced reactions under white light conditions leading to

the occurrence of alcohol functions. However the detailed nature of these reactions remains an open question at this point.

Besides the illumination conditions, the presence of humidity strongly influences the photo oxidation of P3HT as presented in sections III.2.2.5 and III.2.3.2. Water in itself does not react with P3HT at significant rates in the absence of light and oxygen, but acts as a promoter increasing the photo oxidation rate of P3HT films. During the photo oxidation process the reaction rate strongly increases in the presence of humidity. This might be explained by the increasing hydrophilicity of the film during degradation due to the formation of polar reaction products e.g. carbonyl and SO_x species. Consequently the concentration of adsorbed humidity in the film is increased and the accelerating effect becomes more pronounced.

These considerations lead to the question about the detailed nature of the accelerating effect of H_2O during the photo oxidation of P3HT. First of all water may act as solvent facilitating the diffusion of reactants (although it has no effect on the diffusion of oxygen) or stabilizing intermediates. Secondly water may open additional reaction pathways, acting as a catalyst or reactant during the reaction. Interestingly the FTIR reaction spectra in section III.2.3.2 reveal that the concentration of adsorbed water in the polymer film is way below the detection limit of the spectrometer even in the case of the degradation carried out at 100% rel.hum. At the same time the product evolution during photo oxidation is modified by the appearance of new hydroxyl species and the strongly reduced concentration of alcohol groups. This strongly suggests that water is consumed during the photo oxidation process to some extent. Experimental evidence of this interpretation comes from the presence of deuterium und ^{18}O in the reaction products during degradation in the presence of D_2O and $H_2{}^{18}O$. Therefore water is acting at least as reactant during the degradation process.

Although water is evidently consumed, the absence of a significant isotopic effect on the reaction rate in the UV/Vis reveals that the accelerating effect is not limited by the splitting of water molecule itself. Therefore it seems that the water molecule reacts with highly reactive intermediates, possibly a hydroxyl radical according to scheme 3:

Scheme 3: Possible reactions of the a hydroxyl radical with H_2O, D_2O and $H_2{}^{18}O$.

$$OH\cdot + H_2O \rightarrow H_2O + OH\cdot$$
$$OH\cdot + D_2O \rightarrow H_2O + OD\cdot$$
$$OH\cdot + H_2{}^{18}O \rightarrow H_2O + {}^{18}OH\cdot$$

The reactions presented in scheme 3 present a hopping transport of the reactive centre which may lead to the enhanced diffusion respectively of reactive species. Furthermore it might give a hint how the different isotopic markers discussed before are able to be incorporated into the reaction products.

The diffusion of reactive intermediates within the polymer film may also explain the activation energy of the photo oxidation process of 26 kJ/mol presented in section III.2.2.3. Generally this value points to the presence of a thermally activated diffusion process and thus a reaction limited by the diffusion of a reactant. Interestingly the activation energy of the photo degradation and the oxygen diffusion in the polymer film show the same value of 26 kJ/mol. However the photo oxidation is clearly not limited by the diffusion of oxygen as discussed above. A possible explanation for this low activation energy may be the presence of hydroperoxide species. These species are thermally unstable and decompose into hydroxyl radicals. Thus, either the decomposition of these species or the diffusion of the created hydroxyl radicals may be the origin of the observed activation energy. With the experimental data at hand this cannot be unambiguously stated.

Finally the structure of the polymer dramatically influences the degradation process as presented in section III.2.2.6. So far the results of the regio-regular P3HT were discussed as this isomer is of tremendous importance in the field of organic electronics. However the comparison with the degradation of the regio- random isomer gives valuable information about the general degradation mechanism. Regio-random P3HT degrades by about a factor of five faster than its regio-regular isomer. Its UV/Vis absorption spectrum also exhibits a significant blue-shift during degradation (by about 100 nm), which is not observed for regio-regular P3HT, suggesting that the fragmentation of the conjugated π-system in rra-P3HT takes place in a more random fashion than in rre-P3HT, thus producing a random distribution of π-conjugated fragments whose average shifts to shorter conjugation lengths throughout the degradation process, very similar to what has been observed for the singlet oxygen driven photo-oxidation of P3HT in solution[20]. The different degrees of regio-regularity have several consequences on the properties of the films, such as higher mobilities of the polymer chains and low molecular weight species, etc. for the random isomer. The most striking difference of the two isomers lies in their grossly different triplet yields. While films of the regio-regular isomer are reported to have triplet yields of $\phi_T < 10^{-3}$, the regio-random polymer shows significantly higher triplet yields[113] which might even approach the solution value of $\phi_T \approx 0.7$ [114]. As oxygen diffusion is not rate-limiting, as shown above, and triplet states are photochemically much more active than singlet excited states, due to their longer life-time, the higher triplet yield is most probably the reason for the accelerated photo-oxidation of the regio-random polymer. A possible pathway of triplet-induced photo-oxidation might be the sensitization of singlet oxygen (see Scheme 1), which has been shown to be the species responsible for the photo-oxidation of P3HT in solution[20,21]. These considerations are further supported by the activation spectrum of the regio-random P3HT which reveals that the effectiveness of the photo reaction follow the absorption spectrum of the polymer.

Although the discussion so far may not result in the presence of a degradation mechanism in detail it is worth trying to summarize the observed data. In summary the described degradation kinetics of the

regio-regular P3HT and their dependencies on environmental factors are summarized sufficiently well by the empirical expression:

$$-\frac{dE}{\varepsilon_T \cdot dt} = -\frac{dn_T}{A \cdot dt} = \frac{\Im\left(p_{O_2} \to \infty, \lambda, T\right) \cdot I_0(\lambda)}{1 + b(T) \cdot p_{O_2}^{-1}} + c\left(p_{O_2}, T\right)$$

where E represents the absorbance of the film, ε_T the extinction coefficient of one thiophene unit, A the unit area, n_T the number of moles of thiophene rings, I_0 the incident photon flux, p_{O_2} the oxygen partial pressure. $\Im$ is the effectiveness, b and c are constants, T is the temperature and λ is the irradiation wavelength. Typical values for these constants for a film of about 100 nm in thickness are $\Im\left(p_{O_2} \to \infty, 334\,nm, 300\,K\right) \approx 9 \cdot 10^{-6}$ and $b(298\,K) = 1.24\ bar$. Thermolysis of P3HT at moderate temperatures ($T < 400\,K$) under air in the dark, described by constant c, is negligible as compared to the photo-oxidative degradation of regiorandom P3HT, even at low light levels[23]. Similarly, photolysis in the absence of oxygen[105] takes place on the time scale of years.

V. Summary

In the present work, the degradation of the polymeric semiconductor poly-3-hexylthiophene (P3HT) has been investigated in thin film (~100nm) in order to elucidate a detailed understanding of the physical/chemical mechanism under ambient conditions. As a large number of possible reaction pathways may be present, the dominating degradation pathway was identified first. Therefore the aging of the polymer films was performed under different, controlled environmental conditions (light intensity, wavelength distribution, temperature, humidity, oxygen partial pressure and ozone) and investigated quantitatively using UV/VIS, FTIR, XPS/UPS and Photoluminescence spectroscopy. In order to establish defined environmental conditions, the degradation experiments were carried out in specially designed reaction cells. These cells allow the degradation of polymeric samples under defined, constant environmental conditions which are monitored online via sensors. At the same time, the degradation can be traced online using UV/VIS spectroscopy in transmission mode. The construction and setting up of the equipment for the measurement system was the first part of this work.

The following degradation studies revealed that the photo oxidation of the material is the major reaction pathway which is strongly enhanced in the presence of humidity. Other pathways like thermal oxidation, direct hydrolysis or ozone degradation are negligible under ambient conditions. Nevertheless the ozone degradation of P3HT was investigated in more detail as local ozone concentrations may be present during application or daily use of P3HT based devices. Ozone primarily attacks the π-conjugated system with subsequent oxidation of the sulfur position.

In order to elucidate the promoting effect of humidity during the photo oxidation of P3HT, FTIR spectroscopy was employed to study the product evolution. Here it turned out that humidity changes the product distribution. Isotopic labeling with D_2O and $H_2{}^{18}O$ was used to state that water at least acts as reactant with both, hydrogen and oxygen out of the water molecule being incorporated into reaction products. The promoting effect may originate from the enhanced diffusion of reactive species.

As the degradation of P3HT under white light conditions may consist of several photo-induced reactions, the wavelength dependence of the photo-oxidation was investigated using monochromatic illumination experiments. Surprisingly, the effectiveness of the aging increases by more than one order of magnitude towards the UV and does not follow the absorption of the polymer which is mainly located in the visible range. This suggests that the photochemistry in the film changes upon illumination with UV or VIS light and furthermore, that the white light degradation is dominated by the UV part of the incoming light. Using FTIR spectroscopy the presence of at least two different, photo-induced reactions was indentified. Illumination with visible light leads to the destruction of the π-conjugated system via the oxidation of the thiophene ring. Photo-oxidation in the presence of UV

light additionally influences the σ-framework of the polymer. During degradation the aliphatic side chain is detached from the molecule via a Norrish reaction and desorbs from the surface. Due to this detachment radical species occur which further promote the degradation.

Both the reaction kinetics and the product evolution during degradation are very similar using UV or white light. The aliphatic side chain is also detached under white light. Therefore the dominating reaction pathway under white light conditions is most probably also radical based and does not proceed via reactive species sensitized by the polymer. In order to investigate the role of the α-side chain position which was so far suggested to be the starting point of degradation in literature, P3HT was degraded which was selectively deuterated in this position. Using FTIR spectroscopy it turned out that this position is not preferentially attacked during degradation, thus it most probably not the origin of the degradation process. The nature of the photo chemically created oxygen species which initially triggers the degradation cannot be unambiguously stated. However the presence of superoxide ions seems to play a minor role whereas the presence of singlet oxygen attacking the thiophene ring is more probable. As the oxidation of the sulfur position could not be addressed in the FTIR spectra, the white light degradation of P3HT was additionally investigated using XPS. The sulfur position is completely oxidized and strongly correlated to the loss of the optical signal. Additionally to the detachment of the side chain, volatile species occur which contain significant amounts of sulfur. Therefore the molecule is completely decomposed under white light conditions.

During these investigations it turned out that the photo oxidation of P3HT in early stages leads to the modification of the electronic structure. These modifications where subsequently addressed in more detail using XPS/UPS and fluorescence spectroscopy. Here the presence of both reversible and irreversible effects was identified. Short time exposure to light and oxygen leads to the p-doping of the material and the partial quenching of fluorescence via the formation of a metastable polymer:oxygen complex. Both of these effects are reversible upon thermal annealing under vacuum or nitrogen conditions. Simultaneously to these reversible effects, the polymer is irreversibly oxidized leading to the formation of additional quenching sites for emissive states. However these quenching sites do not alter the electronic structure. Both the reversible doping of P3HT and the partial quenching of fluorescence occur in early stages of degradation where less than 3% of the UV/VIS signal is lost respectively 97% of all thiophene rings are still intact.

In order to understand the degradation process concerning the observed reaction kinetics and to support mechanistic statements a numerical simulation about the photo degradation in thin films was established. The algorithm can deal with both monochromatic and polychromatic illumination conditions and calculates both the UV/VIS reaction spectra as well as the kinetics of the thiophene ring concentration in the film. The simulation supports that the degradation of P3HT cannot be explained by the presence of a classical photo reaction which is due to the absorption of the polymer itself. More likely the reaction proceeds via a radical based mechanism with the reactive intermediates being highly reactive under UV illumination.

VI. Zusammenfassung

In der vorliegenden Arbeit wurde die Degradation des polymeren Halbleiters Poly-3-hexylthiophen (P3HT) in dünnen Schichten (~100nm) untersucht. Ziel war hierbei ein detailiertes Verständnis des physikalisch chemischen Degradationsmechanismus unter realistischen Umweltbedingungen. Da hierbei eine große Anzahl einzelner Reaktionspfade vorliegen kann, wurde zunächst der dominierende Degradationspfad isoliert. Dazu wurde die Alterung der Polymerschichten unter variierenden, kontrollierten Umweltbedingungen durchgeführt (Lichtintensität, spektrale Verteilung, Temperatur, Feuchtigkeit, Sauerstoffpartialdruck und Ozon) und mittels spektroskopischer Methoden verfolgt (UV/VIS, FTIR, XPS/UPS und Photolumineszenz). Um klar definierte Umgebungsbedingungen zu etablieren, wurden die Experimente in speziell gefertigten, geschlossenen Reaktionszellen durchgeführt. Diese Reaktionszellen ermöglichen die Degradation polymerer Proben unter definierten, konstanten Bedingungen, die in Echtzeit mittels Sensoren überwacht werden können. Die Degradation kann dabei ebenfalls in Echtzeit mittels UV/VIS Transmissionsspektroskopie untersucht werden. Die Entwicklung und der Aufbau von Apparaturen zur definierten Degradation polymerer Materialien mittels der oben genannten Umwelteinflüsse war der erste Teil der vorliegenden Arbeit.

Bei den folgenden Alterungsstudien konnte gezeigt werden, dass die lichtinduzierte Oxidation des Materials bestimmend für die Alterung ist, wobei die Gegenwart von Luftfeuchtigkeit die Reaktion um den Faktor 3 beschleunigt. Andere Reaktionswege wie thermisch induzierte Oxidation, direkte Hydrolyse oder der Angriff von Ozon sind vernachlässigbar. Die Degradation in der Gegenwart von Ozon wurde dennoch weiterhin untersucht, da erhöhte lokale Ozonwerte während der Herstellung oder späterem Einsatz von P3HT basierten Bauteilen vorhanden sein können. Ozon greift primär das das π-konjugierte System an zufälligen Positionen an was anschließend zu einer Oxidation der Schwefelposition führt. Die aliphatische Hexyl-Seitenkette bleibt dabei nahezu unberührt. Um den beschleunigenden Effekt von Luftfeuchtigkeit auf die Degradationsrate zu verstehen wurden die Entstehung von Reaktionsprodukten mittels FTIR Spektroskopie untersucht. Dabei zeigte sich, dass die Gegenwart von Wasser während der Photooxidation zu einer Veränderung der Produktverteilung führt. Durch Isotopenmarkierung mittels D_2O und $H_2{}^{18}O$ konnte gezeigt werden das Wasser zumindest als Reaktand agiert. Dabei wird sowohl Wasserstoff als auch Sauerstoff des Wassermoleküls in Reaktionsprodukte eingebaut. Der beschleunigende Effekt kann möglicherweise durch eine verbesserte Diffusion von Radikalen erklärt werden.

Da die Degradation von P3HT unter Weisslicht möglicherweise eine Überlagerung mehrerer photoinduzierte Reaktionen darstellt, wurde die Wellenlängenabhängigkeit der Photooxidation mittels Experimenten bei monochromatischer Bestrahlung untersucht. Überraschenderweise nimmt die Effektivität der Alterung in Richtung von UV Strahlung um mehr als eine Größenordnung zu und folgt nicht im Geringsten dem Absorptionsspektrum des Polymers, was hauptsächlich im sichtbaren Spektralbereich liegt. Dies lässt stark darauf schließen, dass sich die Photochemie im Film zwischen

Bestrahlung im sichtbaren und ultravioletten Bereich unterscheidet und dass bei Weisslichtbestrahlung der UV Anteil den Degradationsprozess dominiert. Mittels FTIR Spektroskopie zeigte sich die Gegenwart von mindestens 2 unterschiedlichen, photoinduzierten Reaktionen. Bestrahlung mit sichtbarem Licht führt zur Zerstörung des π-konjugierten Systems durch die Oxidation des Thiophenrings. Photooxidation in der Gegenwart von UV Licht beeinflusst zusätzlich das σ-System des Polymers. Während der Degradation wird die aliphatische Seitenkette vom Rest des Polymers durch eine Norrish Reaktion abgetrennt und desorbiert von der Oberfläche. Durch diese Spaltung entstehen radikalische Spezies die den Degradationsprozess beschleunigen. Sowohl die Reaktionskinetik als auch die Produktverteilung während der Degradation unter Weisslicht ist der unter UV Licht sehr ähnlich. Auch hier spaltet die aliphatische Seitenkette vom Polymergerüst ab. Daher scheint der dominierende Reaktionspfad auch hier radikalbasiert zu sein und verläuft nicht über reaktive Spezies die durch die Absorption des Polymers verursacht werden. Um die Rolle der α-Seitenkettenposition zu untersuchen die bisher als Startpunkt der Degradation gilt, wurde P3HT untersucht, dass an dieser Stelle selektiv deuteriert ist. Hierbei zeigte sich mittels FTIR Spektroskopie, dass diese Stelle nicht bevorzugt angegriffen wird. Daher ist diese Stelle sehr wahrscheinlich nicht verantwortlich für den Degradationsprozess. Die Natur der photochemisch aktiven Sauerstoffspezies kann nicht einwandfrei geklärt werden. Aufgrund der vorliegenden Ergebnisse spielen jedoch superoxidionen keine dominierende Rolle. Viel wahrscheinlicher hier ist die Präsenz von Singulett O_2 was direkt an den Thiophenring addiert. Da die Oxidation der Schwefelposition im Thiophenring nicht einwandfrei mittels FTIR Spektroskopie untersucht werden konnte, wurde die Degradation unter Weisslicht zusätzlich mittels Photoelektronenspektroskopie untersucht. Diese Untersuchungen zeigten dass die Schwefelposition während der Reaktion vollständig oxidiert wird und mit dem Verlust an optischer Absorption korreliert. Weiterhin konnte gezeigt werden, dass neben der Abspaltung der aliphatischen Seitenkette auch flüchtige Reaktionsprodukte entstehen müssen die Schwefel enthalten und das die Reaktion homogen im gesamten Film verläuft. Daher wird das Polymer unter Weisslicht völlig in flüchtige Reaktionsprodukte zerlegt.

Während dieser Reaktionen zeigte sich qualitativ, dass die Photooxidation in frühen Stadien zur Modifizierung der elektronischen Struktur von P3HT führt. Diese Effekte in frühen Stadien der Degradation wurden dann mittels XPS/UPS und Fluoreszenzspektroskopie detailliert untersucht. Dabei konnte nachgewiesen werden das sowohl reversible wie irreversible Effekte auftreten. Der kurzzeitige Kontakt von P3HT mit Licht und Sauerstoff führt zu einem metastabilen Polymer:Sauerstoff Komplex was zu einer p-Dotierung des Materials und partieller Löschung der P3HT Fluoreszenz führt. Beide Effekte sind reversible und können durch Heizen unter Vakuum oder Stickstoff rückgängig gemacht werden. Simultan zu diesen reversiblen Effekten wird das Polymer irreversibel oxidiert. Diese irreversiblen Defekte agieren als zusätzliche Quenchzentren für die Fluoreszenz des Polymers sind aber in Hinblick auf die elektronischen Eigenschaften des Polymer inaktiv und führen nicht zu Dotierung. Sowohl die Löschung der Fluoreszenz als auch die reversible

Dotierung von P3HT treten in frühen Stadien der Degradation auf solange weniger als 3% der vorhandenen Thiophenringe zerstört sind bzw. weniger als 3% Verlust an Absorption im UV/VIS Spektrum zu beobachten sind.

Um die experimentellen Befunde der Degradation in Hinblick auf die beobachtete Reaktionskinetik zu verstehen und mechanistische Vorstellungen zu untermauern , wurde eine numerische Simulation der P3HT Photooxidation in dünnen Schichten erstellt. Der Algorithmus kann sowohl monochromatische Experimente als auch Weisslichtexperimente erfassen und dabei UV/VIS Reaktionsspektren als auch die Kinetik der Thiophenringkonzentration berechnen. Diese Simulation unterstützt die Aussage, dass die Degradation sich nicht mittels einer klassischen Photoreaktion erklären lässt, bei der die Degradation durch die Absorption des Polymers verursacht wird. Vielmehr liegt ein radikalbasierter Mechanismus vor der über Zwischenprodukte verläuft die unter UV Bestrahlung hoch reaktiv sind.

VII. Appendix

Appendix A: Numerical algorithm of matlab simulation about the polymer degradation

In the following the matlab algorithm of the complete simulation will be explained from the initial light absorption to the chemical reaction of polymer chains within the random chain or end chain scission mechanism. Finally the two limiting cases about the mobility of the reactive center are introduced. The basic differential equation used in the matlab algorithm for the photochemical decomposition of P3HT is given by:

$$\frac{dc}{dt} = I_{Absorbed}(\lambda) \cdot \Phi(\lambda) \qquad \textbf{Eq. 43}$$

with c being the concentration of a chemical species i, t the time, $I_{Absorbed}$ the number of photons absorbed per unit volume by the species i and Φ as the wavelength dependent quantum efficiency of the photo reaction. The number of absorbed photons $I_{Absorbed}$ per unit volume is given by is the difference of primary intensity I_0 and transmitted intensity I:

$$I_{Absorbed}(\lambda) = I_0(\lambda) - I(\lambda) \qquad \textbf{Eq. 44}$$

Using the Lambert Beer law

$$-dI(x) = \varepsilon(\lambda) \cdot c(d) \cdot I(x) \cdot dx \qquad \textbf{Eq.45}$$

and integration to:

$$I(x) = I_0 \cdot 10^{-\varepsilon(\lambda) \cdot c(x) \cdot x} \qquad \textbf{Eq. 46}$$

This becomes:

$$I_{Absorbed}(\lambda) = I_0(\lambda) \cdot (1 - 10^{-\varepsilon(\lambda) c(x) x}) \qquad \textbf{Eq. 47}$$

Therefore the differential equation for a photochemical reaction becomes:

$$\frac{dc}{dt} = I_0(\lambda) \cdot (1 - 10^{-\varepsilon(\lambda)c(x)x}) \cdot \Phi(\lambda) \qquad \textbf{Eq. 48}$$

The numerical algorithm (written in Matlab®) will be explained in the following and is visualized in Fig. 78:

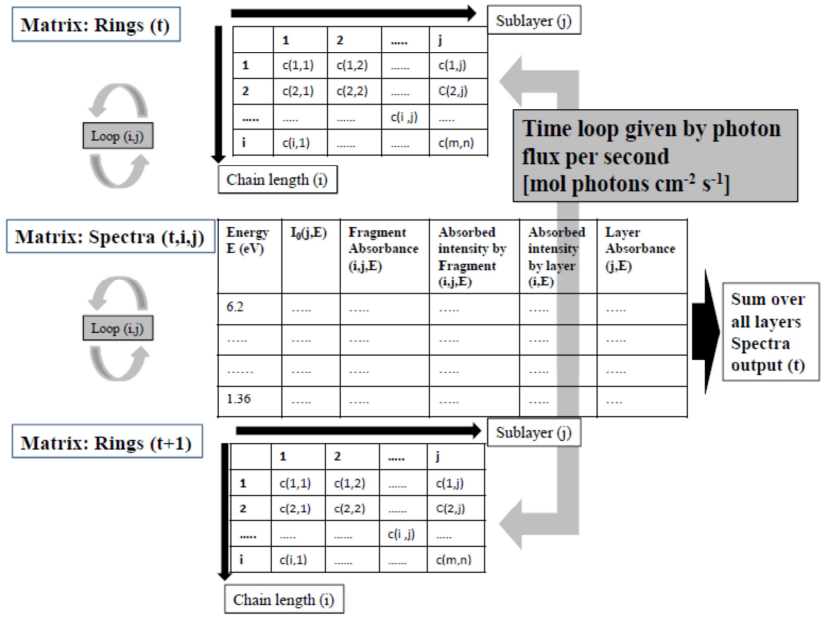

Fig. 78 Scheme of the numerical algorithm for the simulation of the photochemical decomposition of a P3HT thin film. The matrix element (i,j) in the matrix Rings contains the concentration c(i,j) of thiophene rings for a fragment consisting of i conjugated thiophene rings which is located in sublayer j. The Number of sublayers in the complete polymer film is given by n whereas m is the chain length of conjugated thiophene rings at t=0.

Step 1: Generation of Matrix Rings (t)

A matrix called *Rings* is generated which consists of n columns (j). Each column represents a sub layer of the polymer film with a thickness of 1 nm. The matrix has m = 300 rows, each representing a certain length of π-conjugated fragments. The index i of a given row is identical to the number of thiophene rings in the corresponding thiophene oligomer. At time zero (indicated in the algorithm by

the time index zero) only the last row (chain length 300) has entries of c(t = 0) = 10 mol/L for each column (each sub layer) which corresponds to the concentration of thiophene rings in undegraded P3HT films.

Step 2: Generation of absorption spectra in the matrix *Spectra*

For each time t, the matrix *Rings* is evaluated column by column to obtain the absorption spectra of each layer. For each matrix element (polymer fragment) a Gaussian function is created representing the main UV/VIS absorption band of the corresponding polymer fragment. The maximum position of the Gaussian function is correlated to the chain length of the p-conjugated fragment according to table Tab. 10

Tab. 10 Maximum absorption position of oligomers with length of n thiophene units used in the matlab algorithm[35]

Oligomer [n]	Absorption Position E_{max} [eV]	Absorption Position E_{max} [nm]	Oligomer [n]	Absorption Position E_{max} [eV]	Absorption position E_{max} [nm]
1	4.51	274.8	5	2.50	495.9
2	3.60	343.8	6	2.30	539.0
3	2.90	427.5	7	2.27	546.2
4	2.60	476.9	≥8	2.24	553.5

The height of the function is given by the product of the non-normalized Gaussian, the molar absorption coefficient $\varepsilon = 10^4\ M^{-1}cm^{-1}$,the corresponding concentration c(i,j) and the sublayer thickness d. The absorbance of the fragment of length i in layer j at a given energy E, Abs(i, j, E), is then given by:

$$Abs(i,j,E) = \varepsilon \cdot c(i,j) \cdot d \cdot e^{-\frac{(E-E_{max})^2}{2 \cdot FWHM^2}} \qquad \textbf{Eq.49}$$

The spectra are calculated on the energy scale with a constant halfwidth of 0.2067 eV for all chain lengths. Finally, the absorption spectrum of a specific layer, j, is calculated by summing over the absorption spectra of all fragments i in this layer:

$$Abs(j,E) = \sum_{i=1}^{300} A(i,j,E) \qquad \textbf{Eq.50}$$

The resulting spectra, Abs(j,E), are converted to the wavelength scale, A(j,λ), according to

$$\lambda[nm] = \frac{hc}{E[J]} \cdot 10^{-9} = \frac{6.63 \cdot 10^{-34}[J] \cdot 2.998 \cdot 10^{8}[ms^{-1}]}{E[eV] \cdot 1.602 \cdot 10^{-19}[J \cdot eV^{-1}]} \cdot 10^{-9} \qquad \textbf{Eq.51}$$

Step 3: **Absorption of light in Matrix *Spectra***

The number of photons absorbed by each fragment i in the sublayer j at the wavelength λ is calculated according to:

$$I_{Abs\ Fragment}(i,j,\lambda) = I_0(j,\lambda)(1-10^{-Abs(i,j,\lambda)}) \qquad \textbf{Eq. 52}$$

with $I_0(j,\lambda)$ being the primary intensity of the incoming light in the sub layer j at the wavelength λ.

The total number of photons absorbed, integrated over the whole spectrum is obtained by summing over all wavelengths:

$$I_{Abs\ Fragment}(i,j) = \sum_{\lambda} I_0(j,\lambda)(1-10^{-Abs(i,j,\lambda)}) \qquad \textbf{Eq.53}$$

The number of photons absorbed at wavelength λ in the layer j is obtained from the absorbance of all fragments i present in this layer:

$$I_{Abs\ layer}(j,\lambda) = I_0(j,\lambda)(1-10^{-Abs(j,\lambda)}) \qquad \textbf{Eq.54}$$

This number is used to calculate the primary intensity for the next sub layer. I_0 has to be recalculated for each sub layer, as the light intensity is reduced step by step according to the Lambert-Beer law. The absorption of light is also used as time counter in the simulation as the incoming light is given as

mol photons per second and unit area. Therefore each time loop represents one second of illumination with the intensity I_0.

Step4: **Reaction: Destruction of thiophene rings in Matrix *Rings1***

The concentration of reacting thiophene rings $c_{react}(i,j)$ in the corresponding fragment class after the absorption of light is then given by:

$$\frac{\Delta c_{react}(i,j)}{\Delta t} = I_{Abs\ Fragment}(i,j,\lambda) \cdot \phi_{\lambda} \qquad \textbf{Eq.55}$$

Where ϕ is the photochemical quantum yield. For the moment, we set the quantum efficiency to unity. Although this is most probably not the case, this number is only a linear scaling factor for the time scale as can be seen in Eq. 49.

The corresponding concentration for the fragments of length i in layer j for the next time index t+1 due to the destruction of rings is thus given by:

$$c(i,j,t+1) = c(i,j,t) - \Delta c_{react}(i,j) \qquad \textbf{Eq.56}$$

Due to the destruction of thiophene rings, the π-conjugated segments are split into shorter fragments consisting of i' and i" thiophene rings. For each split segment of row i, the concentration of thiophene rings in the corresponding rows, i' and i", has to be increased by the corresponding values, c(i') and c(i"). Assuming that each destructed ring leads to the splitting of exactly one polymer chain, the concentration of polymer chains which have to redistributed into shorter classes of chain lengths is also $\Delta c_{react}(i,j,t)$. The corresponding concentration loss of thiophene rings in row i is thus given by

$$\Delta c_{redistribute}(i,j) = \Delta c_{react}(i,j,\lambda) \cdot i \qquad \textbf{Eq.57}$$

The overall concentration of rings remaining in row i for the next time step t+1 is given by:

$$c(i,j,t+1) = c(i,j,t) - \Delta c_{redistribute}(i,j) = c(i,j,t) - \Delta c_{react}(i,j) \cdot i \qquad \textbf{Eq.58}$$

In rows i' and i", the concentrations of thiophene rings at time t+1 are

$$c(i',j,t+1) = c(i',j,t) + \Delta c_{react}(i,j) \cdot i' \qquad \textbf{Eq.59}$$

And

$$c(i'', j, t+1) = c(i'', j, t) + \Delta c_{react}(i, j) \cdot i'' \qquad \textbf{Eq.60}$$

With $i = i' + i'' - 1$ **Eq. 61**

Equation 55 takes into account that one thiophene ring is destructed in order to split the chain with length i into segments i`and i``.

The rings to be actually photo-oxidized (to be removed from the matrix) are determined according to the chosen splitting mechanism (end chain or random splitting) as described in the following step 5.

Step5: Splitting of polymer chains in Matrix *Rings1*

There are different ways of distributing the thiophene rings to be destroyed in the polymer fragments. Two extreme cases will be considered in the following: destruction of terminal rings only ("end chain splitting") and random destruction of rings ("random splitting").

End chain splitting:

In this case, it is assumed that only the terminal rings of the conjugated segments are destroyed. Consequently, in Eq.55, i' = i-1 and i" =0. According to Eqs. 50 and 51, the concentrations of fragments of lengths i and i-1 are obtained as

$$c(i, j, t+1) = c(i, j, t) - \Delta c_{react}(i, j) \cdot i \qquad \textbf{Eq.62}$$

$$c(i-1, j, t+1) = c(i-1, j, t) + \Delta c_{react}(i, j) \cdot (i-1) \qquad \textbf{Eq.63}$$

All terminal rings in the considered region (either in the same layer or in the whole film, depending on the chosen mechanism - see below) have the same probability of being photo-oxidized.

Random splitting:

In this case, all rings of the considered polymer fragment are destroyed with equal probability using a random number out of a uniform distribution [0:1]. The chain lengths of the two fragments, i' and i"

depend on the position of the destroyed ring in the initial segment of length i. This position, p, is chosen randomly

$$p = 1 + RandomNumber[0 : (i(t) - 1)] \qquad \textbf{Eq.64}$$

Thus

$$i'(t+1) = p - 1 \qquad \textbf{Eq.65}$$

$$i''(t+1) = i(t) - p \qquad \textbf{Eq.66}$$

With the concentration of thiophene rings according to:

$$c(i', j, t+1) = c(i', j, t) + \Delta c_{react}(i, j) \cdot (p-1) \qquad \textbf{Eq.67}$$

$$c(i'', j, t+1) = c(i'', j, t) + \Delta c_{react}(i, j) \cdot (i(t) - p) \qquad \textbf{Eq.68}$$

Step 6 Time loop closes

The matrix *Rings* contains the concentration of thiophene rings for the time index t. Simultaneously a matrix *Rings1* is used to save the concentrations for the time index t+1. In order to iterate the concentrations of the time index t+1 are handed over to the index t which remains in the working memory of the matlab software. Then the calculations start again. The reaction spectrum at the time index t of the complete film is saved in an external file.

Mobility of the reactive centre created after the absorption process

1) "Localized reactive centre- Classical photochemical reaction"

This model represents a mechanism where molecules react only from their excited state. Molecules in their ground state are not affected. The mechanism is realized by oxidizing only those thiophene rings which are contained in fragments of the same length i as the fragment in the same layer which has absorbed the photon. As pointed out above, the number of reacting thiophene rings per absorbed number of photons of a fragment of length i in the sublayer j is given by:

$$\frac{\Delta c_{react}(i,j)}{\Delta t} = I_{Abs\ Fragment}(i,j,\lambda)\cdot\phi_{\lambda} \qquad \textbf{Eq.69}$$

2) " Mobile reactive centre "

This model represents a mechanism where the absorption of a photon by a molecule produces a reactive species which destroys a thiophene ring in the same molecule or in other close by molecules with equal probability. Therefore also molecules in their ground state are affected by the degradation process which were not involved in the absorption process.

In a first approach the reactive reactive centres are free to move within the complete polymer film. The model is based on the consideration that diffusion of the reactive centre might be much faster than the destruction of thiophene rings.

The total number of reacting rings in the complete polymer film is given by:

$$\frac{\Delta c_{react}}{\Delta t} = I_{Abs\ Film}(\lambda)\cdot\phi \qquad \textbf{Eq. 70}$$

As the reactive centre is now mobile in the complete polymer film the number of reacting thiophene rings is given by comparing the concentration of thiophene rings c(i,j) in the fragment class i in a sublayer j compared to the overall concentration of thiophene rings in the complete film (i,j)

$$\Delta c_{react}(i,j) = \frac{c(i,j)}{\sum_j \sum_i c(i,j)} \cdot \Delta c_{react} \qquad \textbf{Eq.71}$$

The following steps of the algorithm, chain splitting and redistribution of thiophene rings is calculated as presented in section III.3.1.

VIII. Literature

1 Fix W., Ullmann A., Ficker J., Clemens W., *Appl. Phys. Let.t*, **2002**, *81*, 1735-1737

2 NREL – National renewable energy laboratory, USA, **Rev.4-2011**

3 Waltera M. G.,Rudineb A.B., Wamser C.C., *J. Porphyrins Phthalocyanines*, **2010**,14, 760–792

4 Green M.A., Emery K., Hishikawa Y., Warta W., *Prog. Photovolt: Res. Appl.*, **2011**,19,84–92

5 Brabec C.J. , Gowrisanker S. ,Halls J.J.M., Laird D., Jia S. , Williams S.P., *Adv. Mater.*, **2010**, 22, 3839–3856

6 Jørgensen M., Norrman K., Krebs F.C., *Solar Energy Materials & Solar Cells*, **2008**, M. G., 686–714

7 Thompson B.C., Frechet J.M.J., *Angew. Chem. Int. Ed.* , **2008**, 47, 58–77

8 Kalowekamo, J., Baker, E, *Sol.Energy*, **2009**, doi:10.1016/j.solener.2009.02.003

9 Lungenschmied C., Dennler G., Czeremuszkin G., Latreche M., Neugebauer H., Sariciftci N.S., *Proc. of SPIE*, 6197, 619712-3

10 Cros S., De Bettignies R., Berson S., Bailly S., Maisse p., Lemaitre N., Guillerez S., *Solar Energy Materials & Solar Cells*, **2011**,95,65–69

11 Manceau M., Rivaton A., Gardette J.L., Guillerez S., Lemaître N., *Solar Energy Materials and Solar Cells*, **2010,** 95, 5, 1315-1325

12 Norrman K., Madsen M.V., Gevorgyan S.A., Krebs F.C., *J. AM. CHEM. SOC.* , **2010**, *132*, 16883–16892

13 Hauch J.A., Schilinsky P., Choulis S.A., Childers R., Biele M., Brabec C.J., *Sol. Energy Mater. Sol. Cells*, ***2008***, *92*, 727–731

14 Manceau M., Bundgaard E., Carl J.E., Hagemann O., Helgesen M., Søndergaard R., Jørgensen M., Krebs F.C., *J. Mater. Chem.*, **2011**, 21, 4132–4141

15 Seemann A., Egelhaaf H.-J., Brabec C.J., Hauch J.A., *Org. Electron.*, **2009**, 10, 8, 1424-1428

16 Manceau M., Rivaton A., Gardette J.L., Guillerez S., Lemaître N., *Solar Energy Materials*

and Solar Cells, **2010,** 95, 5, 1315-1325

[17] Schafferhans J., Baumann A., Wagenpfahl A., Deibel C., Dyakonov V., *Organic Electronics* , **2010**, 11, 1693-1700

[18] Seemann, A.; Egelhaaf, H.-J.; Brabec, C.J.; Hauch, J.A. *Org. Electron*., **2009**, *10*, 1424-1428

[19] Ogawa, S.; Naijo, T., Kimura, Y. Ishii, H.; Niwano, M. *Japanese Journal of Applied Physics* **2006,** *45*, 530–533

[20] Abdou, M.S.A.; Orfino, P.; Holdcroft S. *J. Am. Chem. Soc.*, ***1997***, *119*, 4518-4524

[21] Koch, M.; Nicolaescu R.; Kamat P.V. *J. Phys. Chem. C*, **2009**, *113*, 11507-11513

[22] Manceau, M.; Rivaton, A.; Gardette, J.-L.*Macromol. Rapid Commun.*, **2008**, *29*, 1823–1827

[23] Abdou M.S.A., Holdcroft S., *Can. J. Chem.*, **1995**,73, 1893-1901

[24] Manceau, M.; Rivaton, A.; Gardette, J.-L.; Guillerez, S.; Lemaitre, N. *Polymer Degrad. Stab.*, **2009**, *94*, 898–907

[25] Hintz, H.; Egelhaaf, H.-J.; Peisert, H., Chassé, T. *Polymer Degradation and Stability*, **2010**, *95*, 818-825

[26] Ljungqvist, N.; Hjertberg, T. *Macromolecules*, **1995**, *28*, 5993-5999

[27] Chen Y., Zhou G.X., Brown N., Wang T., Ge Z., *Analytica Chimica Acta*, **2003**, 497, 155–164

[28] Gross T.,Pippig F., Merz B., Merz R., Vohrer U., Mix R., Steffen H., Bremser W., Unger W.E.S., *Plasma Process. Polym.*, **2010**, 7, 494–503

[29] Seah M.P., Densch W.A., *Surface and interface analysis*, **1979** ,1

[30] Barbarella G., Bonghi A., Zambianchit M., *Macromolecules*, **1994**,27, 3039-3045

[31] Brown P.J., Thomas D.T., Koehler A., Wilson J.S., Kim J.-S., Ramsdale C.M., Sirringhaus H., Friend R.H., *PHYSICAL REVIEW B* , **2003**, 67, 06420, 1-13

[32] Rabek, J.F., Handbook of Polymer Photo degradation, Chapman Hall

[33] Audouin, L.; Langlois, V.; Verdu, J; de Bruin, J.C.M. *J. Mater. Sci.*, **1994**, *29*, 569 - 583

[34] Egelhaaf H.-J., Dissertation, Tübingen 1996

[35] Gierschner, J; Cornil, J.; Egelhaaf, H.-J. *Adv. Mater.*, **2007**, *19*, 173-191

[36] Andrady, A.L. *Advances in Polymer Science*, **1997**, *128*, 48-94

[37] Numeric Simulation provided by PD. Dr H.-J. Egelhaaf

[38] Ocean Optics, Manual Maya2000pro

[39] Hesse R., Chassé T., Szargan R., *Anal. Bioanal. Chem.*, **2003**, *375*, 856

[40] LUXEON Rebel Direct Color Portfolio, Technical Datasheet DS65

[41] Cook S., Furube A., Katoh R., *Energy Environ. Sci.*, **2008**, 1, 294–299

[42] Lüer, L.; Egelhaaf, H.-J.; Oelkrug, D.; Cerullo, G.; Lanzani, G.; Huismann, H.; De Leeuw, D. *Org. Electron.*, **2004**, *5*, 83–89

[43] Kroeze J.E., Savenije T.J., Vermeulen M.J.W., Warman J.M., *J. Phys. Chem. B*, **2003**, *107*, 7696-7705

[44] Shaw P.E., Ruseckas A., Samuel I.D.W., *Adv. Mater.* , **2008**, 20, 3516–3520

[45] Kaptan, H.Y. *Journal of Applied Polymer Science*, **1999**, *71*, 1203–1207

[46] Horas, J.A., *Journal of Polymer Science: Part B, Polymer Physics*, **1996**, *34*, 1547-1553

[47] Gao, Y.; Maca, A.M.; Wang, B.; Ogilby P.R., *Macromolecules*, **1994,** *27***,** 7041-7048

[48] Egelhaaf, H.-J.; Lüer, L.; Oelkrug, D.;Winter,G.; Haisch,P.; Hanack, M., *Synth. Met.* **1997**, *84*, 897-898

[49] Yan, M.; Rothberg, L.J.; Papadimitrakopoulos, F.;Galvin, M.E.; Miller, T.M., *Phys. Rev. Lett.* **1994**, *73*, 744 - 747

[50] G. Dicker, M. P. de Haas, L. D. A. Seibels, J. M. Warman, Phys. Rev. B, **2004**, *70*, 045203.

[51] Schwieger T., Liu X., Peisert H., Aldolphi B., Kiriy N., Knupfer M., *J. Appl. Phys.*, **2005**, *97*, 1237121-1237125

[52] Chien-Cheng Liu, Chia-Ming Yang,Wen-Hsing Liu, Hua-Hsien Liao,Sheng-Fu Horng, Hsin-Fei Meng, **2009**, 159, 1131–1134

[53] Lu C.-K. , Meng H.-F., *Phys. Rev. B*, **2007**, *75*, 23520611-23520616

[54] Liao H.-H., Yang Ch.-M., Liu Ch.-Ch., Horng S.-F., Meng S.-F., Shy J.-T., *J. Appl. Phys.*,

2008, *103*, 1045061-1045068

[55] Lüer L., Egelhaaf H.-J., Oelkrug D.,*Optical Materials*, **1998**. *9*, 454-460

[56] Hintz H., Egelhaaf H.-J., Lüer L., Hauch J., Peisert H., Chassé T., Chem. Mater., **2011**, *23*, 145–154

[57] Vingarzan R., *Atmos. Environ.*, **2004**, *38*, 3431–3442

[58] Seinfeld J., *Science*, **1989,** *243*, 745-752

[59] Kendrick C., Semancik S., J. *Vac. Sci. Technol.* A, **1998**,*16.5*, 3068-3075

[60] Egelhaaf H.-J., Lüer L., Oelkrug D., Winter G., Haisch P., Hanack M., , *Synth. Met.*, **1997**, *84*, 897 -898

[61] E.J. Meijer, A.V.G. Mangnus, B.-H. Huisman, G.W. 't Hooft, D.M. de Leeuw, T.M. Klapwijk, *Synth. Met.* , **2004**, *142*, 53 - 56

[62] Nowaczyk J., Czerwinski W., Olewnik E., *Polymer Degrad. Stab.*, **2006**, *91*, 2022-2029

[63] Hintz H., Peisert H., Aygül U., Latteyer F., Biswas I., Nagel P., Merz M., Schuppler S., Breusov D., Allard S., Scherf U., Chasse T., *ChemPhysChem*, **2009**, 269-275

[64] Heeg J., Kramer C., Wolter M., Michaelis S., Plieth W., Fischer W.-J., *Appl. Surf. Sci.*, **2001**, *180*, 36-41

[65] Coen M., Keller B., Groening P., Schlapbach L., *J. Appl. Phys.*, **2002**, *92*. 5077-5083

[66] Hopkins J., Badyal J.P.S., *J. Polym. Sci., Part A: Polym. Chem*., **1994**, *34*, 1385-1393

[67] Zhenfeng, Z.; Xingzhou, H.; Zubo, L. *Polymer Degrad. Stab.* **1996**, *5*, 93-97

[68] Andrady A.L., *Final Report to USEPA under contract* # 68-02-4544, Task II-60, January 1991

[69] Andrady, A.L.; Searle, N.D.; Crewdson, L.F.E. *Polymer Degrad. Stab.*, **1992**, *35*, 235-247

[70] Papet G.; Audouin-Jirackova, L.; Verdu, J. *Radiat.Phys.Chem*, **1989**, *33*

[71] Staring, E.G.J.; Berntsen, A.J.M.; Romme, S.T.R.; Rikkeny, G.L.J.A.; Urbach, *P. Phil. Trans. R.Soc. Lond. A* **1997,** *355*, 695-706

[72] Scurlock, R. D., Wang, B., Ogilby, P. R., Sheats, J. R. & Clough, R. L. *J. Am. Chem. Soc.*

1995, *117***,** 10194-10202

[73] Cumpston B. H. , Jensen K. F. *Synth. Met.* **1995,** *73*, 195-199

[74] Cross H., Rolfe A.C., *Trans. Faraday Soc.*, 1951, 47, 354-357

[75] Cross H., Rolfe A.C., *Trans. Faraday Soc.*, 1951, 47, 354-357

[76] Sessler C., Hintz H., Egelhaaf H.-J., Chassé T., in preparation

[77] Wiberg, K.B., Slaugh, L.H., *J. Am. Chem. Soc*., **1958**, 80, 3033

[78] Saunders,W.H., Ashe, Jr. and T.A., *J. Am. Chem. Soc.*, **1969**, 91, 4473

[79] Lynch, R.A., Vincenti, S.P., Lin, Y.T., Smucker, L.D., Subba Rao, S.C., *J. Am. Chem. Soc. 1972*, **1994**, 8351

[80] Hurrell S., Milroy G.E., Cameron R.E., *Polymer 44* , **2003**, 1421–1424

[81] Sammon C., Deng C., Yarwood j., *Polymer 44* , **2003**, 2669–2677

[82] Ping Z.H., Nyugen Q.T., Chen SM., Zhou J.Q., Ding Y.D., , *Polymer 42*, **2001**, 8461-8467

[83] Jaczewska J., Raptis I., Budkowski A.,, Goustouridis D., Raczkowskaa J., Sanopoulou M. , Pamuła E. , Bernasik A., Rysz J., *Journal of Applied Polymer Science*, **2007**, 105, 67–79

[84] Lin P., Yan F., Chan H.L.W., *Langmuir*, **2009**, 25, 7465–7470

[85] J.F. Rabek, Polymer Photodegradation – Mechanism and experimental Methods, Chapman & Hall 1995

[86] Scheirs, J., Carlsson D. J., Bigger S. W., *Polym.-Plast. Technol. Eng.*, **1995**, 34, 97-116

[87] Kodera Y., McCoy B.J., *AIChE Journal* , **1997** , 43, No. 12, 3205-3214

[88] Triacca V., Gloor P.E., Zhu S., Hrymak A.N., Hamielec A.E. Polymer *Engineering and science*, **1993**, 33, 8, 445-454

[89] Staggs J.E.J., *Polymer Degradation and Stability*, **2002**, 76, 37–44

[90] Kang E.T., Neoh K.G., Zhang X., Tan K.L., Liaw D.J., *Surf. Interface Anal.*, **1996**, *24*, 51-58

[91] Kaduk A., Toby S., *Int. J. Chem. Kinet.*, **1977**, *Vol. IX*, 829-840

[92] Bailey P., Hwang H.H., *J. Org. Chem*. **1985**, *50*, 1778-1779

[93] Razumovskii S. D., Lisitsyn D. M., *Polymer Sciene Series A*, **2008**, *50*, 1187-1197

[94] Cataldo F., *Polymer Degradation and Stability*, ***2001***, *73*, *511-520*

[95] Cataldo F., *Polymer Degradation and Stability*, ***2002***, *75*, *93-98*

[96] Allen N.S., Edge M., Mourelatou D., Wilkinson A., Liauw C. M., Parellada M.D., Barrio J.A., Ruiz Santa Quiteria V., *Polymer Degrad. Stab.*, **2003**,*79*, 297–307

[97] Cataldo F., Angelini G., *Polymer Degrad. Stab.*, **2006**, 2793-2800

[98] Chabinyc, M.L.; Street, R.A.; Northrup, J.E.; *Appl. Phys. Lett*., **2007**, *90*, 123508-1-123508-4

[99] Ricci W. , Nesta J.M., *The Journal of Physical Chemistry*, **1976**, 80, 9, 975-979

[100] Yan M., Rothberg L.J., Papadimitrakopoulos F., Galvin M.E., Miller T.M., *Phys. Rev. lett*, **1994**, 73, 5, 744-747

[101] Lu C.-K. , Meng H.-F., *Phys. Rev. B*, **2007**, *75*, 235206-1-235206-6

[102] Yang X., Loos J., Veenstra S.C., Verhees W.J.H., Wienk M.M., Kroon J.M., Michels M.A.J., Janssen R.A.J., *Nano Lett.*, **2005**, 5, 579-583

[103] Marchant S., Foot P.J.S., *Journal of materials science: materials in electronics*, **1995**, 6, 144-148

[104] Seemann A., Sauermann T., Lungenschmied C., Armbruster O., Bauer S., Egelhaaf H.-J., Hauch J. A., *Solar Energy* , **2010** ,84, 6, 1238-1249

[105] Manceau, M.; Chambon, S.; Rivaton, A.; Gardette, J.-L.; Guillerez, S. & Lemaıtre, N. *Sol. Energy Mater. Sol. Cells*, **2010**, *94*, 1572 - 1577

[106] Aguirre A., Meskers, S.C.J., Janssen, R.A.J. Egelhaaf , H.-J., Org. Electron., **2011**,12,1657-1662

[107] Saunders B.B., Kaufman P.C., Matheson M.S., *The Journal of Physical Chemistry*, **1978**, *82*, *2*, 142-150

[108] von Sonntag C., Bothe E., Ulanski P.,Adhikary A., *Radiation Physics and Chemistry*, **1999**, 55, 599- 603

[109] Sperlich A., Kraus H., Deibel C., Blok H., Schmidt J., Dyakonov V., J. Phys. Chem. B , **2011**, 115, 13513–13518

[110] Hartley G. H., Guillet J. E. , *Macromolecules*, **1968**, I, 5, 413-417

[111] Geuskens G., David C., *Pure & Appl. Chem*., **1979**, 51, 233-240

[112] Kuzina S., Mikhailov A.I., *European Polymer Journal*, **2001**, 2319-2325

[113] Österbacka, R.; An, C.P.; Jiang, X.M.; Vardeny, V. *Science*, **2000**, *287*, 839-842

[114] Seixas de Melo, J.; Burrows, H. D.; Svensson, M.; Andersson, M. R.; Monkman, A. P. *J. Chem. Phys.* **2003**, *118*, 1550 – 1556

Danksagung

Zunächst möchte ich mich bei Herrn Prof.Dr. Chassé für die angenehme Zeit in seinem Arbeitskreis bedanken. Insbesondere für das Vertrauen bei Projektanträgen, der Anschaffung neuer Laborgeräte und der täglichen Laborarbeit, die ich als sehr frei und angenehm empfand.

Herrn PD. Dr. Hans-Joachim Egelhaaf möchte ich für die grenzenlose Zusammenarbeit, Diskussionsbereitschaft und das Vertrauen in meine Arbeit danken. Das hat die Arbeit zum Vergnügen gemacht.

Herrn PD. Heiko Peisert für viele kritische Diskussionen und nette Gespräche außerhalb der Wissenschaft.

Herrn Wolfgang Neu für seine herzliche Art und die Chance von ihm zu lernen, egal ob menschlich oder technisch.

Meinem jahrelangen Bürokollegen Florian Latteyer für die vielen, netten Gespräche und produktiven Fachsimpeleien

Dem gesamten Arbeitkreis Chassé und auch den ehemaligen Mitarbeitern für die angenehme Atmosphäre.

Herrn Klaus Schaupp und der gesamten Metallwerkstatt für die Anfertigung meiner endloser Versuchsaufbauten.

Der Deutschen Forschungsgesellschaft (DFG) und dem Bundes Ministerium für Bildung und Forschung (BMBF) für die Finanzierung.

Meiner Familie, Freunden und meiner Verlobten für den ständigen Rückhalt und für das Verständnis der Tatsache, dass Wissenschaft oftmals keine Pause macht.